

Oceanic inspiration for biomaterial formation – investigations into biomimetic synthesis
and characterization of inorganic oxide materials inspired by sea sponges and
diatoms

By

Jenny E. Nesbitt

Dissertation

Submitted to the Faculty of the Graduate School of Vanderbilt University

in partial fulfillment of the requirements for the degree of

DOCTOR OF PHILOSOPHY

in

Chemistry

December, 2016

Nashville, TN

Approved:

David W. Wright, Ph.D.

Janet E. Macdonald, Ph.D.

Charles M. Lukehart, Ph.D.

Scott A. Guelcher, Ph.D.

To my family

ACKNOWLEDGEMENTS

This work was made possible by the financial contributions of the Hercules Fellowship and the D. Stanley and Ann T. Tarbell Graduate Research Fellowship.

I want to thank many people without whom my success would not have been possible. First and foremost, my family has been the most constant, unwavering source of support in my life. Throughout high school, college, and beyond, my parents have extended their wisdom and guidance to me, and my brothers have never been anything but supportive (and fantastic friends, love you two!). My high school chemistry teacher, Mrs. Savage, first sparked my interest in chemistry. As I progressed through high school, I found many other science courses exciting, but I was still drawn to chemistry. Throughout college, I enjoyed learning chemistry, and particularly enjoyed the labs, being able to physically *do* chemistry. My undergraduate research advisor, Dr. Abdessadek Lachgar, introduced me to laboratory skills and practice, experimental design, and inorganic synthesis, and he showed me how much FUN working in a chemistry laboratory can be.

While he was not an advisor or a committee member, Dr. John McLean is a very important reason I attended graduate school at Vanderbilt University. His philosophy about graduate school research as a chemist, the innovation, and the direct implication of the degree itself resonated with me and drew me to Vanderbilt. We have certain skill sets that lend ourselves to the field in which we're most practiced, but our training has led us to be prepared problem-solvers in any situation.

There are many more people who have helped pave my path to this point. Our incoming class to the graduate program could not have been made up of more fantastic people. From midtown nights and trivia our first year to Festivus and after-picnic parties, we always knew how to get along and have a good time.

Without a doubt, my fellow lab members in the Wright lab have been instrumental in my making it through this program. Former wright lab members, Josh Swartz, Becca Sandlin (and her hubby Shane), Stevie Jackson, Chris Gulka, Phillip Budge, Alex Rutledge, Phoebe Penamon, Nicholas Wright, and Nick Adams, all helped make it an enjoyable time, from lab movie nights to beach trips, we always had a great time. Kim Fong, you are so supportive and strong and amazing. I appreciate all of our cell room chats, and I would not have made it through this program without you. You will make an incredible teacher, and those lil kiddos are very lucky! Adam Ryan Travis, my first mentee! Your snarky attitude, quick wit, and brilliance made you a great person to work with, and I know success will follow wherever you go. Danielle Kimmel, even though we only overlapped in the Wright lab for one year, I am extremely grateful that we did. You were always so supportive, both in and out of lab. I am proud of you moving up the ranks at Vandy, and I know that you will pave a career path where people will be proud of and impressed by your work. Anna Bitting, I'm so glad we worked together in the same lab, and I really appreciate your friendship. From your love of corgis, to "do you guys have shuffle board" to Wednesdays at Melrose and Nashville, you always put me in a good mood. GOOD LUCK finishing up, you will do amazing things and I'm so excited for you! Keersten Ricks. My dear, dear Keersten. I never would have guessed

that my first rotation buddy would become one of my best lab, Nashville, and life friends. Do you remember hugging after our rotation presentations?...that should have been a sign. I am so thankful that we got to weather all of the Wright lab experiences together; you were a very supportive rock, and I thank you. We've had some rough times over the past six years, and we were always there for each other. I honestly would not have survived without you, and I love you. Current lab members Christine Markwalter, Lauren Gibson, Alexis Wong, Andrew Kantor, Wes Bauer, Joseph Conrad, and Tom Scherr will make it difficult to leave.

I'd like to thank my committee members, Janet Macdonald, Scott Guelcher, and Chuck Lukehart. Janet was a tough critic, but her pushing me allowed me to grow and develop the skills to handle difficult questions and to get me to think more critically. Scott provided great insight and a different perspective as an 'outsider' from the department of chemical and biomolecular engineering. Chuck was always a very supportive presence, in my exams and even in my departmental presentation that he wasn't required to attend! Finally, I owe thanks to my PI, David Wright, for giving me the opportunity to learn and work in his lab.

TABLE OF CONTENTS

| | Page |
|---|------|
| DEDICATION | ii |
| ACKNOWLEDGEMENTS..... | iii |
| LIST OF TABLES | ix |
| LIST OF FIGURES..... | x |
| Chapter | |
| I INTRODUCTION | 1 |
| Biom mineralization | 1 |
| Inorganic Minerals in Nature..... | 2 |
| Biosilica in Demospongiae | 3 |
| Biosilica in Diatoms | 5 |
| Biomimics of Diatom Structure Directing Agents..... | 7 |
| Typical Metal Oxide Formation..... | 9 |
| Dissertation Scope | 10 |
| II PREPARATION OF A LIBRARY OF BIOMIMETIC DENDRIMERS TO FINE TUNE INORGANIC MATERIAL PRODUCTS AND MORPHOLOGIES | 12 |
| Introduction..... | 12 |
| Experimental Methods..... | 15 |
| Materials | 15 |
| Precipitation of Inorganic Material | 15 |
| Silica Quantification | 16 |
| Titania Quantification | 17 |
| Characterization..... | 17 |
| Results and Discussion | 18 |
| Silica Yield vs. Dendrimers..... | 18 |
| Silica Particle Sizes..... | 21 |
| Titania Yield vs. Dendrimers..... | 22 |
| Titania Particle Sizes | 25 |
| Conclusions | 26 |
| Future Work..... | 27 |

| | | |
|-----|---|----|
| III | BIOLOGICALLY INSPIRED SYNTHESIS OF INORGANIC OXIDE METAL MATERIALS UNDER AMBIENT CONDITIONS BY CATALYSIS OF PRECURSORS WITH PROTEASE ENZYMES..... | 29 |
| | Abstract..... | 29 |
| | Introduction..... | 30 |
| | Experimental Methods..... | 35 |
| | Materials | 35 |
| | Metal Oxide Precipitation..... | 35 |
| | Kinetics of Metal Oxide Precipitation | 36 |
| | Enzyme Denaturation & Inhibition | 36 |
| | Silica Quantification | 36 |
| | Titania Quantification | 37 |
| | Characterization..... | 37 |
| | Results and Discussion | 38 |
| | Protease mimic reactivity with TMOS | 38 |
| | Effect of active site inhibition and 3D structure on reactivity..... | 41 |
| | Protease mimic reactivity with TEOS..... | 44 |
| | Silica morphology differences between proteases | 46 |
| | Protease mimic reactivity with TiBALDH..... | 47 |
| | Conclusions | 50 |
| IV | NANOSPHERE LITHOGRAPHY FOR THE TEMPLATED FORMATION OF ENZYME-MEDIATED METAL OXIDES IN ZEPTOLITER CHAMBERS | 52 |
| | Introduction..... | 52 |
| | Experimental Methods..... | 54 |
| | Materials | 54 |
| | Templating Si Wafers..... | 55 |
| | Templated Metal Oxide Formation | 55 |
| | Characterization..... | 57 |
| | Results and Discussion | 57 |
| | Templating Surfaces..... | 57 |
| | Imaging Templated Surfaces..... | 60 |
| | Silica ‘Flowers’ on Substrates..... | 61 |
| | Conclusions | 63 |
| | Future Work..... | 64 |
| V | DEVELOPMENT OF A SCREENING ASSAY PLATFORM AS A NOVEL APPROACH TO MATERIAL FABRICATION AND DESIGN USING THE MODEL DIATOM <i>THALASSIOSIRA PSEUDONANA</i> | 66 |
| | Abstract..... | 66 |
| | Introduction..... | 67 |

| | |
|---|---------|
| Typical High Throughput Screening | 68 |
| Unique Aspects of HTS for Material Development | 68 |
| Diatom Screening Platform | 69 |
| Potential Applications | 70 |
| Chapter Aims | 71 |
| Experimental Methods | 72 |
| Materials | 72 |
| Culture Conditions | 73 |
| Silica Quantification | 73 |
| Flow Cytometry | 75 |
| Imaging | 76 |
| Plate Analysis and Processing | 76 |
| Results and Discussion | 77 |
| Culturing and Stock Growth | 77 |
| Translation to Microtiter Plate Format | 80 |
| DMSO resistance | 80 |
| PDMPO Fluorescent Probe for Silica Quantification and Imaging | 82 |
| Plate Processing by Cell Separation | 86 |
| Flow Cytometry as an Alternative to Washing | 95 |
| Limitations and Future Work | 98 |
| VI RESEARCH SYNOPSIS AND FINAL THOUGHTS | 101 |
| REFERENCES | 104 |
| CURRICULUM VITAE | 115 |

LIST OF TABLES

| | Page |
|--|------|
| 1. Specific Activities of PAMAM Dendrimers with TMOS | 19 |
| 2. Specific Activities of PAMAM Dendrimers with TiBALDH..... | 24 |

LIST OF FIGURES

| | Page |
|--|------|
| 1. (a) Calcium carbonate shell of coccolithophore <i>E. huxleyi</i> ¹ and (b) calcium carbonate coral in Hawaiiin coral reef ⁶ | 2 |
| 2. SEM images of <i>Suberites domuncula</i> (a) axial filament and (b) silica spicules ⁸ | 3 |
| 3. Fluorescent (PDMPO) stained <i>T. pseudonana</i> during cell division ⁹ | 7 |
| 4. Structure of Silaffin 1A ₁ from <i>C. fusiformis</i> ² | 8 |
| 5. Structure of poly (amido amine) dendrimer, generation 2 | 14 |
| 6. Structure of (a) tetramethyl orthosilicate and (b) titanium (IV) bis (ammonium lactato) dihydroxide | 16 |
| 7. Silica yield of PAMAM dendrimer reactions with TMOS | 18 |
| 8. SEM images of silica particles from PAMAM reactions with TMOS | 22 |
| 9. Titania yield of PAMAM dendrimer reactions with TiBALDH | 23 |
| 10. SEM images of titania particles from PAMAM reactions with TiBALDH | 25 |
| 11. Representative schematic of AFM dip-pen lithography with PAMAM dendrimers and metal oxide precursors | 28 |
| 12. Proposed <i>in vitro</i> mechanism for silicatein with TMOS ¹⁰ | 32 |
| 13. Active sites of (a) papain (b) trypsin and (c) modified cathepsin L as silicatein representative | 34 |
| 14. Silica precipitation from TMOS with enzyme (a) papain and (b) trypsin | 39 |
| 15. Infrared spectroscopy of silica from (a) papain and (b) trypsin reactions with TMOS | 40 |
| 16. Relative activities of papain versus inhibited papain (a) protease activity and (b) TMOS activity | 42 |

| | |
|--|----|
| 17. Relative trypsin activities native versus inhibited (a) protease activity and (b) TMOS activity | 44 |
| 18. Kinetics of particle formation in TMOS + enzyme reactions | 45 |
| 19. Kinetics and yields of particle formation in TEOS + enzyme reactions | 45 |
| 20. SEM images of silica from reactions with (a) papain with TMOS (b) trypsin with TMOS (c) papain with TEOS and (d) trypsin with TEOS | 47 |
| 21. Reactions of enzymes with TiBALDH (a) titania yield versus papain concentration (b) native versus inhibited papain activity with TiBALDH (c) titania yield versus trypsin concentration and (d) native versus inhibited trypsin activity with TiBALDH..... | 48 |
| 22. SEM images of titania particles from TiBALDH reactions with (a) papain and (b) trypsin..... | 49 |
| 23. Schematic of nanosphere lithography ⁷ | 53 |
| 24. Two-phase reaction between papain and TMOS | 56 |
| 25. Scheme of templating silicon wafers | 57 |
| 26. Ring patterns formed by silica beads on silicon wafer (a) SEM image of representative substrate (b) SEM image of substrate with beads (c) distance between rings | 58 |
| 27. AFM topography image of bead-formed rings | 59 |
| 28. AFM analysis of trichloro(octadecyl) silane template silicon surface (a) topography (b) zoom inset of topography (c) topography trace and (d) lateral force..... | 60 |
| 29. AFM analysis of trichloro(octadecyl) silane template silicon surface (a) topography and (b) topography trace | 61 |
| 30. AFM analysis of silica ‘flowers’ (a) topography (b) topography retrace (c) topography trace of (a), (d) topography trace of (b) and (e) zoomed inset topography..... | 62 |
| 31. SEM images of silica ‘flowers’ on silicon surface | 63 |
| 32. Workflow for the development of a typical high-throughput screen..... | 68 |

| | |
|---|----|
| 33. Schematic of the formation of a colorimetric Si-Mo structure under certain conditions | 73 |
| 34. Optimized Molybdenum Blue assay with calibration curve..... | 74 |
| 35. Experimental and Theoretical silica content of <i>T. pseudonana</i> cells across variations cell densities using Molybdenum Blue colorimetric assay | 75 |
| 36. Structure of Chlorophyll A..... | 78 |
| 37. Correlation between <i>in vivo</i> fluorescence and <i>T. pseudonana</i> cell densities (a) up to 20 million cells/mL and (b) below 5 million cells/mL..... | 78 |
| 38. <i>T. pseudonana</i> cell growth and death measured by IVF across various inoculation conditions in (a) 250 mL and (b) 125 mL Erlenmeyer flasks | 79 |
| 39. Edge effects of 96-well plate on day 2 of culture (a) all wells and (b) center 60 wells..... | 80 |
| 40. DMSO resistance of <i>T. psuedonana</i> culture..... | 81 |
| 41. Dose-response curves of <i>trans,trans</i> -2,4-decadienal in <i>T. pseudonana</i> after (a) 2 days and (b) 6 days of incubation | 82 |
| 42. Structure of PDMPO (LysoSensor Yellow/Blue DND-160)..... | 83 |
| 43. Excitation/Emission spectra of PDMPO under varying pH conditions in the (a) absence and (b) presence of polymerized silicic acid ⁵ | 83 |
| 44. (a) PDMPO emission spectra in the presence and absence of polymerized silicic acid and (b) ratio of 510:450 fluorescence of PDMPO as a function of silicic acid concentration | 84 |
| 45. Ratio of 510:450 PDMPO fluorescence after incubation with cells or media in the presence of absence of silicon | 85 |
| 46. Cell content in washing steps of 96-well plates measured by IVF after (a) 1 day and (b) 3 days of growth | 86 |
| 47. Cell content in washing steps of 96-well v-bottom plates measured by IVF..... | 87 |
| 48. Silicon content in samples before and after processing through 96-well filter plates | 88 |

| | |
|--|----|
| 49. (a-c) calibration curves processed through a 96-well filter plate compared to (d) calibration curve not filtered through plate and (e) silicon content of 40 ppm Si samples processed through a 96-well filter plate | 90 |
| 50. <i>T. pseudonana</i> cell growth in filter plates (blue) and flat bottom plates (black) of the (a) 96-well format and (b) 384-well format..... | 91 |
| 51. IVF of the supernatant of <i>T. pseudonana</i> culture incubated in the (a) absence and (b) presence of chitin magnetic beads | 92 |
| 52. IVF of the supernatant of <i>T. pseudonana</i> culture in microcentrifuge tubes incubated with a titration of poly(ethyleneimine) coated magnetite particles..... | 93 |
| 53. Percentage of <i>T. pseudonana</i> cells captured (black) and lost in a wash (blue) as a function of the number of PEI-magnetic beads present | 94 |
| 54. Percentage of <i>T. pseudonana</i> cells in the steps of cell processing by PEI-coated beads with elution methods of (a) high pH and (b) low pH conditions | 94 |
| 55. Cell density measurements by flow cytometry (black) and hemocytometer (blue) methods..... | 95 |
| 56. Flow cytometry analysis of <i>T. pseudonana</i> culture incubated with or without Si in the presence or absence of PDMPO showing (a) cell density and (b) percentage of PDMPO positive cells..... | 96 |
| 57. Percentage of PDMPO positive cells as a function of PDMPO concentration | 97 |
| 58. Variation in cell signal on flow shown by cell counts in control versus lysed cell samples..... | 98 |
| 59. Confocal microscopy image of <i>Navicula radiosa</i> cells stained with PDMPO | 99 |

CHAPTER I

INTRODUCTION

Biom mineralization

In Nature, many organisms deposit inorganic minerals *via* polymerization by organic material¹¹. This biom mineralization process occurs across all evolutionary levels, from single cells to animals¹², and is an inspiration for inorganic material formation *in vitro*. More than 50% of life's essential elements are deposited as biom minerals¹³. There are two different types of inorganic biom mineralization, biologically induced mineralization and biologically controlled mineralization. One impressive feature of biologically *controlled* mineralization is the exquisite control that these biological systems have over a number of size-scales¹⁴. In order to harness this control, many scientists study *in vitro* mimics of the organic facilitators in biological settings of mineralization. This dissertation will focus on the interplay between these organic mediators and the resulting inorganic features.

Biologically synthesized inorganic minerals can provide a variety of functions, including structural support and more specialized functionality, such as magnetic sensors. In magnetotactic bacteria, the formation of iron oxide nanoparticles is used as an internal compass to navigate and orient themselves using Earth's magnetic pull^{15, 16}. Many yeasts impressively mineralize CdS quantum dots in an effort to sequester toxic cadmium¹³. Biom mineralization is a great source of inspiration for the material scientist

due to the mild synthetic conditions, control, and functionality of inorganic materials produced in biological systems.

Inorganic Minerals in Biological Systems

There is a plethora of examples of inorganic material deposition in biology. Calcium carbonate is present in the shell of molluscs¹⁷, intricate outer plates of some phytoplankton known as coccolithophores¹⁸ (Figure 1a), and the skeletons of coral¹⁹ (Figure 1b). In humans, our bones are made up of an inorganic-organic hybrid of mostly calcium phosphate (hydroxyapatite) and collagen, which allows bones to

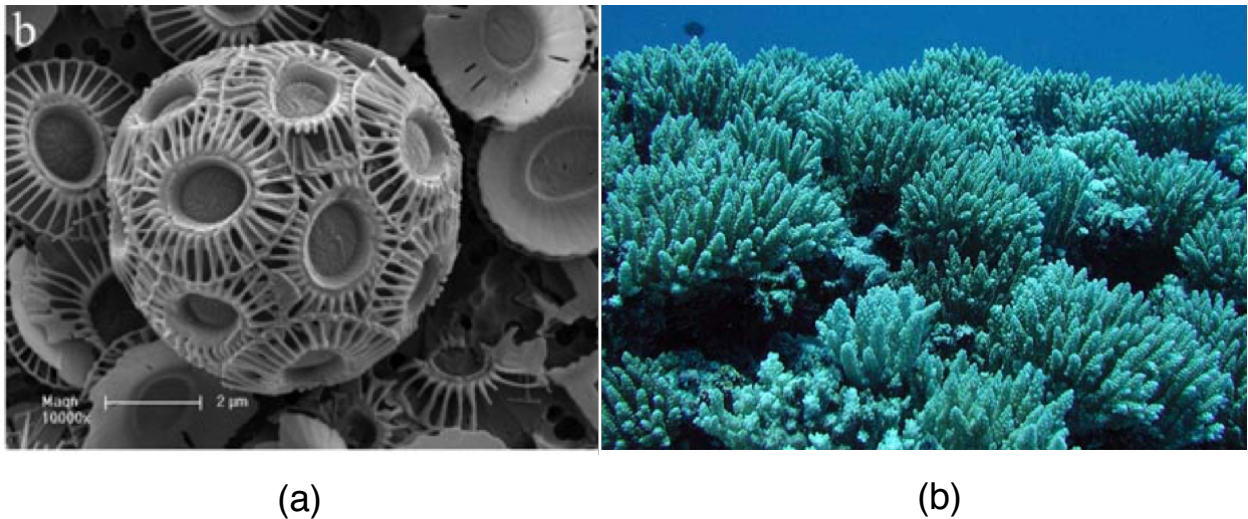


Figure 1. (a) Coccolithophore *E. huxleyi*¹ showing calcium carbonate shell, scale bar 2 μ m; (b) calcium carbonate *Acroporidae* in Hawaiian coral reef⁶

maintain the rigidity and strength of the inorganic material as well as the flexibility of organic material^{20, 21}. This dissertation focuses on the biomineralization of one mineral in particular, silica, and the process of biosilicification in two different organisms. The primary sources of biosilica are sponges, sea-dwelling animals with a siliceous exoskeleton, and diatoms, photosynthetic single-cell eukaryotes that mineralize a silica

cell wall. From these two systems, we can find inspiration to develop *in vitro* techniques to control silica formation and expand them to a variety of metal oxides. Current methods of silica processing are limited in the amount of control we have over scale and patterning. Silica biomineralization by both systems is species controlled and results in unique patterns ranging from the nano-scale to the micro-scale, and even to the macro scale, in sponges. This type of hierarchical control would be highly advantageous for material processing *in vitro*.

Biosilica in Demopongiae

In some classes of Porifera sea sponges, the structural exoskeleton is comprised of concentric circles of silica deposited around a center organic region (Figure 2a). Specialized cells, called sclerocytes, take up silicic acid from the environment through

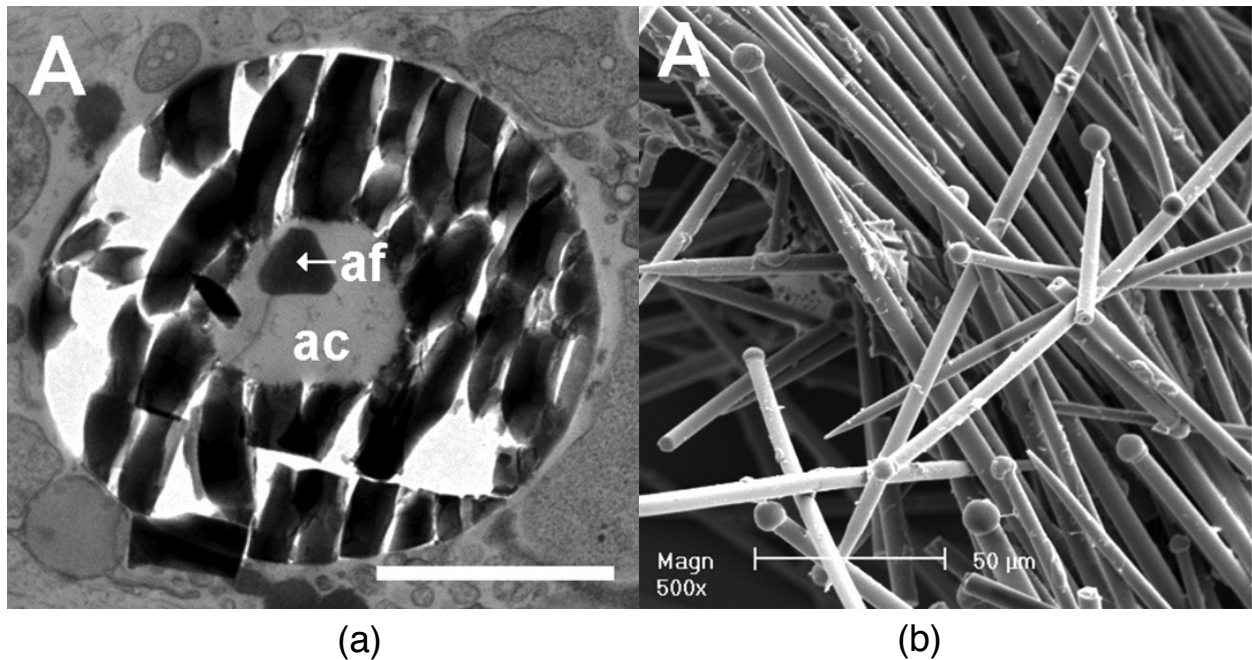


Figure 2. SEM images of *Suberites domuncula* (a) axial filament (af) inside the axial canal (ac) surrounded by silica spicules (b) silica spicules⁸

transporters⁸. This precursor is then polymerized by an organic material and subsequently deposited around this material, known as the axial filament, that becomes the center of the spicule (Figure 2b). This spicule precursor is then extruded from the cell into the extracellular space, where more layers (called lamellae) of silica are deposited concentrically. Much like typical sol-gel reactions, a stage of syneresis, or water expulsion, causes shrinking and hardening of the biosilica, allowing it to be rigid and strong as an exoskeletal structure. In the Demospongiae class, these layers then sinter together to form a single layer, called the mantel²².

The axial filament is able to guide the formation of silica by self-assembled enzymes, called silicateins, that polymerize and condense silicic acid into silica^{11, 23-26}. These proteins make up the majority of the axial filament, and are also located in the extracellular space to add silica to the growing spicule. The most abundant isomorph, an approximately 24 kDa protein called silicatein- α , is also capable of hydrolyzing silicon alkoxide precursors to form silica *in vitro*¹⁰, and as such represents an opportunity for biomimicry.

Sponges also exhibit an enzyme, silicase, which is overexpressed upon an increase in silicon concentration and breaks down amorphous and crystalline silica²⁷. As the counter-enzyme to silicatein, the two enzymes together result in the patterns of the siliceous spicules that are unique to each species. Similar in sequence to carbonic anhydrase II, it has a catalytic triad of three histidine residues coordinated to a zinc ion that hydrolyzes the polymeric silica chain, releasing silicic acid, $\text{Si}(\text{OH})_4$ ²⁸. The formation and control of silica processing in sponges is the only known catalytically

driven silicification in nature; studying this system will lead to potentially new ways of catalyzing mild material fabrication *in vitro*.

Biosilica in Diatoms

Diatoms, unicellular algae that essentially reside in a 'glass house', have developed an exquisite control over the formation of their unique cell wall – an organic-inorganic hybrid of amorphous silicon dioxide surrounded by an organic matrix. The silica portion of the cell wall, known as the frustule, is composed of two valves, the hypotheca and epitheca, which fit together like the halves of a petri dish. These halves are held together by silica girdle bands around the circumference. The patterning of the frustule differs in a species-dependent manner, but is highly conserved within a species, indicating a genetic control over the organization of this inorganic material. Silica deposition in these cells has been attributed to a number of organic molecules, including long chain polyamines (LCPAs), silacidins, cingulins, and highly post-translationally modified peptides known as silaffins. While these organic facilitators have been identified and shown to assemble as the template for silica formation²⁹, the mechanism by which diatoms organize the self-assembly to control the patterning of the frustule is still being fully elucidated.

In order to form the silica frustule, diatom cells need silicon from their environment. A soluble form of silica, silicic acid, is present at low concentrations, $\sim 70\mu\text{M}$ in seawater and as low as $10\mu\text{M}$ at the sea surface³⁰. Silicic acid is taken up by the cell through a number of silicon transporter proteins (SITs). These proteins are

~550 amino acids in length with 10 highly conserved α -helical units that span the cell wall membrane, and a more variable c-terminal coiled coil³¹. Silicic acid accumulates in intracellular pools at concentrations as high as 58mM to 340mM, substantially higher than the extracellular concentration, and varies in concentration during the cell cycle³². At this level, silicic acid is unstable in a dissolved state and will spontaneously condense to silica³³; however, in diatoms the silicic acid remains soluble and does not efflux out of the cell despite the large concentration gradient across the cell membrane. To prevent these occurrences, silicon is likely stored in a different form inside the cell. It has been suggested that monomeric silicic acid is likely stabilized in the cells by the interaction with organic material. Small amounts of lowly polymerized silicic acid may also be stabilized in cells by organic components in order to prevent cell membrane damage³². More recently it has been suggested that silicic acid is taken up by the model diatom, *T. pseudonana*, and is stored as pre-condensed silica³⁴. While the form of Si that is stored by diatoms may not be identified for all species, the location within the cell of Si polymerization into silica is well established. Frustule formation occurs in an acidic environment known as the silicon deposition vesicle (SDV). Inside the SDV, the organic mediators (LCPAs, silaffins, cingulins, silacidins) polymerize silica; the SDV membrane, the silicalemma, along with the cytoskeleton helps shape the solid silica. Once formed, the frustule is exocytosed along with the SDV; this organic material helps prevent silica dissolution in the diatom's environment^{35, 36}. During cell division, the mother cell expands and the daughter frustule halves begin being polymerized in the SDV, which expands as the frustule forms. In this way, each daughter cell has an epitheca of older

silica from the mother cell and a newly formed hypotheca for which girdle bands are also newly deposited. One can imagine, then, that as the cells divide, the average size of the diatoms decreases with time until a certain minimum size is reached; at this point, the species will continue to reproduce through a sexual reproduction cycle. Interestingly, there are a few examples of diatoms that maintain their size throughout divisions; *T. pseudonana* is one of these due to its flexibility at the girdle bands, where it

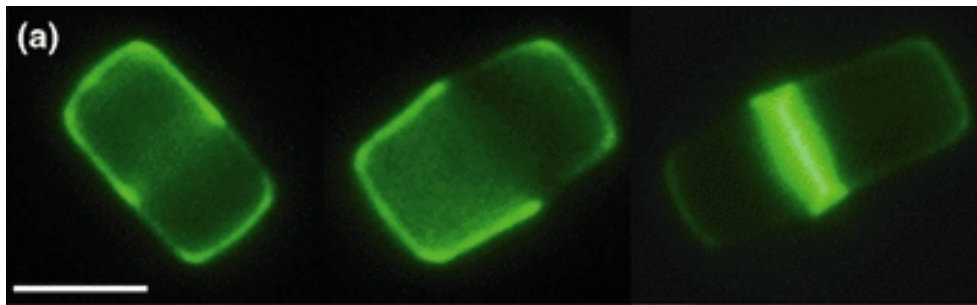


Figure 3. Fluorescent (PDMPO) stained *T. pseudonana* cell division, showing expansion at the girdle bands around the center; scale bar 4 μ m.⁹

expands during cell division to allow the daughter halves to maintain the same size as the mother cell⁹. The work in this dissertation will focus on this species, whose genome has been fully sequenced³⁷.

Biomimics of Diatom Structure Directing Agents

The organic material responsible for silica condensation and patterning in diatoms has previously been studied extensively. Silaffins have been used *in vitro* in the formation of silica nanoparticles; it was shown that each silaffin yields a different average particle size, and the combined silaffins, as seen in diatoms, yield small particles of about 50 nm³⁸. Control of the product from these silaffins *in vitro* has thus far been limited to the size of spherical particle. It is the organization of these small

particles that the diatom has mastered³⁹. Self-assembly is a key feature of silica precipitating organic materials in diatoms. Extracted silaffins without phosphorylated serine groups will not precipitate silica *in vitro*; however, upon addition of phosphate ions, silica will be formed due to the ability of the positively charged silaffins to self-assemble again through negative phosphate ions⁴⁰. Additionally, the long-chain polyamines of diatoms do not contain phosphate groups and must be used in the presence of phosphate ions *in vitro* to cause silica formation⁴¹. *In vivo*, LCPAs organize through silacidins, a group of highly phosphorylated polyanionic peptides that electrostatically interact with positively charged LCPAs²⁹.

Biomimics of these organic mediators have been proposed and studied for potential material synthesis use. One synthetic mimic of silaffin 1A₁ from the diatom *C. fusiformis* (Figure 4) is the R5 peptide, which successfully mediates both silica and

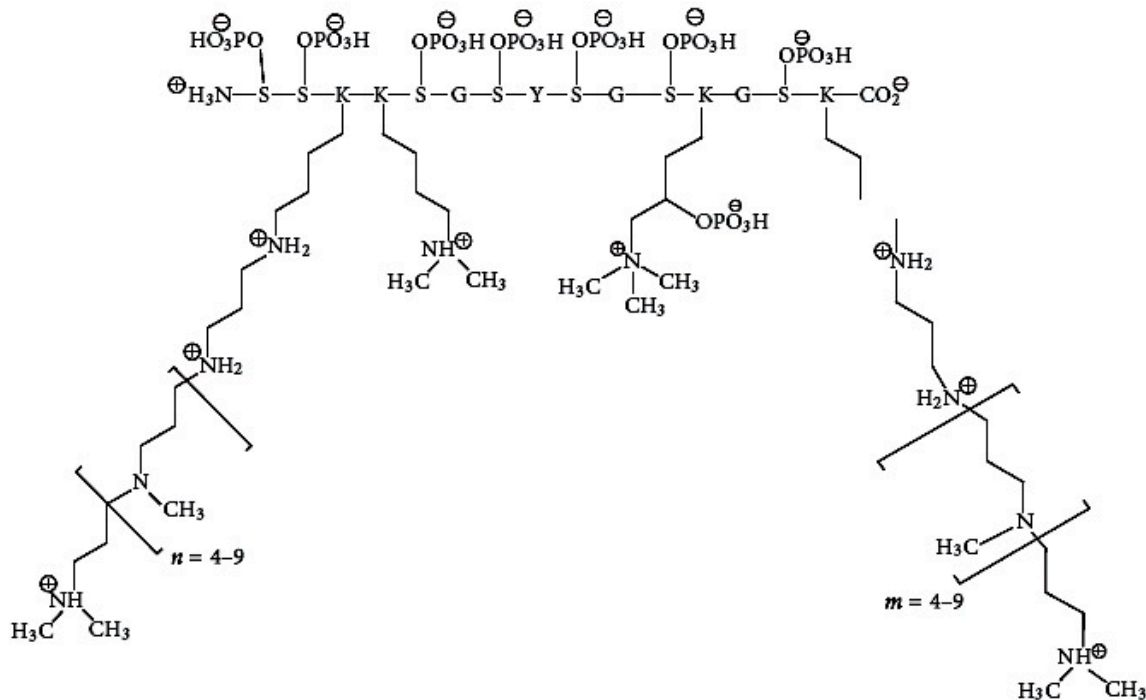


Figure 4. Silaffin 1A₁ structure from *C. fusiformis*, showing the characteristically high PTMs of silaffins: serine phosphorylation and lysine amination²⁻⁴

titania, and has also been used for drug encapsulation and delivery in the biomedical field^{2, 42, 43}. Poly (amido amine) (PAMAM) dendrimers have also been studied as a template for the precipitation of silicon dioxide, due to its many terminal amine groups, similar to the LCPAs and the post-translational modifications of silaffins. PAMAM dendrimers have been shown to precipitate silica, titania, and germania⁴⁴⁻⁴⁶. The investigation of these mimics has shown that these biomimetic templates are advantageous for their low-cost and mild reaction conditions, and could be utilized for lithographic patterning via ink-jet printing⁴⁷, microcontact printing⁴⁸, and dip-pen lithography⁴⁹.

Typical Metal Oxide Formation

Metal oxide glasses and ceramics can be prepared and patterned using a variety of different techniques. One way of preparing glass materials is by extreme heat, raising the temperature above the glass transition temperature, often upwards of 800°C followed by shaping and cooling⁵⁰⁻⁵². One alternative to such an energy-intensive method is the sol-gel process. Sol-gel chemistry consists of a solution phase (sol) of colloidal monomers that develops into a network phase of inorganic polymers (gel). The transition to the gel phase is typically promoted by the addition of a strong acid or base. In the sol-gel preparation, the hydrolyzed metal oxide precursor monomers in a sol condense to form the gel, after which the polymer network condenses further, shrinking and expelling water (syneresis). The gel can then be treated or dried in a number of ways to produce different solids, including a xerogel, aerogel, or solid particles⁵³⁻⁵⁵.

Both of these methods, as well as other techniques commonly used in materials sciences such as chemical vapor deposition, photolithography, and laser ablation, are harsh and have a number of drawbacks, ranging from cost to amount of waste produced, or energy required, and a limit to control of the shape. In hard material fabrication, three-dimensional, non-orthogonal shapes and patterns on the nano-scale or smaller are difficult to obtain. For all of these reasons, the ambient conditions found in biology are appealing!

Biomimetic approaches are a fascinating avenue for *in vitro* inorganic material synthesis in their potential to bring about control and patterning on the same scale as biological systems. The exact mechanism of their control is still in need of exploration, and using mimics is a way to both investigate the biomineralization process and develop practical *in vitro* procedures to expand our control over metal oxide formation under mild conditions at ambient temperature, pressure, and neutral pH.

Dissertation Scope

This work focuses on biomimics of the two examples of biosilification presented in this Introduction. Work in Chapter II aims to develop a library of a dendrimer-based biomimics of diatom structure-directing organic material to make a variety of *in vitro* silica and titania morphologies. In Chapter III, two readily available proteases, trypsin and papain, are investigated as potential biomimics of the silicatein enzyme. Chapter IV discusses a bottom up approach to metal oxide patterning without the use of harsh chemicals typically used in lithography. The templating and metal oxide formation are

characterized using nano-imaging techniques. Chapter V focuses on the biosilicification process in diatoms, presenting work on developing a screening assay of *T. pseudonana*. The purpose of the assay is to determine molecules that probe the silicon metabolic cycle that may result in morphological changes to the silica frustule. Finally, in Chapter VI, conclusions and future directions of this field are discussed, both in terms of specific work discussed in this dissertation as well as in broader applications.

CHAPTER II

PREPARATION OF A LIBRARY OF BIOMIMETIC DENDRIMERS TO FINE TUNE INORGANIC MATERIAL PRODUCTS AND MORPHOLOGIES

Introduction

Dendrimers are large organic polymers characterized by a core group surrounded by concentric layers, where each of these layers is called a generation.⁵⁶ The number of terminal, reactive groups increases with the size of dendrimer and number of generations. Dendrimer synthesis allows for monodisperse, typically symmetrical structures that can be easily functionalized⁵⁷. This has led to their use in a variety of applications, including drug and gene delivery, imaging, biosensing, and inorganic materials synthesis⁵⁸⁻⁶². Branched polymers, including dendrimers, have been studied as facilitators in sol-gel reactions^{63, 64}, which leads them to being good candidates for biomimics for the synthesis of inorganic materials, typically formed *via* sol-gel methods.

Sol-gel chemistry is a well-studied field. The two reaction steps in the sol-gel formation of metal oxides are hydrolysis and condensation. Depending on the reaction conditions, both the mechanism of action and the rate-determining step differs. At pH conditions above the isoelectric point, ~2 to 3 for silica and ~5 to 6 for titania, the growing particles carry an overall negative charge; the hydrolysis reaction is limited, but condensation occurs quickly.⁶⁵ As the particles grow, the negative surface charges

cause inter-particle repulsion, and the resulting particles are larger than those ripening under conditions where this charge is minimized or neutralized. The hydrolyzed substrate immediately condenses onto growing particles due to the fast rate of condensation. The constant source of monomers allows for growth. This type of growth, known as reaction-limited monomer cluster growth, results in distinct particles that will agglomerate slightly or heavily depending on the presence and concentration of counter-ions to neutralize charge on the growing particles. Alternatively, acidic conditions tend to lead to a process known as reaction-limited cluster aggregation. In this case, the relatively high rate of hydrolysis over condensation creates an excess of monomeric silicic acid. As the silicon alkoxide precursor is hydrolyzed, it becomes less likely to be further hydrolyzed due to the mechanism of reaction, and thus, condensation between small oligomers at the outer silicon atoms occurs more readily than condensation at central silicon atoms. This leads to an aggregated three-dimensional network of silica⁵². While the systems studied in this Chapter and in Chapter III are slightly different because they are catalyzed by an organic mediator as opposed to an acid or base, the features of typical sol-gel chemistry help explain differences in the reactions described within these chapters.

Previously in the Wright lab, it has been shown that the dendrimer poly (amido amine), PAMAM, can act as a template for the condensation of silica from silicic acid⁴⁵. Increased localized concentrations of silicic acid at the positively charged, amine-terminated PAMAM dendrimer surface (Figure 5) results in condensation of silicic acid into silica. This process ultimately entraps the organic dendrimer facilitator in the

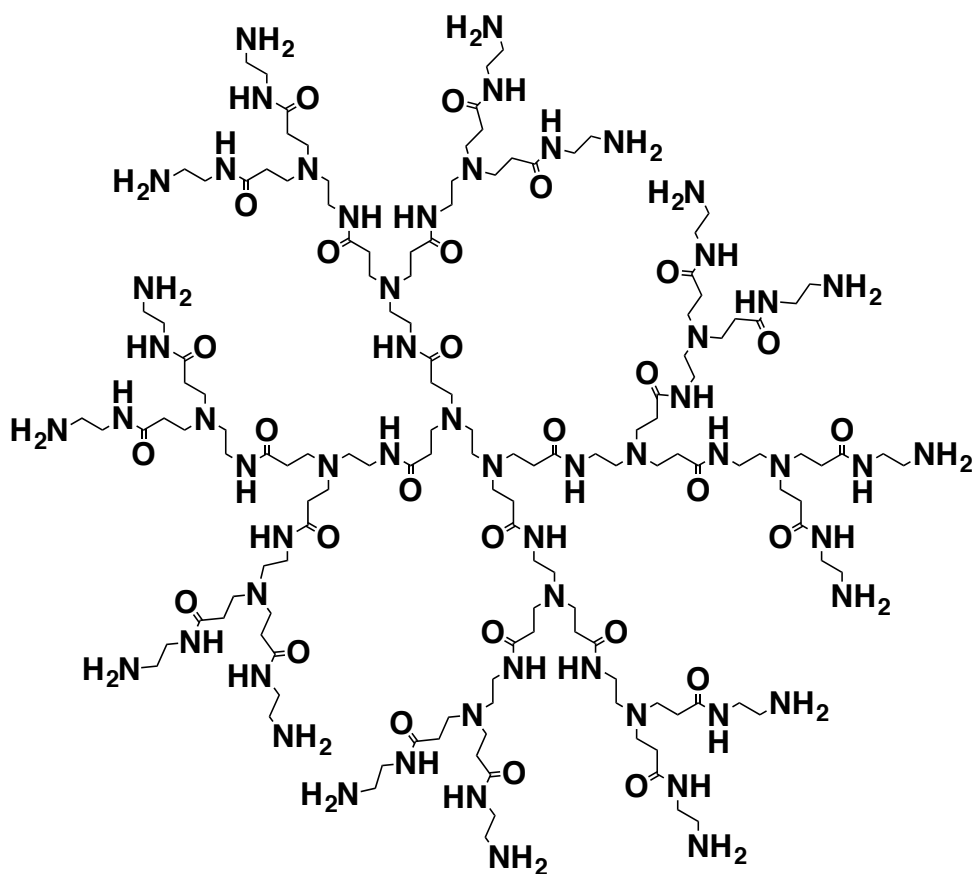


Figure 5. Generation 2 (G2) of poly (amido amine) dendrimer with 16 terminal amine groups; at reaction conditions, pH 7.5, amine groups are protonated and positively charged

growing silica particles, as is seen in biogenic silica, such as the silaffins, pleuralins, and frustulins all found in the frustule of diatoms³. It has been shown that amine groups, like those found in marine sponges and diatoms, are capable of hydrolyzing siloxane bonds for silica precipitation.^{66, 67} Therefore, we want to investigate the ability of PAMAM-based dendrimers to both hydrolyze and condense precursors into different metal oxides. Because dendrimer templates can be simply modified and functionalized with a variety of terminating groups, we can develop a library of similar dendritic platforms with different active groups, i.e. structures with an identical base but unique surface chemistry. We hypothesize that this library will yield a variety of metal oxides with

distinct morphologies. In this way, we propose tailoring dendrimers to provide material with a certain size, shape, and morphology, depending on the desired application. In this Chapter, we investigate a number of differently terminated PAMAM dendrimers and determine their ability to form metal oxides under mild, ambient conditions, as well as characterize the resulting inorganic material.

Experimental Methods

Materials

Solutions of PAMAM dendrimers were obtained from Dendritech, Inc. in a variety of terminating groups: $-\text{NH}_3^+$, $-\text{OH}$, $-\text{COO}^-$, and $-\text{NH}_3^+/\text{OH}$ (50:50, randomly distributed). Sodium phosphate monobasic and dibasic, sodium hydroxide, methanol, tetramethyl orthosilicate (TMOS), and titanium (IV) bis(ammonium lactate) dihydroxide (TiBALDH) were purchased from Sigma. Nitric acid, Si standard (1001 ppm) and Ti standard (998 ppm) were obtained from Fluka, and ammonium (IV) molybdate tetrahydrate was obtained from Acros Organics. Sulfuric acid and ammonium hydroxide were purchased from Fisher Scientific, and Amicon Centrifugal 3KDa MWCO Filters were purchased from Millipore. Silicon-based experiments were performed in plastic (polypropylene) tubes – glassware would result in high silicon background signal.

Precipitation of Inorganic Material

Stock solutions of dendrimer were prepared in 100 mM phosphate buffer (PB) at pH 7.5; substrate stock solutions (1M) of TMOS (Figure 6a) in methanol and TiBALDH

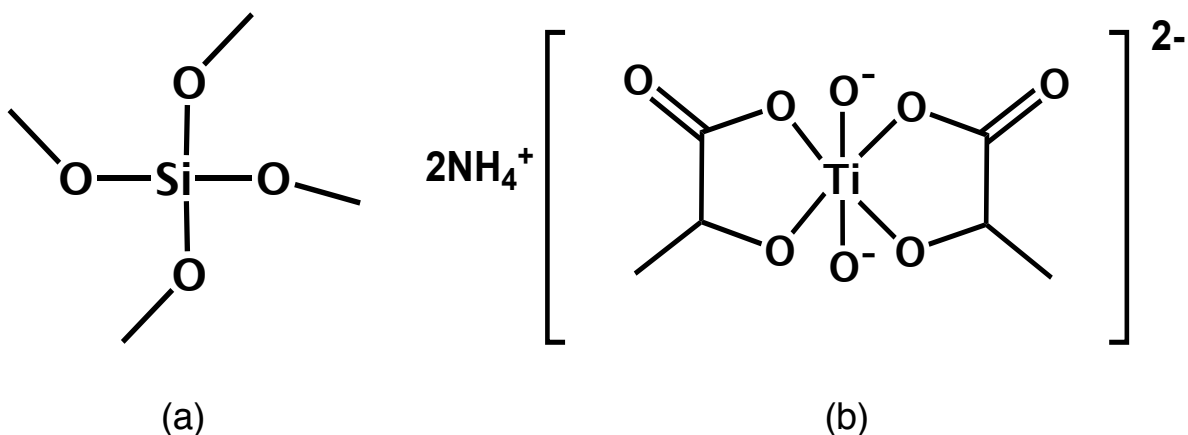


Figure 6. Structures of the metal oxide precursors used; (a) tetramethyl orthosilicate (TMOS) and (b) titanium (IV) bis(ammonium lactato)dihydroxide (TiBALDH)

(Figure 6b) in water were prepared. In triplicate, 200 μL of dendrimer at the desired concentration was reacted with 20 μL of substrate stock solution for 10 minutes while shaking. The reactions were centrifuged at 14000xg, the supernatant was removed, and the precipitates were washed twice with water to remove unreacted starting material.

Silica Quantification

The silica content was quantified by a modified version of the β -silicomolybdate colorimetric assay⁶⁸. Solid samples were dissolved in 500 mM NaOH until full dissolution, which freed encapsulated dendrimers. The dendrimers interfere with the colorimetric assay and were removed using centrifugal filters, with a molecular weight cut-off of 3000 Da; components less than 3000 Da will flow through the filters during centrifugation, and anything above 3000 Da will remain in the filter. 25 μL of each dendrimer-free solution was sampled and added to 100 μL of molybdate reagent (3:1 0.2218M H₂SO₄ to 5% Mo(NH₄)₆•4H₂O in 2.35% NH₄OH); the absorbance of the

resulting yellow solution was measured using a BioTek Synergy H4 Hybrid Reader at 410 nm and quantitated using a calibration curve of silicon standards, ranging from 285 μM – 4.3 mM.

Titania Quantification

The amount of titania precipitated from these reactions was quantified on an Optima 7000 ICP-OES with a Scott spray chamber. Samples were dissolved in 1 mL of 4 M H_2SO_4 and heated to 95°C to ensure dissolution (approximately 1 hour). Samples were prepared for inductively coupled plasma optical emission spectroscopy (ICP-OES) analysis using a 2% HNO_3 matrix. The intensity at 334.94 nm was measured and converted to titanium content using a calibration curve of titanium standards, ranging from 10 ppb to 5 ppm.

Characterization

Kinetic measurements were monitored by the light scattering of particle formation *via* absorbance at 480nm on a BioTek Synergy H4 Hybrid Reader. Scanning electron microscopy (Hitachi S4200) and transmission electron microscopy (CM20 Phillips, operating 200kV) were used to observe morphology, connectivity, and size of particles.

Results and Discussion

Silica Yield vs. Dendrimers

Four differently terminated dendrimers, $-\text{OH}$, $-\text{OH}/\text{NH}_3^+$, $-\text{NH}_3^+$, and $-\text{COO}^-$, were reacted with tetramethyl orthosilicate (TMOS) for 10 minutes. As hypothesized, dendrimers with different terminal groups had different specific activities (Table 1) and different concentration dependent relationships with silica product (Figure 7). PAMAM-

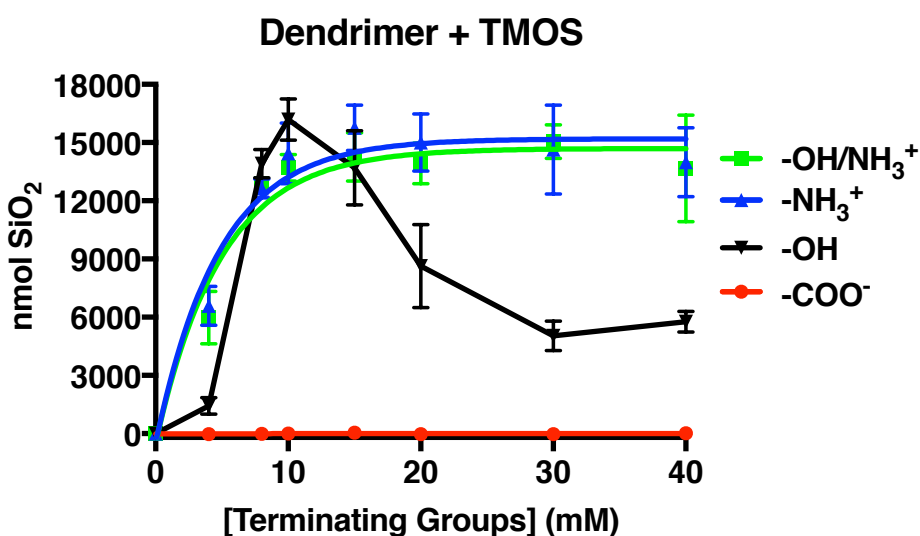


Figure 7. Silica yield vs. concentrations of PAMAM dendrimers after 10 minute reaction with TMOS

NH_3^+ and PAMAM- NH_3^+/OH had similar specific activities and silica precipitation profiles when mediating the formation of SiO_2 from TMOS substrate. This was expected, as it is known that amines facilitate silica formation in sol-gel methods^{67, 69}. As the concentration of the terminating groups increases from 0 to $\sim 10\text{mM}$, precipitated silica product from TMOS increases linearly, and the specific activities did not change. Above concentrations of 10mM terminal groups ($-\text{OH}/\text{NH}_3^+$ and $-\text{NH}_3^+$), increases in dendrimer do not precipitate more silica, despite $\sim 25\%$ of TMOS substrate remaining, and specific

activities begin to fall off due to the increase in dendrimer concentration (denominator) without an increase in the silica product (numerator). This saturation is because, as has been seen with previous organic-mediated sol-gel chemistry^{44-46, 70}, the organic template becomes encapsulated within the growing silica. Addition of TMOS substrate to the reaction does not yield further precipitation. Self-assembly of the organic

| Dendrimer | [Terminal Group] (mM) | Dendrimer (nmol) | SiO ₂ (nmol) | Specific Activity (nmol SiO ₂ /nmol dend * min) | Error (S.D.) |
|--|-----------------------|------------------|-------------------------|--|--------------|
| PAMAM-NH ₃ ⁺ | 4 | 12.5 | 6594 | 52.75 | 8.0 |
| | 8 | 25 | 12645 | 50.58 | 1.9 |
| | 10 | 31.25 | 14445 | 46.22 | 5.0 |
| | 15 | 46.875 | 15768 | 33.64 | 2.5 |
| | 20 | 62.5 | 15000 | 24.00 | 2.3 |
| | 30 | 93.75 | 14645 | 15.62 | 2.5 |
| | 40 | 125 | 13995 | 11.20 | 1.4 |
| PAMAM-NH ₃ ⁺ /OH | 4 | 12.5 | 5986 | 47.89 | 10.8 |
| | 8 | 25 | 12891 | 51.57 | 1.2 |
| | 10 | 31.25 | 13700 | 43.84 | 2.2 |
| | 15 | 46.875 | 14268 | 30.44 | 2.7 |
| | 20 | 62.5 | 13934 | 22.29 | 1.7 |
| | 30 | 93.75 | 15045 | 16.05 | 0.9 |
| | 40 | 125 | 13662 | 10.93 | 2.2 |
| PAMAM-OH | 4 | 12.5 | 1432 | 11.45 | 3.3 |
| | 8 | 25 | 13916 | 55.67 | 2.9 |
| | 10 | 31.25 | 16190 | 51.81 | 3.4 |
| | 15 | 46.875 | 13705 | 29.24 | 4.1 |
| | 20 | 62.5 | 8638 | 13.82 | 3.4 |
| | 30 | 93.75 | 5042 | 5.38 | 0.8 |
| | 40 | 125 | 5762 | 4.61 | 0.4 |

Table 1. Compilation of specific activities from different reactions of PAMAM dendrimers with TMOS substrate. Specific activities (nmol silica product per nmol dendrimer substrate and time in minutes) are reported for each concentration of dendrimer (reported as concentration of terminating group); S.D. = standard deviation

template is an important part of the biomineralization of silica in both diatoms and sponges^{26, 40, 43, 71, 72}. In fact, when silaffins are extracted from diatom frustules, they lose post-translational modifications that prevents them from self-assembling, and silica formation does not occur *in vitro*. However, when phosphates are added back to the solution, silica precipitation returns. The reactions studied here are run in phosphate buffer, which allows the positively charged amine-terminated dendrimers to assemble through the negatively charged phosphate ions. The positively charged dendrimers can also shield the negative charge of the growing silica particles.

The precipitation profile of PAMAM-OH with TMOS differs from the $-NH_3^+$ and $-NH_3^+/OH$ profiles. From 0 to ~ 15 mM terminal $-OH$, silica precipitation increases, as is described above for the amine-terminated templates. Unlike with $-NH_3^+$ and $-NH_3^+/OH$, however, silica precipitation does not stabilize at a maximum, but falls off after 15 mM $-OH$. This is likely due to the electrostatic repulsion between the negative surface of the dendrimers and the growing silica network. The dendrimer surface is not positively charged and does not shield the negative charge at the surface of the growing silica particles. Therefore, at higher concentrations of dendrimer with more partially negative charges in solution, less silica will form as fewer monomers will add to the polymerizing silica. After separation of the solid silica product from the supernatant reaction, addition of substrate to the supernatant results in further silica precipitation. This indicates that not all of the PAMAM-OH dendrimer is encapsulated in the solid silica, further supporting the effect electrostatics has on the reaction. The electrostatics may also be affecting kinetics; if allowed to react for longer than 10 minutes, high concentrations of

dendrimer (corresponding to 30 and 40 mM on the graph in Figure 7) will eventually yield more silica.

The PAMAM-COO- dendrimer does not react with TMOS to form silica. This can be explained by electrostatics, similar to those described above. The carboxylate-terminated dendrimer has a far more negative surface than the hydroxyl-terminated dendrimer. The carboxyl group is negatively charged at pH 7.5, and thus does not allow the formation of silica to occur. The dendrimers are not able to self-assemble through electrostatics, and there is too much negative charge to allow silica particles to grow.

Silica Particle Sizes

The four dendrimers yielded differently sized particles (or no particles), however all particles had relatively monodisperse, spherical morphologies (Figure 8). The size difference can be explained by electrostatics; the more negatively charged dendrimers are less able to shield the growing silica particles, which also share a negatively charged surface. Interestingly, this is the opposite as seen in typical sol-gel chemistry. In typical sol-gel chemistry, the more positive counter ions there are in solution, the smaller the particles will be, because they will not repel each other as significantly. However, in the reactions with the dendrimers, the dendrimers are not simple counter ions in the solution. They are the template for the reaction, the source of the hydrolyzed monomer, and the location of particle growth. Therefore, as the negative charge of the surface grows, less monomer (also negatively charged) accumulation and product growth will occur. Additionally, the more positively charged the dendrimer, the more

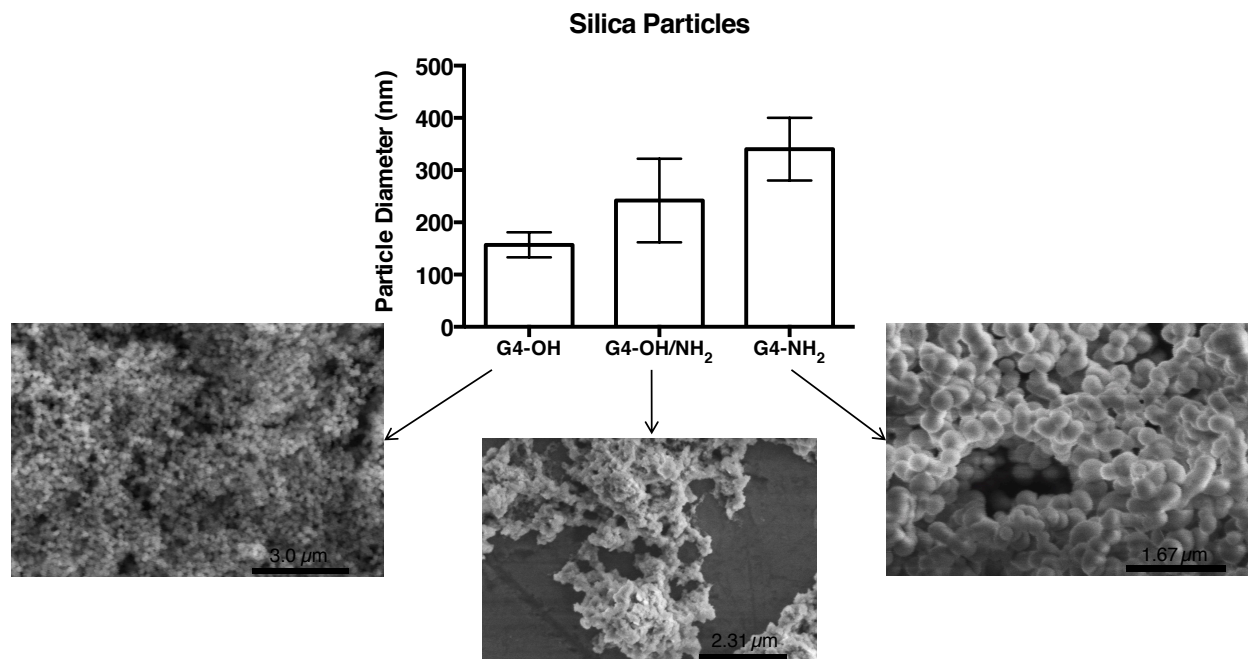


Figure 8. Silica particle sizes and images. Images taken by scanning electron microscopy. Size measurements taken on ImageJ software. Bar graph represents mean of n samples, listed here, and error bar represents standard deviation. G4-OH: n=33; G4-OH/NH₂: n=19; G4-NH₂: n=55

self-assembly can occur through the negative phosphate ions of the buffer system, thus creating a larger local reaction volume.

Titania Yield vs. Dendrimers

Like with TMOS, PAMAM-NH₃⁺, PAMAM-NH₃⁺/OH, and PAMAM-OH are reactive with TiBALDH to form titania; PAMAM-COO⁻, which was not reactive with TMOS, is reactive with TiBALDH (Figure 9). TiBALDH is a more reactive substrate because it is more susceptible to nucleophilic attack by water.⁵⁴ Titanium is less electronegative than silicon, and the presence of 6 oxygen containing ligands pulling electron density away from the metal atom, despite adding steric bulk (Figure 6), allows for the precursor to be easily hydrolyzed⁵⁴. The PAMAM-NH₃⁺ and PAMAM-OH/NH₃⁺ have similar

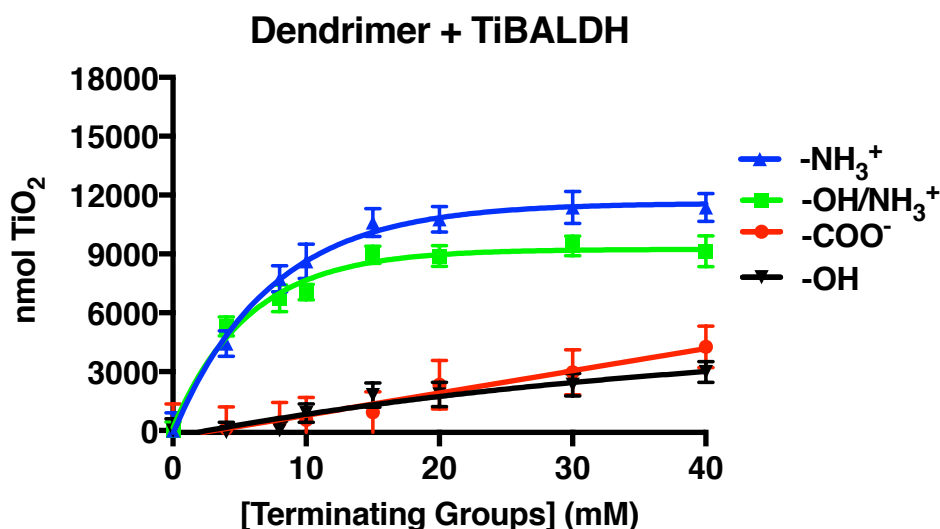


Figure 9. Titania yield vs. concentrations of PAMAM dendrimers after 10 minute reaction with TiBALDH

concentration dependence with TiBALDH as with TMOS, although they produce less precipitate; the specific activities of the -NH_3^+ and $\text{-NH}_3^+/\text{OH}$ dendrimers are less than with TMOS, approximately by half (Table 2). One potential explanation for this decrease, despite being a more reactive substrate, is due to the speed with which these reactions take place. The formation of titania from TiBALDH is much quicker than the formation of silica from TMOS. Because these reactions occur more quickly since, the dendrimer is more quickly encapsulated in the metal oxide network. The organic template that mediates the metal oxide formation is quickly not available in solution and cannot continue facilitating the reaction to titania. Thus, less TiBALDH substrate gets turned over into titania product. The reactions with TiBALDH are over more quickly than TMOS, but both reactions are carried out for 10 minutes. Because the reaction time is taken into account for specific activity and there is less titania yield, the TiBALDH reactions have overall lower specific activities (Table 2).

| Dendrimer | [Terminal Group] (mM) | Dendrimer (nmol) | TiO ₂ (nmol) | Specific Activity (nmol TiO ₂ /nmol dend * min) | Error (S.D.) |
|---------------------------|-----------------------|------------------|-------------------------|--|--------------|
| PAMAM-NH ₂ | 4 | 12.5 | 4437 | 35.50 | 5.3 |
| | 8 | 25 | 7732 | 30.93 | 2.7 |
| | 10 | 31.25 | 8628 | 27.61 | 2.8 |
| | 15 | 46.875 | 10597 | 22.61 | 1.5 |
| | 20 | 62.5 | 10774 | 17.24 | 1.0 |
| | 30 | 93.75 | 11367 | 12.13 | 0.9 |
| | 40 | 125 | 11364 | 9.09 | 0.6 |
| PAMAM-NH ₂ /OH | 4 | 12.5 | 5313 | 42.51 | 3.9 |
| | 8 | 25 | 6742 | 26.97 | 2.7 |
| | 10 | 31.25 | 7051 | 22.56 | 1.3 |
| | 15 | 46.875 | 8952 | 19.10 | 0.9 |
| | 20 | 62.5 | 8895 | 14.23 | 0.9 |
| | 30 | 93.75 | 9406 | 10.03 | 0.5 |
| | 40 | 125 | 9136 | 7.31 | 0.6 |
| PAMAM-OH | 4 | 12.5 | <LOD | | |
| | 8 | 25 | 12 | 0.05 | 1.9 |
| | 10 | 31.25 | 883 | 2.83 | 1.5 |
| | 15 | 46.875 | 1803 | 3.85 | 1.3 |
| | 20 | 62.5 | 1842 | 2.95 | 1.0 |
| | 30 | 93.75 | 2333 | 2.49 | 0.6 |
| | 40 | 125 | 2983 | 2.39 | 0.4 |
| PAMAM-COO- | 4 | 12.5 | 101 | 0.81 | 9.0 |
| | 8 | 25 | 417 | 1.67 | 4.1 |
| | 10 | 31.25 | 534 | 1.71 | 3.7 |
| | 15 | 46.875 | 935 | 2.00 | 2.3 |
| | 20 | 62.5 | 2334 | 3.73 | 2.0 |
| | 30 | 93.75 | 2969 | 3.17 | 1.2 |
| | 40 | 125 | 4265 | 3.41 | 0.9 |

Table 2. Compilation of specific activities from different reactions of PAMAM dendrimers with TiBALDH substrate. Specific activities (nmol titania product per nmol dendrimer substrate and time in minutes) are reported for each concentration of dendrimer (reported as concentration of terminating group); S.D.= standard deviation

Titania Particle Sizes

Titania particle sizes are overall larger than silica (Figure 10). We hypothesize that this is due to the higher isoelectric point of titania when compared to silica. The growing titania is less negatively charged than the silica surface. While in typical sol-gel chemistry, the negative surface charge causes inter-particle repulsion and allows for larger particles, we propose that this causes the exact opposite in our system. Because the particles are forced to nucleate and ripen at the dendrimer surface, the titania particles, which are less repelled than one another, can aggregate together, forming overall larger particles.

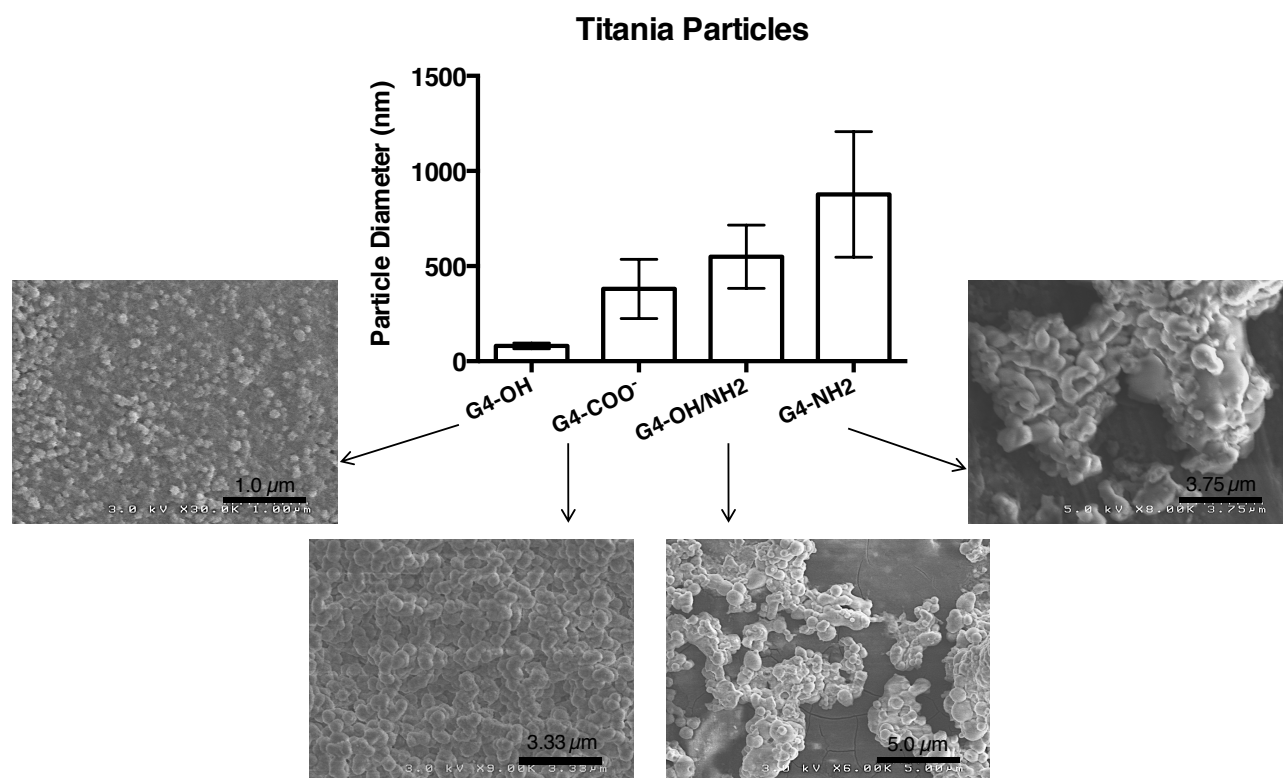


Figure 10. Titania particles, imaged using a scanning electron microscope. Sizes were taken using ImageJ software. Bars represent multiple measurements, as described here, and error bars represent standard deviation. G4-OH: n=24; G4-COO⁻: n=47; G4-OH/NH₂: n=49; G4-NH₂: n=16

Titania particles follow the same size trend as silica particles produced from the same dendrimers, with PAMAM-OH producing smaller particles than $-OH/NH_3^+$, and those smaller than $-NH_3^+$. The anomaly in this case is PAMAM-COO⁻. Despite it being more negatively charged than PAMAM-OH, it actually produces larger particles. The electrostatics described so far have dealt with partial negative charges, discussing the balance between the dendrimers acting as a template for the silica, the dendrimers ability to self-assemble, and the ability of the dendrimers to shield the growing particles. However, the carboxy-terminated dendrimer is significantly negatively charged compared with the others. This may allow the reaction to proceed under more typical sol-gel conditions. We hypothesize that the dendrimers fully repel each other, resulting in no self-assembly. There is also the least amount of even partial positive charge in the solution. Therefore, whenever monomers are able to be hydrolyzed, they condense and titania particles ripen as in typical sol-gel reactions, repelling one another, until the dendrimer is encapsulated in the reaction. Not many monomers are even hydrolyzed, as the carboxy-terminated dendrimer is not very reactive, with a specific activity an order of magnitude less than amine-terminated dendrimer.

Conclusions

We have tested a number of differently terminated PAMAM dendrimers and found that they produce different morphological products. PAMAM-OH, PAMAM-NH₂, and PAMAM-NH₂/OH dendrimers all react with TMOS to form silica. The size of silica

particles increases with increasing positive charge of the dendrimer: PAMAM-OH forms the smallest, and PAMAM-NH₂ forms the largest particles.

The dendrimers above, as well as PAMAM-COO⁻, react with TiBALDH to form titania. Overall, the titania particles are larger than silica particles. They follow the same size trend as silica, but PAMAM-COO⁻ is a bit larger than PAMAM-OH mediated particles, rather than a bit smaller, despite the increase in negative charge.

In general, these reactions are dictated heavily by electrostatics, where the dendrimer acts as both a counter ion and as a template. The balance between these two roles leads to a number of differently sized products. While the final metal oxides may vary in size and degree of interconnectivity, each reaction yields spherical particles that are highly fused.

Future Work

These dendrimers could be studied in combinations with one another, as was previously done with silaffins *in vitro*; this could result in even more potential sizes, due to added complexity to the electrostatic relationships in the solution.³⁸ Self-assembly could occur without the need for added phosphate buffer. Additionally, electronic shielding at the metal oxide surface could be affected. Expanding this work to other metal oxides may reveal more insight into the electrostatic interactions at play, and help fill in understanding where there is still confusion, such as the PAMAM-COO⁻ size and specific activity with TiBALDH.

In order to form different shapes and patterns, printing techniques could be used. Dip-pen lithography with these dendrimers could be used to pattern dots and lines at the nano-scale. The dendrimer itself could first be patterned with an AFM tip, and then the surface could then be incubated with the metal oxide precursor. Or, using a technique previously published by de La Rica et al⁷³, the dendrimer could be added to a substrate and incubated with the metal oxide precursor. Then, the AFM tip could be dipped in the

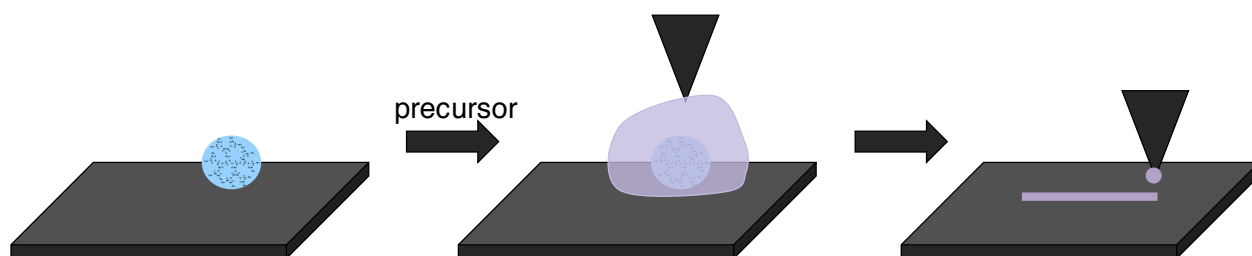


Figure 11. Depiction of AFM dip pen lithography; on a solid substrate, the solution precursor is deposited and left to react; the AFM tip can then be dipped into the solid suspension and subsequently 'drawn' across the substrate surface

'ink' of metal oxide particles and then printed in the desired way (Figure 11). This allows for 2-dimensional control with line widths of less than 100nm. Secondly, the heat and friction expels water from the metal oxide products, leading to crystalline patterns from amorphous metal oxide inks.

CHAPTER III

INVESTIGATIONS OF ENZYME BIOMIMICS FOR *IN VITRO* INORGANIC OXIDE MATERIAL FORMATION UNDER AMBIENT CONDITIONS

The work presented in this chapter investigates the enzymes papain and trypsin as potential biomimics of silicatein to precipitate silica from TMOS *in vitro* and identifies mechanistic similarities between silicatein and trypsin, yet not papain. The importance of fully investigating biomimics *in vitro* is made clear by the discrepancies between papain and trypsin, enzymes with similar native mechanisms, when used with non-native substrates; each enzyme represents a biological system (of biosilica) and can be used *in vitro* to form morphologically different silica under ambient, environmentally conscious conditions.

Abstract

In some classes of the phylum Porifera, sea sponges have an extracellular structure consisting of needle shaped siliceous spicules organized in unique patterns. Enzymes for both the formation and degradation of silica control its organization and patterning, which is the only known enzymatic process of biosilicification. Silicatein, the enzyme that catalyzes the condensation of orthosilicic acid into silica for the formation of spicules, has inspired many mimetic approaches to silicon dioxide formation. Highly homologous to the papain family of proteases, silicatein is capable of hydrolyzing silicon

alkoxide precursors *in vitro* to form silica networks. Here we explore the proteases papain and trypsin, enzymes with similar hydrolytic mechanisms as proposed for silicatein *in vitro*, as potential biomimics. We investigate these hydrolytic proteins' reactivity with metal and semi-metal oxide precursors, to determine how these enzymes interact with non-native substrates in the formation of oxide materials. We have determined that while both enzymes are native hydrolytic enzymes, they do not necessarily behave as such with non-native substrates.

Introduction

Nature is particularly adept at controlling the formation of inorganic material for structural and functional use in organisms. Magnetotactic bacteria navigate using the Earth's magnetic field with the help from biogenic, single-domain magnetite (Fe_3O_4) or greigite (Fe_3S_4). Proteins and biopolymers within the bacteria mineralize iron taken up from the microbes' environment into monodisperse, uniformly shaped nanoparticles organized in a singular chain.^{15, 16} A second example of iron biomineralization in nature can be found in almost any living organism: the iron-storing protein ferritin. Ferritin is a large, 24-subunit protein that sequesters toxic Fe^{2+} , converts it to Fe^{3+} , and stores it in the biomineral ferrihydrite.^{23, 74} While iron-based biominerals are found often in Nature, the most commonly found biomineral is silica (SiO_2). Si is the second most abundant element on Earth, and it can be found as an oxide across many evolutionary levels in Nature. In many plants, Si is deposited as hydrated silica in micro-particles called phytoliths. These protective particles are formed in a wide variety of shapes and sizes,

including dumbbells and bowls. They form a hard barrier in cell walls that keeps out fungi and bacteria. They also absorb light across a variety of wavelengths to promote cooling and photosynthetic processes within the plant.⁷⁵⁻⁷⁷ Biogenic silica also provides protective and structural support in ocean-dwelling sponges of the phylum Porifera. In these sponges, silicon dioxide in the spicules provides extracellular structure; the growth, degradation, and specific patterning of the biogenic silica are controlled through a self-assembled enzymatic filament. The spicules result from concentric layers of silica deposited around a center organic component, known as the axial filament.⁷⁸ The primary component of these axial filaments is a family of enzymes known as silicateins ($-\alpha$, $-\beta$, and $-\gamma$) that condense the silicic acid substrate, taken up by sponges from their environment, into silica.⁷⁹ The most abundant isoform, silicatein- α , is a member of the papain family of cysteine proteases.⁸⁰ The 23 kDa mature enzyme is 44.0% and 45.1% homologous with proteases human cathepsin L1 and cathepsin S, respectively, with conservation of both the histidine and asparagine residues of the active site, and the cysteine residue of the cathepsins replaced with serine in silicatein.⁸¹ Porifera spicules are the only known form of enzymatically-produced biosilica. Silicatein- α has been studied *in vitro* and has been shown to precipitate silica from non-native silicon substrates tetramethyl orthosilicate (TMOS)⁸² or tetraethyl orthosilicate (TEOS).¹⁰ The proposed mechanism of this precipitation is based on the classic mechanism of triad active site hydrolytic enzymes. The silicatein active site acts as a general acid/base catalyst whereby the hydroxyl group of Ser-26 is more nucleophilic upon deprotonation by the nearby imidazole ring of His-165 (Figure 12). The hydrolysis of the methoxy

bond of TMOS by the active site of silicatein is a two-step process; first nucleophilic attack of the TMOS silicon by the serine oxygen results in a covalent bond between the TMOS substrate silicon and the serine oxygen. Secondly, water attacks the silicon center, releasing the serine active site-substrate bond. The free $(\text{MeO})_x\text{Si}(\text{OH})_{4-x}$ now initiates hydrolysis of more TMOS substrate, and the condensation to silica proceeds.¹⁰ Silicatein- α - cathepsin L chimera mutants and a series of site-directed mutagenesis experiments on recombinant protein support this mechanism.^{10, 24, 83} Silicatein has also

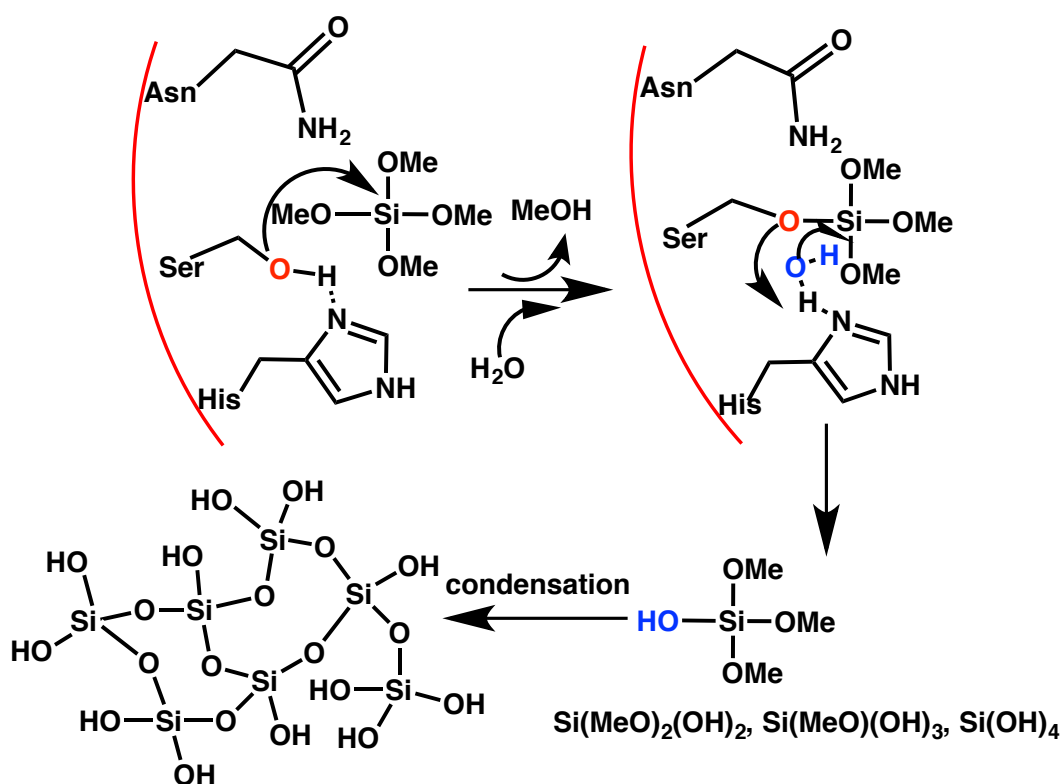


Figure 12. Proposed *in vitro* mechanism for active site silicatein mediated silica formation from TMOS¹⁰

been shown to mediate the formation of other metal oxides zirconium dioxide⁸⁴, titanium dioxide⁸⁵, gallium oxohydroxide, and gallium oxide⁸⁶, and catalyze their formation under mild conditions as opposed to the typically used acids or bases.⁵³ This biomineralization

process has inspired biomimetic routes to silica processing; silicatein is not easily extracted or recombinantly expressed, and using easily obtainable mimics would be advantageous. Additionally, identifying multiple biomimics of silicatein may offer different silica or metal oxide products.

The importance of the hydrolytic mechanism at the active site of silicatein has led to an interest in alternative, more readily available, hydrolytic enzymes, such as proteases. A variety of proteases, including trypsin, chymotrypsin, pepsin, and papain have been investigated as possible biological catalysts of metal oxide formation. Previous studies show inconsistencies in levels of reactivity, substrate specificity, and proposed mechanisms. It is therefore important to further explore the reaction of these types of enzymes for biomimetic approaches.

Since it is part of the same protein family, papain shares a similar sequence with silicatein (28% homology)⁸¹ and has a similar active site, with the serine residue of silicatein replaced by another nucleophilic amino acid, cysteine. This makes papain a natural choice as a silicatein biomimic. An additional feature that lends itself to a good biomimic is papain's active site, which stretches across 7 amino acids⁸⁷ (Figure 13a) that typically accommodates large peptide substrates; this allows large non-native substrates the opportunity to fit and react with the active site.

A second protease with a large, accommodating active site is trypsin (Figure 13b), which retains the serine nucleophilic active site of silicatein (Figure 13c). However, because it is not a member of the same family and has low homology with silicatein, we might expect differences. In order to investigate these proteins as

potential biomimics, we titrate papain and trypsin with a number of different metal oxide precursors to determine their specific activities. We also analyze the morphological differences of the products. Additionally, we determine the involvement of the active site of each enzyme by comparing the native protein to the irreversibly, small molecule inhibited protein.

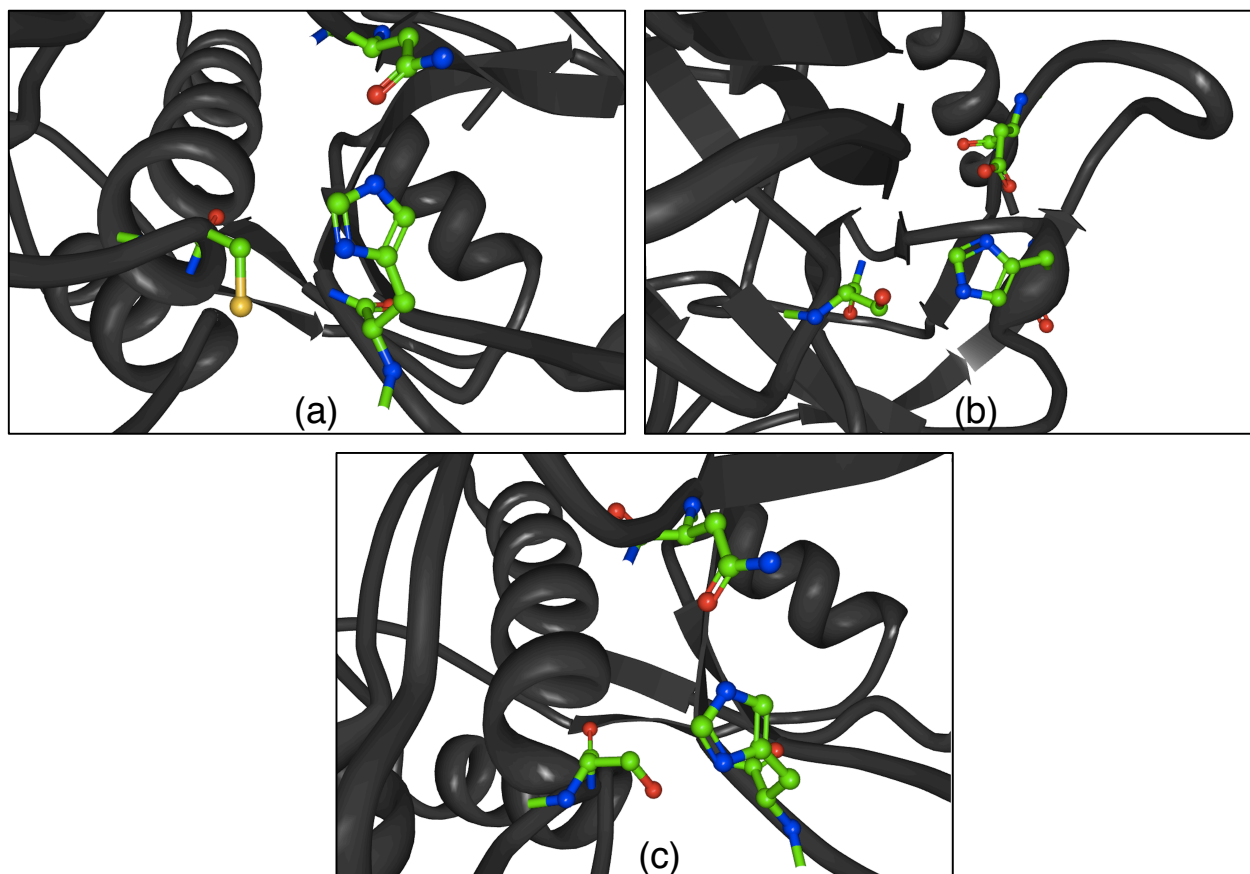


Figure 13. Active sites of a) papain, b) trypsin, and c) silicatein representative using cathepsin L with a cysteine to serine mutation as a substitute, since the crystal structure of silicatein has not been solved; green represents carbon, blue represents nitrogen, yellow represents sulfur, and red represents oxygen

Experimental Methods

Materials

Papain from *Carica papaya* (76216) and trypsin from bovine pancreas (T8802) were obtained from Sigma-Aldrich. Tetramethyl orthosilicate (TMOS), tetraethyl orthosilicate (TEOS), and titanium(IV) bis(ammonium lactate) dihydroxide (TiBALDH) were also obtained from Sigma-Aldrich. Ammonium molybdate (VI) tetrahydrate and mercury(II) chloride were purchased from Acros. Phenylmethanesulfonyl fluoride (PMSF) was purchased from Research Products International Corp. Silicon standard (1001 ppm) and titanium standard (998 ppm) from Fluka Analytical were used, and Amicon Ultra Centrifugal Filters with a 3kDa molecular weight cut off from Millipore Inc. were used. EnzChek protease Assay Kit (E6638) was obtained from Invitrogen.

Metal Oxide Precipitation

Stock solutions of trypsin and papain were made using 10mM phosphate buffer, pH 7.5, for each experiment. Substrate stock solutions were 1M solutions of TMOS in methanol, TEOS in ethanol, and TiBALDH in water. All reactions were run in triplicate with 200 μ L of enzyme stock and 20 μ L of substrate stock at the desired final concentration of enzyme. Reactions were shaken for 10 minutes (except the reaction with TEOS, which ran for 24 hours) and centrifuged at 14,000 g for 5 minutes. The pellet was subsequently washed twice with water and quantitated by the β -silicomolybdate colorimetric assay⁶⁸ or inductively coupled plasma optical emission spectrometry (ICP-OES).

Kinetics of Metal Oxide Formation

Reaction kinetics of metal oxide formation were obtained by monitoring light scattering of the precipitate at 480 nm on a BioTek Synergy H4 Hybrid Reader.

Enzyme Denaturation and Inhibition

Papain and trypsin were denatured by heating the enzyme solutions to 95°C for 10 minutes.

Papain inhibition was achieved by incubating the enzyme with shaking for 4 hours with excess mercuric chloride at room temperature. Inhibited enzyme was purified from excess mercury (II) chloride on a G-15 Sephadex size exclusion column or Amicon centrifugation filters. To verify that the mercury(II) ions did not bind to other cysteine residues and cause unfolding of the protein, circular dichroism spectra were taken for each enzyme state: native, denatured, and inhibited. Native protease activities were determined using a fluorescent protease activity kit.

Trypsin inhibition was achieved by incubation of the enzyme with the common serine protease inhibitor, phenylmethylsulfonyl fluoride (PMSF), at a 10mM final concentration.

Silica Quantification

The silica content was quantified by a modified version of the β -silicomolybdate colorimetric assay.⁶⁸ Silica precipitates were dissolved in 500mM NaOH until full dissolution, which freed encapsulated enzymes. These enzymes interfere with the

colorimetric assay and were removed using centrifugal filters. Each solution was sampled and added to the molybdate reagent; the absorbance of the resulting yellow solution was measured using a BioTek Synergy H4 Hybrid Reader at 410 nm and quantitated against a calibration curve of silicon standards, ranging from 285 to 4300 μM .

Titania Quantification

The amount of titania precipitated from these reactions was quantified on an Optima 7000 ICP-OES with a Scott spray chamber. Samples were dissolved in 1 mL 4M H_2SO_4 and heated to 95°C to ensure dissolution (approximately 1 hour). Samples were prepared for ICP-OES analysis using a 2% HNO_3 matrix. The intensity at 334.94 nm was measured and converted to titanium content using a calibration curve of titanium standards, ranging from 10 ppb to 5 ppm.

Characterization

Characterization by SEM was performed on a Hitachi S4200 high-resolution scanning electron microscope X-ray diffraction as performed on an Xgen-4000 Advanced Diffraction System from Scintag Inc, USA. CD spectra were collected on a circular dichroism spectrometer, Model 215, from AVIV instruments, Inc. Infrared spectroscopy was performed on a ThermoMattson Satellite FTIR. Electrostatic potential at the surface was mapped using the Swiss-PDBViewer program.⁸⁸ The Poisson-

Boltzmann equation was used to map the electrostatic potential, with a dielectric constant for the protein at $\epsilon=4$, which is most commonly used for proteins.⁸⁹

Results and Discussion

Protease Mimic Reactivity with TMOS

While the hydrolysis and condensation of tetramethyl orthosilicate into silica in a buffered system at pH 7.5 is slow, on the order of days, the integration of one of two hydrolytic enzymes, papain or trypsin, into the system significantly increases the reaction to a matter of minutes. Papain and trypsin are proteases that both naturally cleave after positive amino acid residues arginine and lysine. They have similar active site environments and mechanisms, and have previously been studied as biomimics of silicatein with a silicic acid substrate.⁹⁰ We have expanded the study to unhydrolyzed silicon alkoxide substrates to determine if these enzymes have hydrolytic capabilities as metal oxide mediators. By using fresh stock solutions of tetramethyl orthosilicate in methanol as opposed to hydrochloric acid, we assure that the substrate has not been hydrolyzed to silicic acid (<2% molybdate reactive).

Incubation of each enzyme with the TMOS substrate results in a solid precipitate of silica. While both of these enzymes react in a concentration dependent manner up to a saturation point, the reactions differ between enzymes. A previous study by Smith et al⁹⁰ showed that while papain was reactive with silicic acid, the reactivity was not dependent on the availability of the active site, and silica precipitate formed despite inhibition of papain at the active site. Our study corroborates this information and

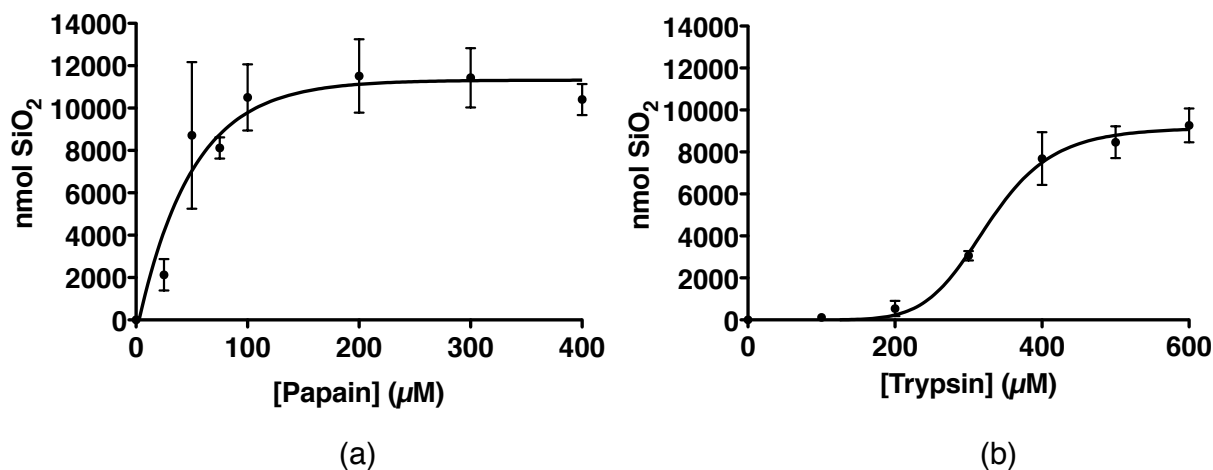


Figure 14. Silica precipitation versus enzyme concentration; a) papain and b) trypsin; each point represents n=3 with error bars of standard deviation

expands it to unhydrolyzed substrate, TMOS. From 25 to 100 μM , increasing concentrations of papain yields more silica product; at 100 μM papain, silica formation plateaus (Figure 14a). At 100 μM , papain has a specific activity of 45 nmol SiO₂/(nmol papain*min). Above concentrations of 100 μM papain, increases in enzyme concentration do not affect silica yield. This is likely due to the encapsulation of a majority of the protein into the growing silica product, as is seen in other organic-facilitated condensation of silica^{2, 40, 91-94}. This is supported by infrared spectroscopy (Figure 15a), which shows carbon-carbon double bonds between 1600 and 1700 cm^{-1} , that can only come from the protein, not the silica material. Additional substrate to the reaction supernatant results in little to no precipitation; measurement of the supernatant shows less than 30 μM papain, which explains the lack of additional precipitate.

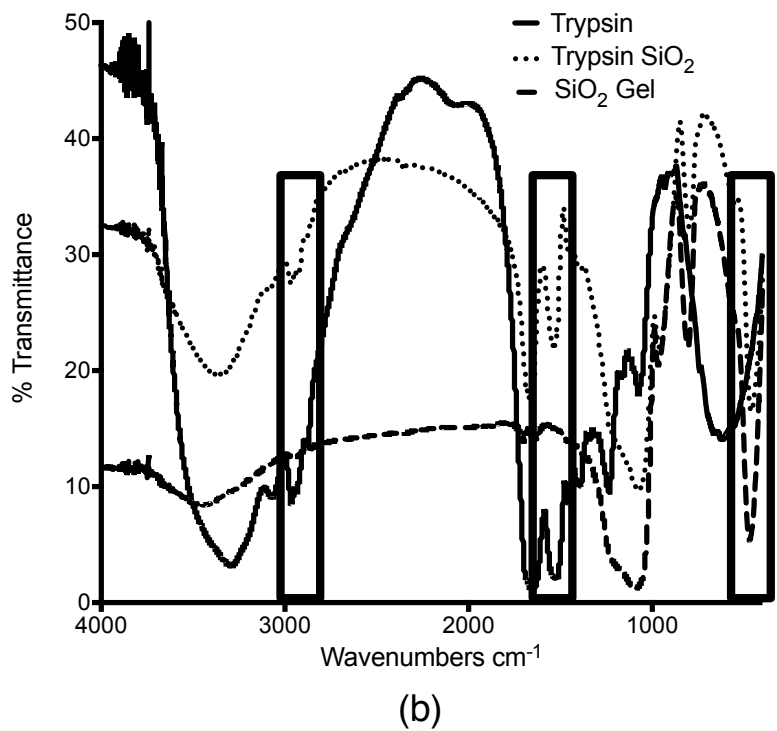
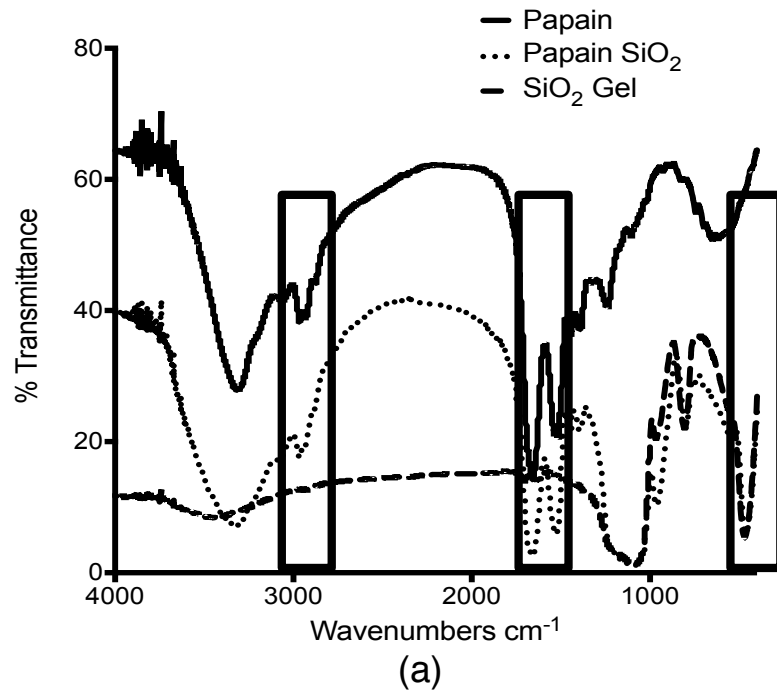


Figure 15. IR spectra for enzyme (solid) silica gel (dashed) and silica product from reaction with enzyme (dotted) for a) papain and b) trypsin; black boxes show protein peak overlaps with the reaction precipitate, indicating protein present in each product

Trypsin reacts differently with TMOS, despite having a similar maximum yield. Silica production by trypsin requires more than eight times higher concentration of enzyme to precipitate silica than papain, $200\mu\text{M}$ versus $25\mu\text{M}$, respectively. The positive correlation between concentration of trypsin and silica yield ends at $400\mu\text{M}$ trypsin. At concentrations above $400\mu\text{M}$ trypsin, increases in trypsin no longer yield additional silica due to the ratio of enzyme to substrate (Figure 14b). Some enzyme is encapsulated within the growing silica product, as is seen with papain, (Figure 15b), but not all of the enzyme is encapsulated. Upon addition of substrate to the reaction, the remaining free trypsin reacts with TMOS to form silica. The saturation comes from the decreased concentration of TMOS, which slows the reaction with trypsin significantly, longer than the 10-minute reaction time used.

Effect of Active Site Inhibition and 3D Structure on Reactivity

To probe the involvement of the active site, the enzymes were inhibited by known active site inhibitors irreversibly. The active site of these enzymes is responsible for hydrolyzing peptide and protein substrates naturally; in order to mimic silicatein, which also hydrolyzes substrates TMOS at the active site, the two proteins need to hydrolyze TMOS at the active site. It cannot be assumed that the active site hydrolyzes TMOS, since other methods of protein facilitated silica production from TMOS are known. In order to determine the importance of 3D folding and structure, the enzymes were denatured by heat, unfolding the proteins.

Papain was incubated with excess mercury (II) chloride in order to form a covalent bond between the cysteine thiol in the active site and mercury. According to hard-soft acid/base theory (HSAB), hard, small, weakly polarizable Lewis acids will bind more favorably with hard Lewis bases, and soft, polarizable acids will bind with soft bases⁹⁵. Thus, the soft thiol group of the active site cysteine residue reacts very favorably with the soft mercuric ion, leading to a strong covalent bond of ~ 272 kJ/mol⁹⁶. Circular dichroism spectra of each form of papain verify that excess mercury did not cause unfolding of the protein. Figure 16 shows the native protease activity and the TMOS activity of different forms of papain. When incubated with excess Hg (II), papain no longer hydrolyzes peptide substrate BAEE provided with the EnzChek protease activity kit. However, mercury-inhibited papain retains its activity with TMOS, indicating that the active site is not required for hydrolysis of the TMOS substrate.

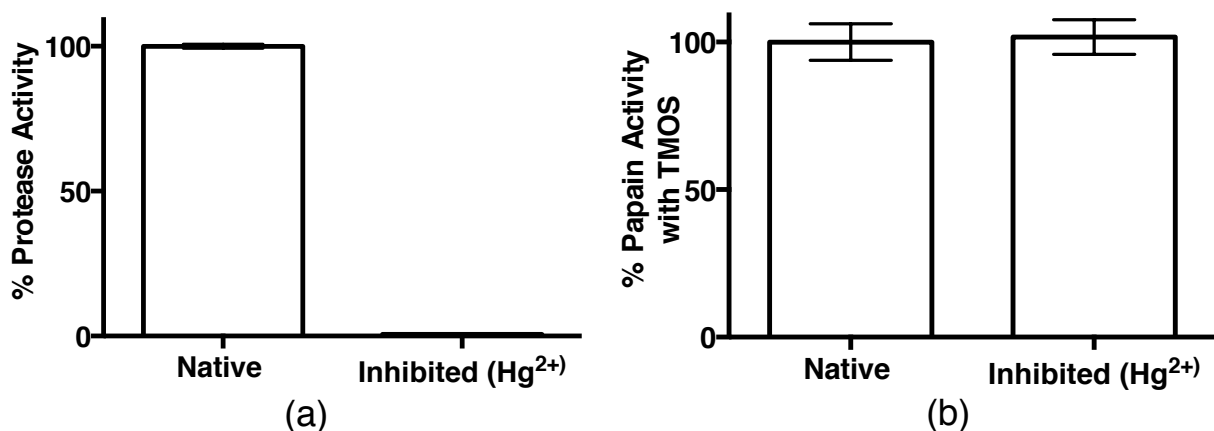


Figure 16. a) protease activity and b) TMOS activity of papain either in the native form or inhibited at the active site by Hg²⁺

We propose, then, that papain acts similarly as mimics of the organic components in a second source of biogenic silica, diatom algae. Long chain polyamines and silaffins, highly post-translationally modified peptides, organize together to precipitate silica in the

cell wall of some unicellular algae as well as *in vitro*.⁹⁷ Mimics of these, such as poly (amido amine) (PAMAM) dendrimers, have been previously studied and found to precipitate TMOS into silica by driving localization at the positively charged surface.⁴⁵ Since the active site is not involved in driving silica formation, we propose that the papain surface is acting as a template, much like PAMAM dendrimers. Papain, when folded, has large positively charged surface patches, as determined by a Poisson-Boltzmann distribution calculation.⁸⁸

In order to inhibit trypsin at its active site, the enzyme was incubated with excess phenyl methyl sulfonyl fluoride (PMSF), a small molecule that reacts specifically with the active site serine residue, forming a covalent bond between oxygen and sulfur that precludes future nucleophilic attack by serine.

We found that while trypsin is less homologous to silicatein than papain, the active site is involved in the hydrolysis of TMOS to form silica. At pH 7.5, trypsin has cationic patches on the surface, but is less charged than papain. Papain is more charged than trypsin by almost 50%, making it much more likely than trypsin to act as a sink for precursor localization. We hypothesize that this difference in charge causes the difference in reactivity of these two enzymes with TMOS. Trypsin does not cause as much localization of TMOS at its surface because it has less overall positive charge; thus, there is less precursor to hydrolyze, and lower precursor concentration that will result in less self-condensation. We hypothesize, then, that in reactions between trypsin and TMOS, the surface chemistry is not enough to cause precipitation, and something else is required to facilitate the reaction. This facilitator is the active site,

which has the same nucleophilic serine residue as silicatein does. This was tested by inhibition of the active site of trypsin and subsequent comparison of this inhibited protein with native trypsin. Upon inhibition of the protein with the small molecule PMSF (Figure 17a), precipitation of silica is reduced significantly, to ~20% of the silica yield from uninhibited trypsin protein (Figure 17b). Some TMOS substrate can be catalyzed to silica formation by the presence of the positive patches on the trypsin surface, but this is significantly decreased as compared with papain due to the decreased positivity of the trypsin surface compared with papain.

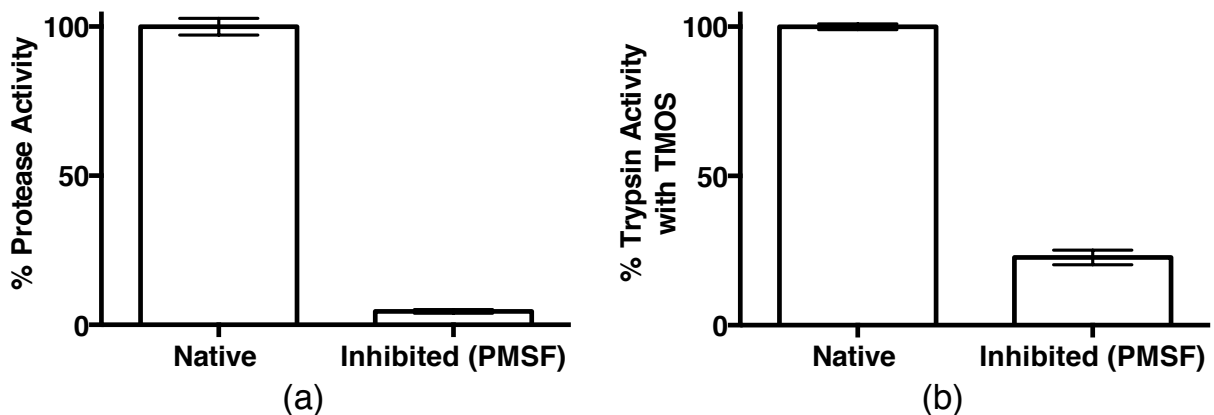


Figure 17. Trypsin activity with a) native substrate BAEE and b) non-native TMOS substrate

Despite both being hydrolytic enzymes, we found interesting differences between papain and trypsin in terms of what is responsible for reacting with the unnatural TMOS substrate. In fact, papain does not use its hydrolytic active site to facilitate the hydrolysis and condensation of TMOS to silica, while trypsin does.

Protease Mimic Reactivity with TEOS

Using the substrate TEOS significantly slows the formation of silica induced by papain and trypsin as compared to the substrate TMOS. Whereas silica formation

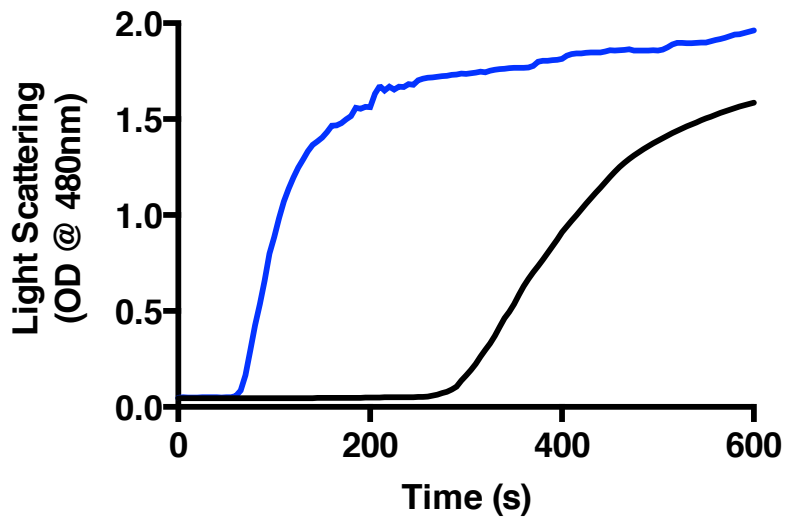


Figure 18. Kinetics of reactions between TMOS and papain (blue) or trypsin (black), showing the formation of particles at 65s for papain and 275s for trypsin

appears within minutes from the substrate TMOS (Figure 18), silica formation occurs over the span of 24 hours with TEOS. This can be attributed to the limited solubility of TEOS in buffer. Due to the increased time of the reaction, the amount of silica in the control without protein is not negligible and must be accounted for in the samples. Since

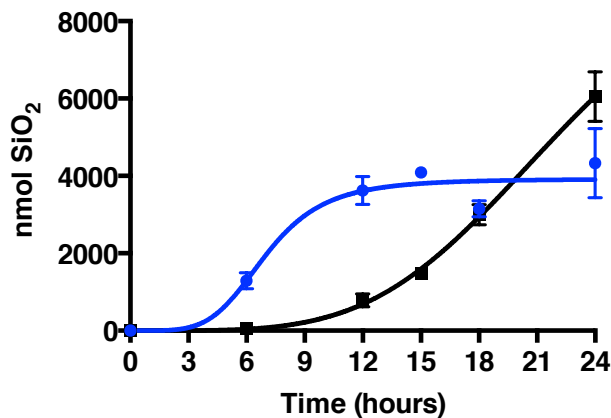


Figure 19. Yield of silica over time for reactions between TEOS and papain (blue) or trypsin (black)

this reaction occurs closer to the time scale of the gel point of the substrate TEOS in buffer, the increase in the silica content of the samples with trypsin and papain over the amount in the buffer control is due to the enzyme presence. While both reactions were significantly slowed with TEOS as compared with TMOS, papain reacts more quickly than trypsin with TEOS to form silica product (Figure 19), as is seen with TMOS (Figure 18). Larger substrates such as tetrapropyl orthosilicate or tetraisopropyl orthosilicate are impractical substrates for these enzymes due to their immiscible nature with aqueous solutions.

Silica Morphology Differences Between Proteases

Papain precipitates spherical, monodisperse silica particles, averaging 472 ± 87 nm (Figure 20a) for TMOS and 790 ± 260 nm (Figure 20c) for TEOS. Trypsin, on the other hand, produces a highly aggregated network of indistinctly shaped and sized silica with TMOS or TEOS (Figure 20b,d). We propose that the morphological differences are due to the different hydrolysis mechanisms; hydrolysis of the precursors happens mainly at the active site of trypsin, and mainly at the surface of papain. As the substrate is hydrolyzed by trypsin, it may be expelled from the active site, and thus not further hydrolyzed. When this occurs, condensation will happen at the outer silicon atoms, not at central atoms, leading to an aggregated network. This is known as reaction-limited cluster aggregation. In typical sol-gel chemistry, this process is induced by acidic conditions that favor hydrolysis and cause condensation to be the rate-determining step; while this may not be the exact cause in these reactions, the end result, where

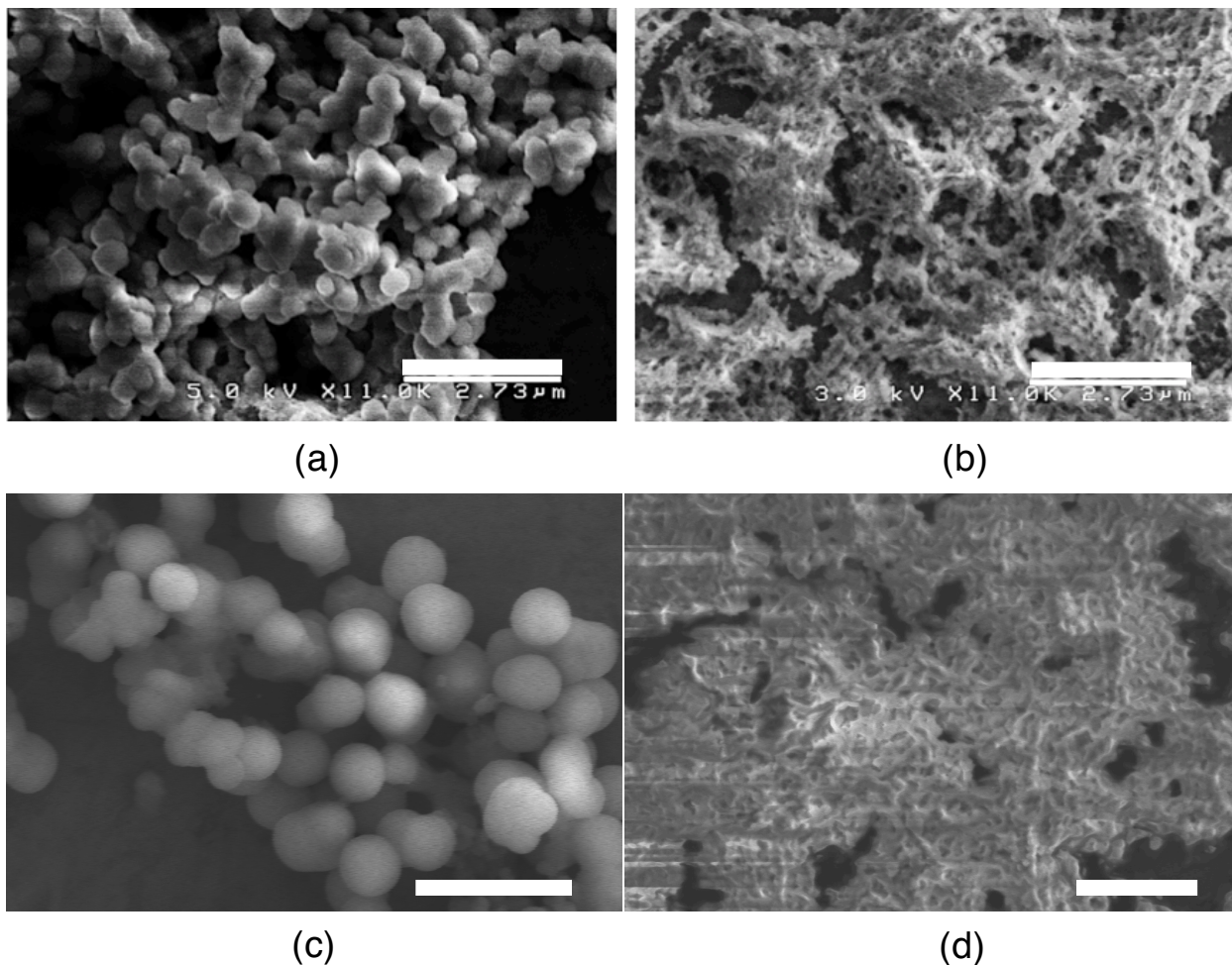


Figure 20. SEM images of silica particles from reactions between enzymes and silicon alkoxides (a) papain with TMOS, (b) trypsin with TMOS, (c) papain with TEOS, and (d) trypsin with TEOS; scale bars 3 μm for (a) & (b); 2.33 μm (c) & (d)

condensation occurs at outer silicon atoms and oligomers, yields an aggregated network.

Protease Mimic Reactivity with TiBALDH

Since silicatein was able to precipitate a variety of metal oxides, including titania, we decided to examine the activity of each biomimic with TiBALDH to expand our knowledge of these biomimics to other metal oxide precursors. We found that titania precipitation from either papain or trypsin is immediate, as has been reported for the

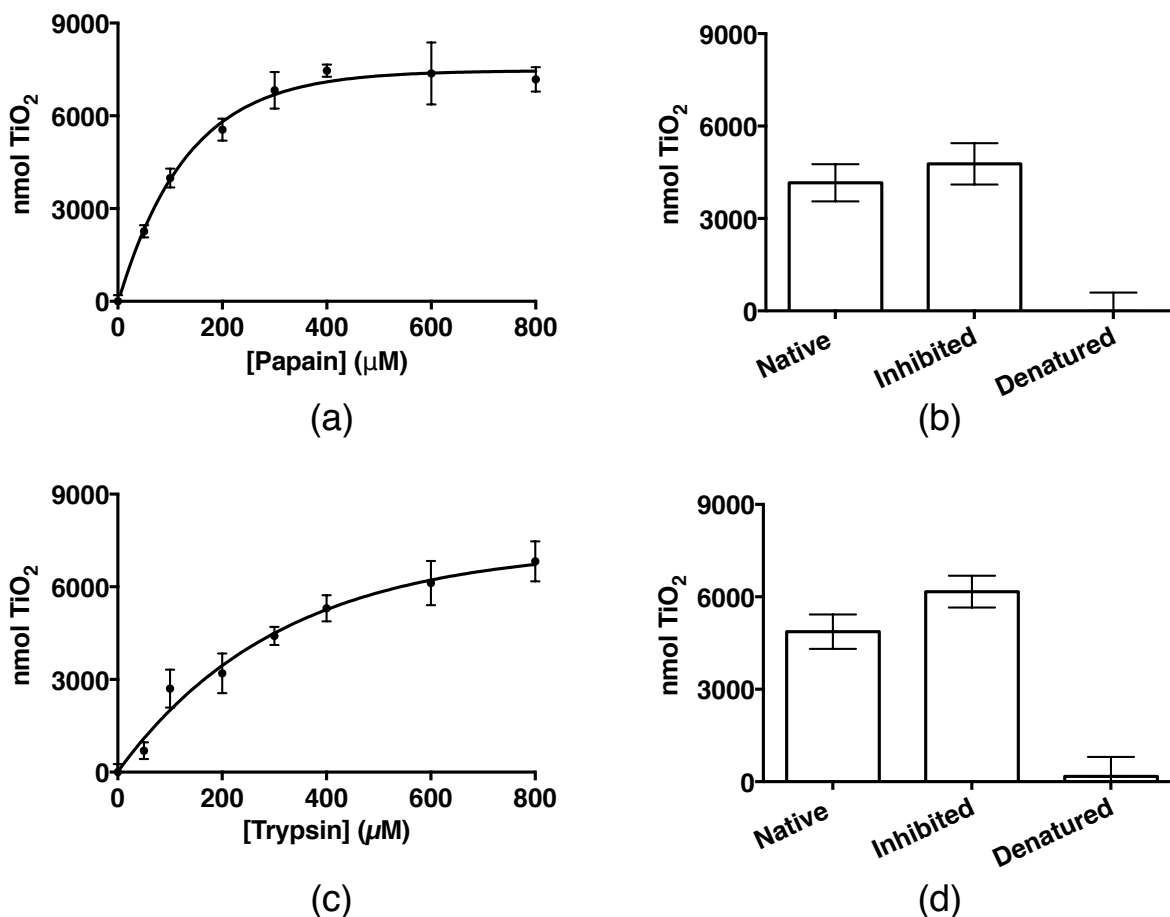


Figure 21. a) titania yield as a function of papain concentration; b) titania yield from reactions with 3 different states of 100 μM papain: untreated, inhibited with Hg²⁺, or denatured by heat; c) titania yield as a function of trypsin concentration; d) titania yield from reactions with 3 different states of 400 μM trypsin: untreated, inhibited with PMSF, or denatured by heat

formation of silica particles through organic template-driven condensation of silicic acid.⁹¹ As the concentration of either trypsin or papain increases, the titania yield increases (Figure 21a,c); at 400 μM enzyme, this correlation ends and titania formation plateaus at about 6000 nmol TiO₂. This is due to encapsulation of the enzymes into the titania network, which is supported by IR spectroscopy. Little precipitation of titania occurs upon addition of new TiBALDH substrate to the reaction supernatant. The slight difference in specific activities of papain (~8.5 nmol titania/nmol papain*min) and trypsin

(~ 7 nmol titania/nmol trypsin *min) at $400 \mu\text{M}$ is likely due to the decreased positive charge of trypsin compared to papain. We hypothesize that the decrease in yields and specific activities of these proteins with TiBALDH as compared with TMOS is due to the speed with which the reactions occur. Because the formation of particles occurs immediately, the protein template is immediately encapsulated within the particles and is no longer present to further drive condensation of precursor to titania.

When irreversibly inhibited by Hg^{2+} for papain and PMSF for trypsin, as described above, both enzymes retain their reactivity with TiBALDH and precipitate titania (Figure 21b,d). Neither biomimic requires availability of the active site to hydrolyze the substrate; however, the overall structure and folding of the protein is important, as heat denaturation results in a loss of titania formation. Trypsin with TiBALDH, unlike with TMOS, does not require the active site to aid in hydrolysis and condensation of the metal oxide precursor; the surface positive patches are enough to cause substrate hydrolysis. This is likely due to the increased electrophilicity of the titanium(IV) metal

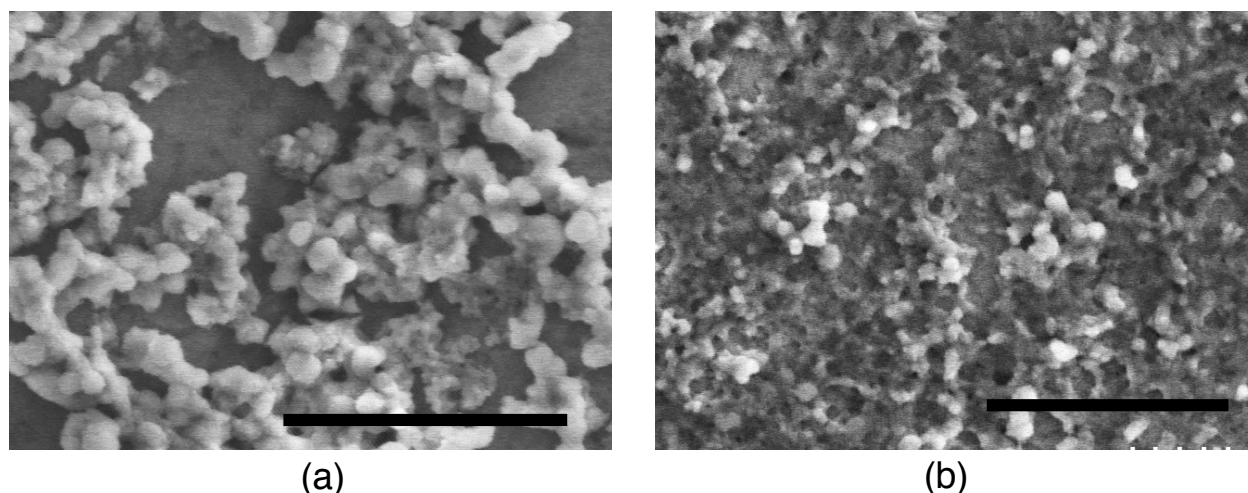


Figure 22. SEM images of titania particles precipitated from reactions with (a) $100 \mu\text{M}$ papain and (b) $400 \mu\text{M}$ trypsin, scale bars $3 \mu\text{m}$. particle sizes (a) $201 \pm 44 \text{ nm}$ and (b) $305 \pm 61 \text{ nm}$

and the weaker bonds between the titanium(IV) metal center and the 6 ligand oxygen atoms relative to TMOS; TiBALDH is known to be much more reactive in typical sol-gel chemistry than TMOS.⁵⁴ The morphologies of the products is consistent between the biomimics; both reactions yield a network of spherical, relatively monodisperse titania particles (Figure 22).

From these experiments, we found that the only conditions studied so far that leads to the use of the hydrolytic active site of the biomimic is when trypsin is reacted with a silicon alkoxide precursor like TMOS. The high reactivity of TiBALDH compared to TMOS means that the both proteins are able to facilitate titania from TiBALDH without the use of the active site. The surface charge differences between papain and trypsin influence the reactions with TMOS; papain does not require the active site to facilitate silica precipitation, but the less positive trypsin does.

Conclusions

We have verified that the proteases trypsin and papain are both reactive with tetramethyl orthosilicate, as well as tetraethyl orthosilicate. However, while they are hydrolytic enzymes, they are not guaranteed to react with non-native substrates at their active site. Hydrolysis by the nucleophilic active site residue in papain is in fact not a key step in the formation of silica from TMOS; yet in trypsin, the active site is required. The tertiary structure of both proteins is vital, as seen by heat denaturation of the proteins; once unfolded, the proteins do not react with TMOS to precipitate silica. When the proteins are unfolded, their overall surface chemistry is altered and no longer has

the cationic patches that are present on the three dimensional surface. This alteration diminishes the ability of the metal oxide precursors to react at the protein surface to form metal oxide precipitates. Additionally, the active site for trypsin is no longer in the correct formation and can't act to hydrolyze the TMOS precursor. Both enzymes react with TiBALDH to form titania, regardless of active site availability. In this study, we have identified papain as a biomimic more akin to the organic precipitation platforms previously reported, and trypsin as a biomimic of silicatein with respect to TMOS. However, both of these enzymes can be expanded to alternative metal oxides, such as titanium dioxide. Due to the differences in how each enzyme reacts to non-native substrates, despite having similar native substrates, reactivity, and mechanisms, it is clear how important deeply investigating potential mimics is when using them in non-natural ways.

CHAPTER IV

NANOSPHERE LITHOGRAPHY FOR THE TEMPLATED FORMATION OF ENZYME-MEDIATED METAL OXIDES IN ZEPTOLITER CHAMBERS

Introduction

As was described in Chapters II and III, we are able to precipitate metal oxides in a controlled manner under mild conditions. However, as seen in the images, the resulting materials were almost always spheres, albeit of different sizes and levels of interconnectivity. In order to exercise better control over the patterning of these materials, we propose to use an extension of a templating, bottom-up technique called nanosphere lithography.⁷

Nanosphere lithography is a method based on the formation of a template from the self-assembly and packing of nanospheres, typically polystyrene, in a colloidal solution. As depicted in Figure 23, these spheres are deposited onto a surface and pack, if spherical, in hexagonal close packing; therefore, a template is formed for further material fabrication. The desired material is then added to the masked substrate, and thus is patterned according to the interstitial space between the spheres. The spheres can then be removed, as would be done with the mask in typical lithographic approaches. In some cases, a last step of heating will induce a phase change to a crystalline final material. Depending on the size of the spheres and the number of layers (monolayer vs bilayer) the template can be modified.⁷ In our experiments, we

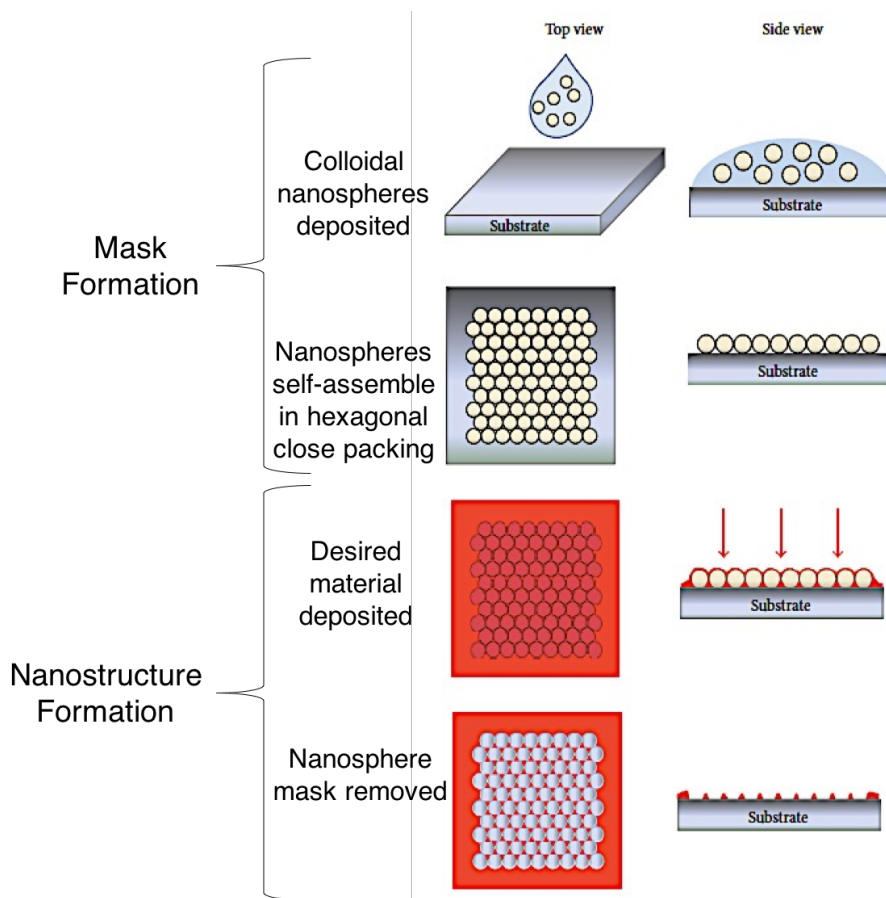


Figure 23. Process of nanosphere lithography from Colson et al⁷ divided into two phases

use this idea to first mask a substrate. However, after this, instead of adding the desired material, we add a reactive alkyl chain that can react with the exposed surface. This alkyl chain will assemble vertically off of the surface, and we subsequently remove the masking beads. The substrate surface is now a hydrophobic alkyl-layer everywhere except the small areas where the beads were touching the surface, where there are pores that expose the original substrate surface. Next, we add the precursors in a way that allows the material of interest to form as a result of a reaction in these specific pores. In this way, we are employing two masking steps. This process will be further outlined and depicted in the following experimental section. By this method, we

can synthesize small, nanosized metal oxides across a substrate. In order to facilitate imaging of the template, in addition to scanning electron microscopy, which has been used in previous chapters, we will use atomic force microscopy (AFM).

Since its invention in the 1980s, AFM has been used across many scientific fields, from biology to materials science.⁹⁸ It's been used to study cells, DNA, and other biological features, as well as hard and soft materials.⁹⁹⁻¹⁰⁴ With a high resolution of typically less than 1nm, this technique will be particularly useful for the analysis of the substrates prepared, particularly in the z-direction, orthogonal to the substrate surface. The templated substrates will have pores, and determining their depth with SEM would not be possible.

In this Chapter, we template silicon wafer substrates under a few different conditions and image the results. We then use the reactions described in Chapter II to form metal oxides in the pores of the substrate. Analysis of the substrates by SEM and AFM reveals patterned 'flowers' of silica.

Experimental Methods

Materials

Trimethoxy(octadecyl) silane, trichloro(octadecyl) silane, papain from *Carica papaya* (76216), tetramethyl orthosilicate, titanium (IV) bis(ammonium lactate) dihydroxide, sodium phosphate monobasic and dibasic, and hydrogen peroxide were from Sigma-Aldrich. Silicon wafers (4", 5x7mm chips) were obtained from Ted Pella, Inc. Silica microparticles (500nm) were purchased from Polysciences, Inc. HPLC

grade, submicron filtered water, toluene, acetone, and sulfuric acid were obtained from Fisher Chemical. Ethanol from Decon Laboratories, Inc was used.

Templating Si Wafers

A bead stock was prepared by washing 250 μL of beads (Polysciences, Inc. 24232-15) twice with DI water and diluting to 1.5mL. Silicon wafers were cleaned with piranha (3:1 18 M H_2SO_4 to 30% H_2O_2) for 30 minutes and subsequently washed with water. The bead suspension (10-20 μL) was added to each clean, dry substrate surface, in order to fully cover the surface. A 0.1% or 1% trimethoxy(octadecyl) silane or trichloro(octadecyl) silane solution in toluene dried over molecular sieves was prepared. Once the bead suspensions fully dried, the bead-coated silicon wafers were incubated in the silane solution or plain toluene over night at 70°C. In order to remove the beads, the substrates were vigorously washed *via* 10-minute sonication steps in ethanol, water, ethanol, acetone, ethanol, and water. The last wash was in HPLC-grade water. Templated substrates were allowed to dry and subsequently characterized to verify a patterned surface. Multilayers of beads may occur, but this does not need to be avoided because it doesn't affect the availability of the exposed substrate surface.

Templated Metal Oxide Formation

Once substrates have been identified as successfully templated, they are incubated with 1mM or 0.1mM papain in phosphate buffer. Each sample is placed half-in the papain solution and slowly drawn vertically out of solution, using the step motor of

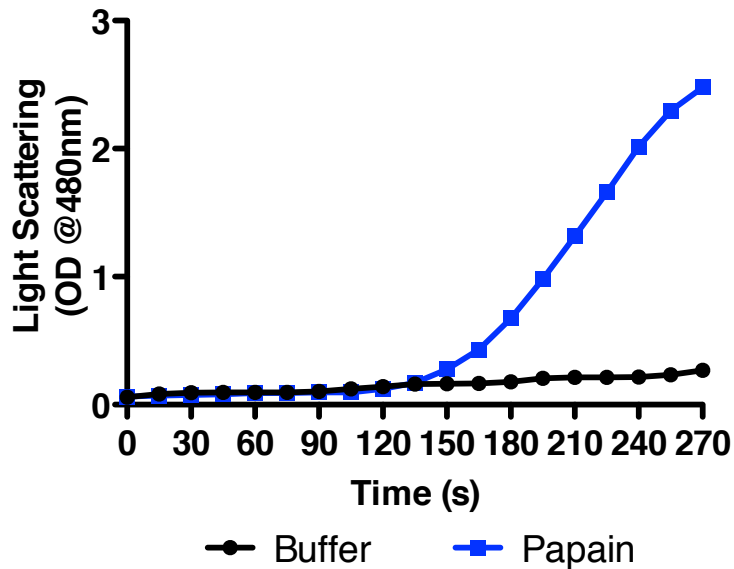


Figure 24. 2M TMOS in toluene added to aqueous papain or buffer solution. Particles form and scatter light when papain is present, but not with just buffer; TMOS diffuses to the aqueous layer without being in a water-miscible stock

the AFM instrument. In this way, each substrate is half treated with papain and half untreated. Samples are then placed in a solution of 2 M TMOS in toluene or in pure toluene and incubated for 30 minutes. As described in Chapter III, reactions between papain and TMOS are typically done in aqueous solutions, with TMOS in methanol since it is miscible with the aqueous papain solution. In this way, both the enzyme and the substrate are in one solution phase. Because toluene is not miscible with aqueous solutions, we first needed to verify that the TMOS would diffuse into the aqueous solution (Figure 24). The increase in absorbance at 480nm indicates the occurrence of light scattering due to insoluble particles forming in solution, meaning the TMOS substrate is able to transfer phases from the organic toluene to the aqueous phosphate buffer and reach the papain.

Characterization

Scanning electron microscopy was performed on a Zeiss MERLIN. Atomic force microscopy was performed on a Keysight Technologies 5500 AFM.

Results and Discussion

Templating Surfaces

In order to create zeptoliter-sized reaction vessels, we template a silicon substrate, as previously published by Englade-Franklin et al.¹⁰⁵ A silicon substrate is cleaned with piranha solution, exposing $-OH$ groups at the silicon surface. The substrate is then covered in spherical silica beads that organize in hexagonal close packing. Thus, the majority of the silicon wafer is still exposed, with only the bottom tip

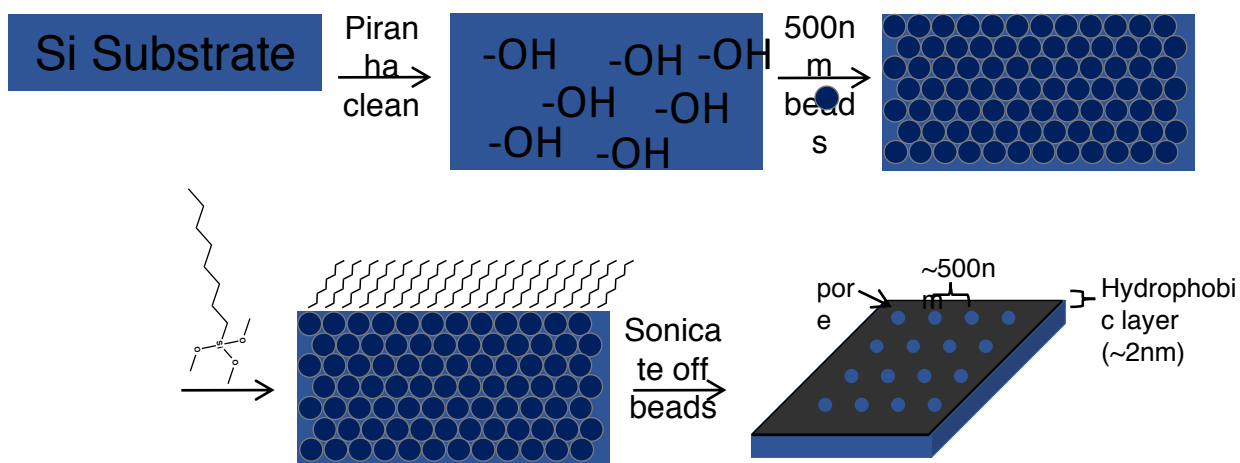


Figure 25. Scheme of templating silicon wafers. Clean the silicon surface with piranha (3:1 18M H_2SO_4 to 30% H_2O_2), exposing hydroxyl groups. Add 500 nm silica beads to coat surface, incubate masked surface with trichloro(octadecyl) silane or trimethoxy(octadecyl) silane, depicted here. Finally surfaces are sonicated in various solvents to remove beads.

of each bead touching the surface. When a reactive species, either trichloro(octadecyl) silane or trimethoxy(octadecyl) silane, is incubated with the substrate, most of the

substrate surface reacts, leaving only $\sim 50\text{nm}$ of surface at each bead unreacted. The octadecane chains of the silane will stick out from the surface, although at different angles depending on the reacted oxygen link, which typically accounts for ~ 1 to 2 nm of added height. Then the 500 nm beads can be removed by sonication (Figure 25). In this way, the silicon wafer becomes patterned with pores approximately 500nm (the size of the beads) apart.

Using AFM and SEM, we analyzed the resulting templates of a variety of templating conditions, differing the silane itself and the silane concentration. Previously,

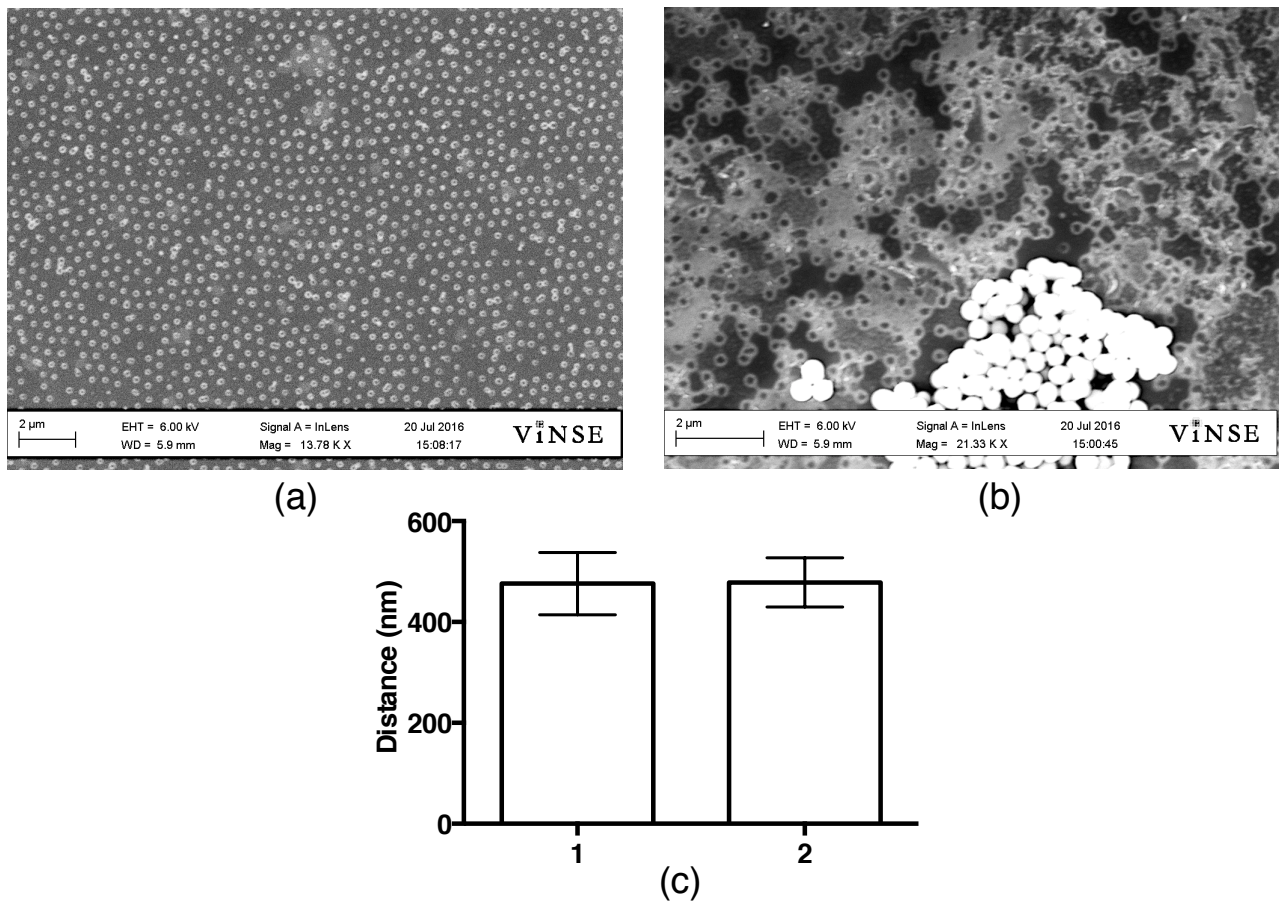


Figure 26. (a) SEM image of substrate I surface after beads were added and removed (b) SEM image of substrate II with beads in bottom center; (c) distance between rings on different substrates, matching the 500 nm beads used to template

templates had been seen sometimes as simple pores and sometimes as raised rings surrounding a pore, likely due to the accumulation of polysiloxane around the bead. We hypothesized that the less reactive trimethoxy(octadecyl) silane would tend towards the ring pattern, and the trichloro(octadecyl) silane would result in pores, under similar conditions.

Interestingly, we found that the ring pattern occurred even when no silane was added. When the substrate was treated with beads, incubated in pure toluene, and then cleaned as described for all other conditions, the substrate surface when imaged showed a pattern of rings (Figure 26). Using AFM, we found that these rings present heights that are shorter (~2 nm) than what may be expected from polysiloxane rings during templating (~5-15 nm) (Figure 27). This requires further investigation, but it could possibly be due to insufficient washing of the original bead stock. However, we are confident in the 1 to 2 nm pores found in the trichloro(octadecyl) silane templated surfaces, described in the section below.

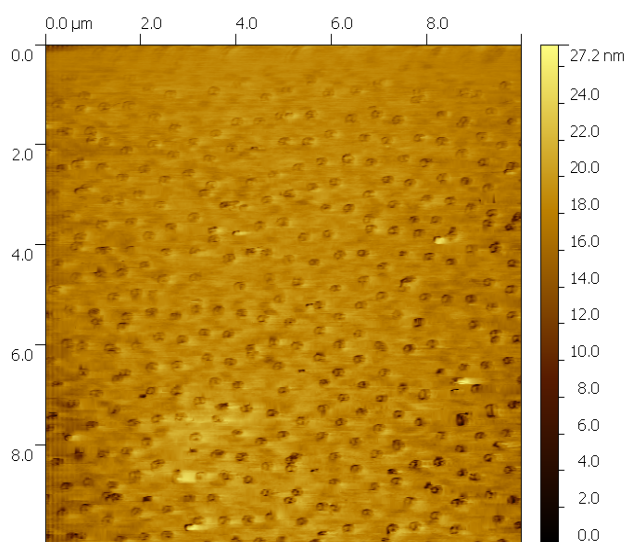


Figure 27. AFM topography image of rings after silicon surface coated with beads that were then removed

Imaging Templated Surfaces

By templating using trichloro(octadecyl) silane, the surface is coated with a hydrophobic alkyl chain with a height dependent on how fully alkyl-ated the surface is. The more alkyl-silanes that are packed into a particular area, the more upright the alkyl chains are and the higher the height is over the surface (meaning the deeper the pores are). As can be seen in Figure 28, there are pores spaced approximately 500 nm apart

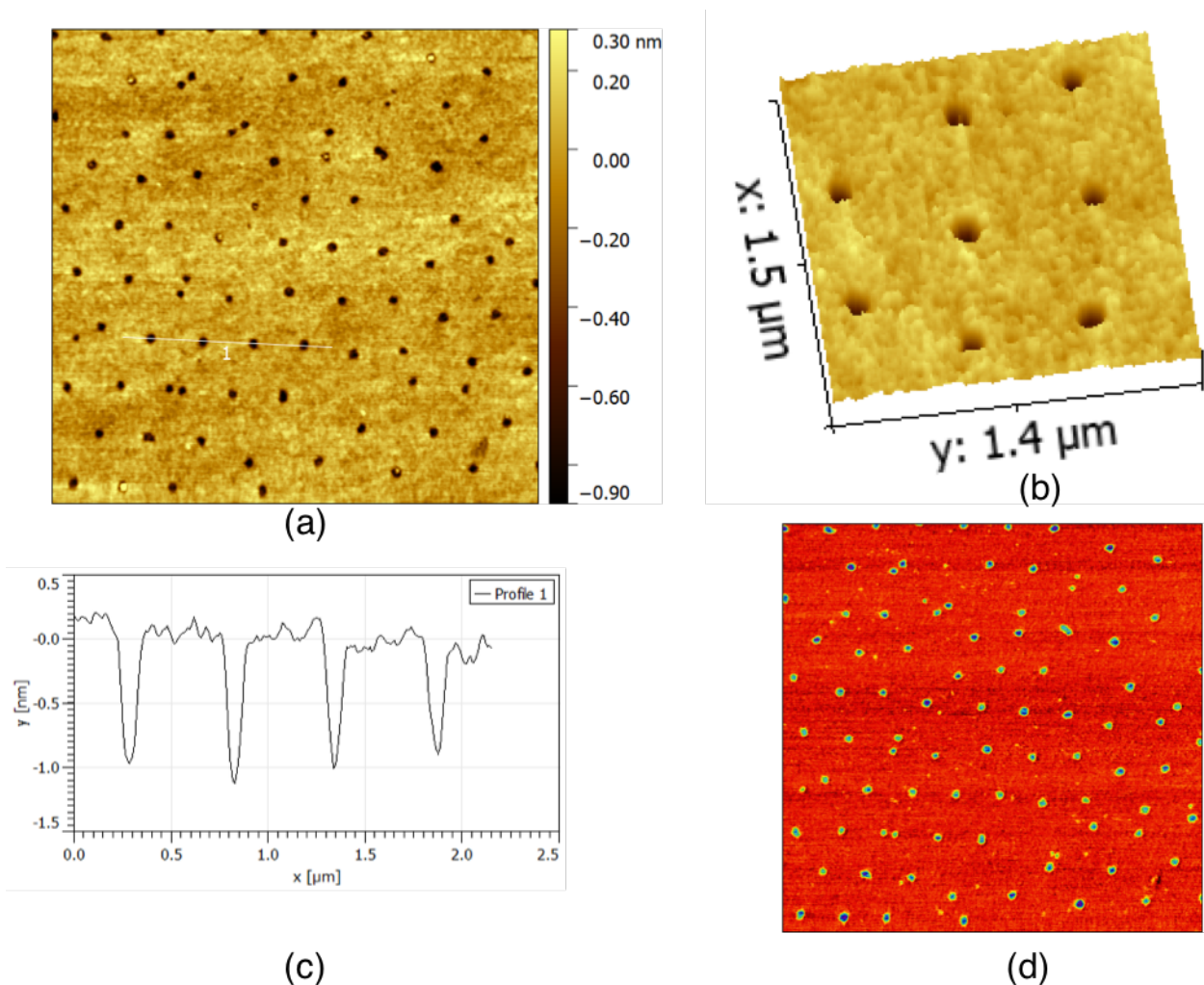


Figure 28. AFM analysis of a trichloro(octadecyl) silane templated surface, as described above, (a) topography (b) zoom topography (c) topography trace with 1 nm deep pores (d) lateral force image, showing different chemistries (or frictions) on the surface, matching the pattern seen in topography images

that range from 1 to 1.5 nm deep. Templating using this technique was repeated multiple times, and another substrate is represented in Figure 29.

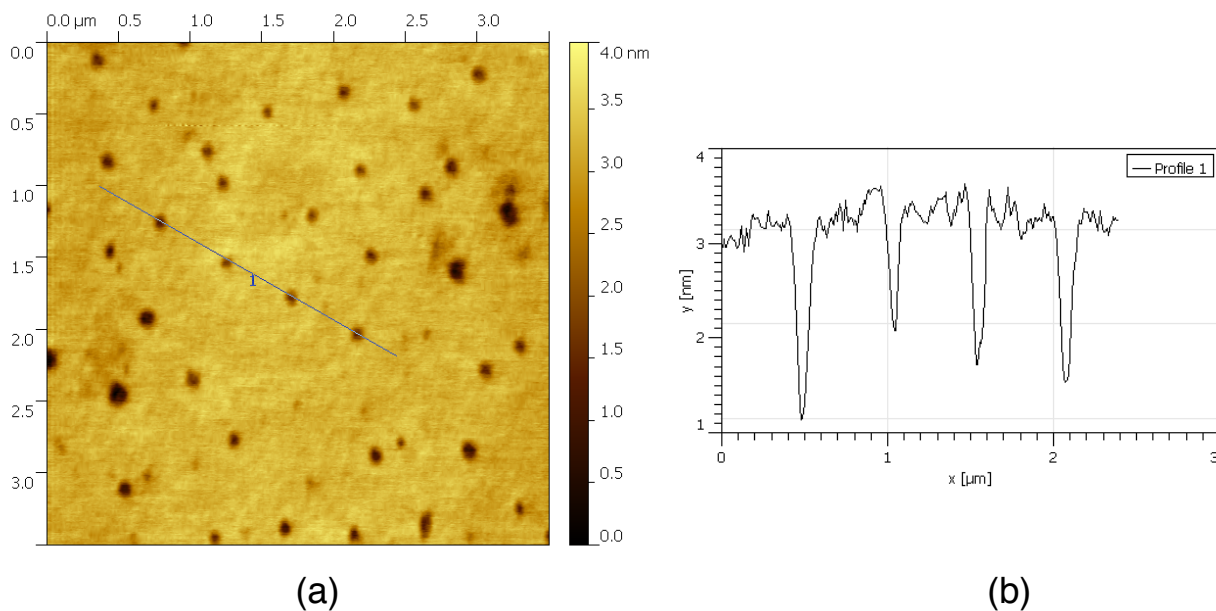


Figure 29. AFM analysis of a trichloro(octadecyl) silane templated silicon substrate (a) topography and (b) topography trace showing pore depth

After verifying the pores of these surfaces, we used trichloro(octadecyl) silane templated surfaces to perform the metal oxide reaction between papain and TMOS.

Silica 'Flowers' on Substrates

We incubated half of a templated surface, as described and imaged above, with 1 mM papain in 100 mM phosphate buffer, pH 7.5. The substrate was slowly removed vertically from the solution using the step motor on the AFM instrument. This allowed the hydrophilic papain solution not to stick to the mainly hydrophobic surface, leaving papain in only the pores. The entire substrate was then submerged in a 2 M TMOS solution in toluene for 30 minutes. The substrate was dipped once in pure toluene as a

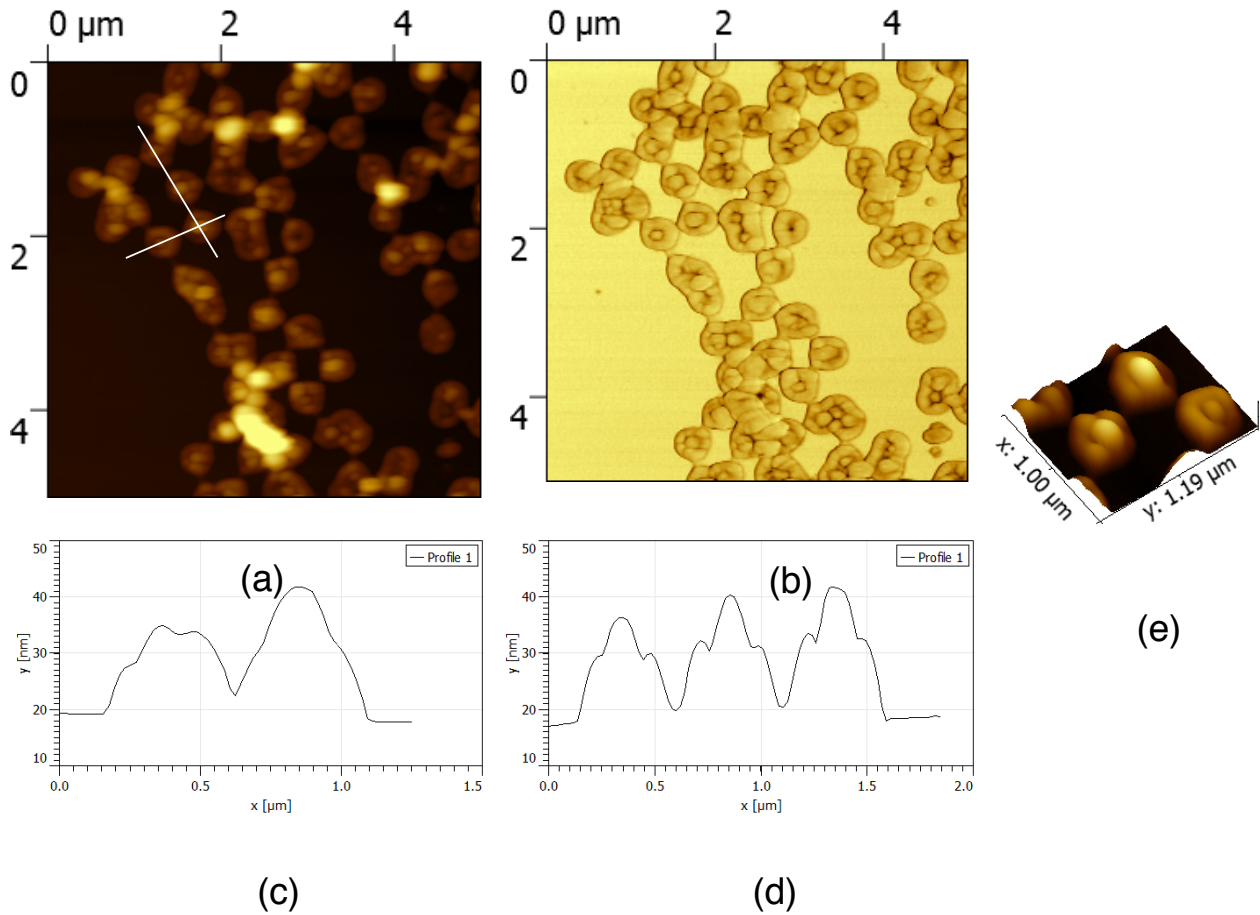


Figure 30. AFM analysis of silica ‘flowers’. (a) topography and (b) topography retrace show center particles with a ring of material surrounding it, (c) topography trace of (a) and (d) topography trace of (b) show 20 to 30 nm heights of the flower centers, (e) zoomed topography

washing step and allowed to dry. The surface was then imaged using AFM and SEM. Using contact mode of AFM, we swept across the surface, which would remove any soft material, such as papain from the surface. In this way, we are confident that the topography shown in Figure 30 is hard material: silica. Secondly, the height of these structures does not decrease over vigorous sweeps. We propose that the reaction occurred in the pores, and as the silica particle grew, it spilled over outside of the pore, causing the ring around the pore – essentially a ‘flower’, as seen by SEM in Figure 31.

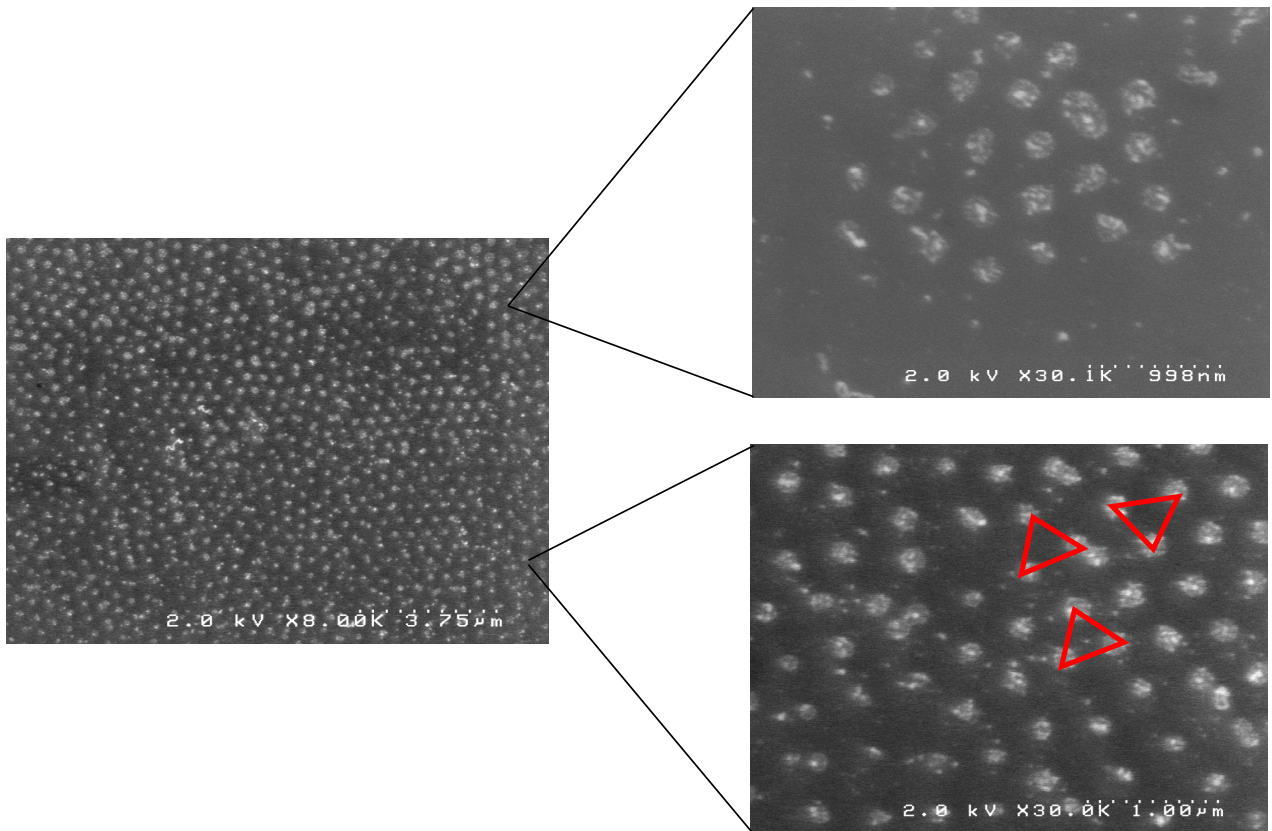


Figure 31. SEM images of silica ‘flowers’; flower size: 159 ± 17 nm; spacing 453 ± 54 nm which matches up with 500nm bead spacing of template

Conclusions

We have deposited silica ‘flowers’ with controllable spacing using a variation on nanosphere lithography. We have begun to determine the differences in templating silicon wafers with two different silanes, and we have noticed a peculiar feature of silica to silicon nanosphere lithography that begs investigation. However, we have consistently formed 1 to 2 nm pores ~ 450 nm apart across silicon substrates using trichloro(octadecyl) silane, and subsequently used these pattern surfaces to precipitate the metal oxide silica in a controlled manner using papain and TMOS.

Future Directions

There are many ways in which this project can be continued. First and foremost, the reason behind the pattern caused by the beads needs to be identified. Extra washing steps of the original bead stock will ensure that there is nothing but pure, DI water in the bead solution to cause a template. If the pattern still occurs, we need to verify conclusively the height of these rings. If the rings are much smaller than what occurs from the silane reaction, then we can differentiate between a silane templated surface and a silicon exposed, bead templated surface. Additionally, we can measure contact angles of the various substrates to determine the relative hydrophobicity of each surface. If the beads themselves do react with the substrate surface, a different type of bead could be purchased. However, because the masked silicon wafer is treated with silane, we could not use polystyrene spheres, which is typically used in nanosphere lithography.

Another way that this project is currently limited is by the difficulty in identifying silica on a silicon surface. In order to avoid this problem, a different metal oxide, such as titania which has also been shown to react with papain in Chapter III, could be formed. By using titania, EDS analysis would show differences in the background silicon substrate and the reaction formed metal oxide (titania).

Continuing this work could provide very interesting patterning techniques. Patterns could be affected by the size of the templating beads used and the length of the alkyl chain of the silane. Combined with the steps described above, these paths

provide the foundation of a solid body of work pertaining to a variation on nanosphere lithography and enzymatically controlled metal oxide formation.

CHAPTER V

DEVELOPMENT OF A SCREENING ASSAY PLATFORM AS A NOVEL APPROACH TO MATERIAL FABRICATION AND DESIGN USING THE MODEL DIATOM *THALASSIOSIRA PSEUDONANA*

Abstract

The previous chapters have investigated a few different avenues of *in vitro* metal oxide formation and patterning. In Chapters II and III, we investigated a number of biomimics that result in different reactivity levels and some different minor features of the resulting inorganic material, most notably size. In Chapter IV, we were able to begin organizing and patterning these metal oxide materials on the nano-scale, but we are still limited to mainly two dimensions. In order to expand our control over the formation of these materials, we need to investigate a new avenue of bio-inspiration. Rather than mimic another biological method of formation *in vitro*, in this Chapter we describe the development of a method to directly use a biological system to manipulate a biomineral *in vivo*. We use the diatom *Thalassiosira pseudonana*, that mineralizes silica as part of its cell wall. In doing this, we allow the diatom to form its organic framework for silica deposition and execute the exquisite hierarchical control over silica formation that it naturally possesses.

Introduction

Typical High-throughput Screening

High throughput screening (HTS) emerged as a method of testing a large volume of compounds, typically hundreds of thousands to millions over a short period of time to determine biological activity. Assays usually aim to identify compounds for therapeutics or biological probes¹⁰⁶. Biological screening assays come in two varieties: phenotypic (cell-based) and target-based (biochemical). Target-based, *in vitro*, assays are more easily adapted to the miniature HT format, in 384-well or 1564-well plates; however, they don't always perfectly represent biological, *in vivo*, conditions and don't always predict the outcomes in real biological settings. Phenotypic assays, on the other hand, are more representative of biological conditions, as the drugs are directly interacting with cells or even a whole-organism, but can be more difficult to adapt to HTS format.

In either case, the biological system must first be studied in order to represent it the best in a microtiter plate format. The workflow of designing an HTS assay is depicted in Figure 32. The type of assay must then be chosen; in cell-based assays, one must determine what phenotypic change is desired, and how they will detect this. In target-based assays, one must determine the specific target and again how this will be detected. The plate assay conditions must be optimized, and then control plates are tested to validate both negative and positive controls and verify their difference is substantial, represented by the z-factor.¹⁰⁷ As the control plates are being modified, scientists take into account a number of features, including sensitivity of their assay, plate-to-plate and well-to-well reproducibility, and even the cost. Once all of these

parameters are optimized, a pilot screen or initial test screen is performed. If needed, the optimization process is restarted until a successful screen emerges.

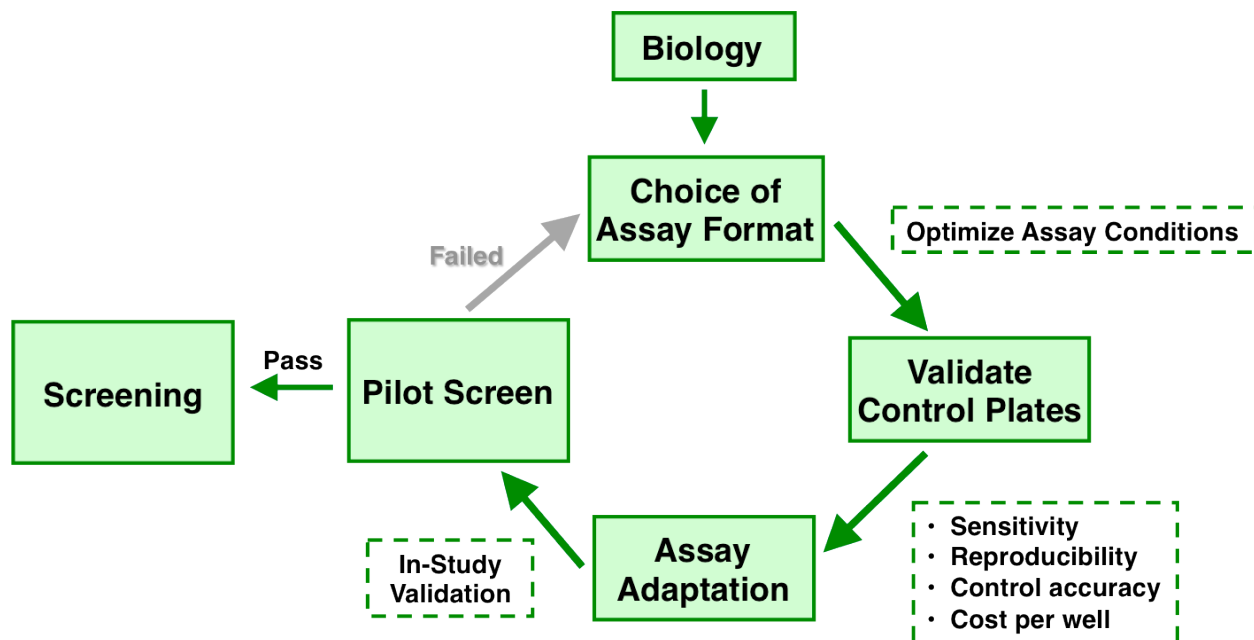


Figure 32. Typical workflow for the development of a high-throughput screen

Unique Aspects of HTS for Material Development

While screening approaches have been utilized often for drug discovery¹⁰⁸, the application of a screening technique for the development of nano-scale materials will bring an interesting combination of biology and materials science. The field of biomimetic material science involves the formation of inorganic materials on a molecular level but with control and order on a larger scale¹³. By allowing these processes to occur naturally, rather than taking the chemical mineralization process out of the biological system, we can use diatoms to design the material for us – the level of control that the organism has over its silica cell wall will be available to our materials. In this

way, we can produce with a high degree of reproducibility a large amount of non-orthogonal three-dimensional structure with nanoscale patterning; this process will also afford us the opportunity to pick exactly what type of pattern or morphology is needed for a desired use and guaranteeing a cost-effective, large quantity of material of that shape.

Diatom Screening Platform

We will exploit the diatoms' control of silica patterning by adding small molecules to the diatom environment to induce changes in the silica formation process leading to different silica frustules. This has been previously done by incorporating metal ions, such as tin¹⁰⁹, mercury¹⁰⁹, nickel¹¹⁰, and germanium, as well as small molecules¹¹¹ such as colchicine, cycloheximide, 2,4-dinitrophenol, and cytochalasin D, into the growth medium and allowing the diatoms to uptake these non-native molecules. However, there are not many molecules that have been investigated for frustule morphological changes; with this work, we aim to take these singular instances and turn them into a robust, higher-throughput screening assay. By doing this, we can more rapidly examine a large library of diverse small molecules to maximize the possible morphological changes of the frustule. In doing this screen, we propose to reach a higher resolution of inorganic material patterning that is currently difficult to achieve *in vitro*. As we have progressed through the biomimic studies, we have found that the pattern of material oxide product is still difficult to control. An understanding of the functions of these mimics is important to allow different product yields and morphologies, but the

organization of these materials on a higher level is still unattained. To further advance this field, we propose a new approach to forming materials that will be both three-dimensional and patterned on the nano-scale. We propose that this approach will lead to a variety of new patterns and shapes of inorganic material that can be chosen for use at one's discretion. Additionally, the identification of compounds that interact with the diatom and result in phenotypic changes will allow further exploration into the understanding of the biochemical processes at work.

Potential Applications

This screen has the potential to bring a variety of patterns and applications, some of which may not be realized until the completion of the screen. However, it is possible to already see the benefit of this screen in many applications, such as biosensing¹¹², filtration¹¹², gaseous chemical sensing¹¹³, microfluidics¹¹⁴, drug delivery³⁹, and energy storage¹¹⁵. Due to the alternating, periodic changes in the dielectric constant of the frustule (between the silica and air or solvent), these cleaned frustules can act as photonic crystals and exhibit interesting optical properties. Some species have been shown to have a blue photoluminescence, and a weak yellow photoluminescence¹¹⁶, that can be exploited for gas sensing, as the presence of gas molecules that adsorb to the surface has been shown to quench the photoluminescence of the frustules¹¹³. It can be imagined that differences in the pore size and patterning (that can be realized by the screening process described) will affect the surface area, which will affect gas adsorption and photoluminescent properties. Silica surfaces are also easily

functionalized, and as such can be modified with antibodies or other biomolecules; interactions at the silica surface can then be identified by changes to the luminescence spectrum (shifts, increased intensity, quenching). We propose that by changing the pore sizes and patterning of the frustule, the resulting photoluminescence will shift, or perhaps be enhanced. In this way, a variety of platforms will be available for detection of different gas molecules or for functionalization with biomolecules to create an array of detectors with different photoluminescence (and thus detection) properties. Additionally, silica can be transformed into silicon, an important conductor for electronics, *via* incubation at high temperature. This screening assay will allow us to create a library of novel silica patterns.

Chapter Aims

This chapter focuses on works towards the development of a screening assay, not the final assay results. Appropriate conditions for diatom culturing are investigated, and these growth conditions are again optimized upon translation to a microtiter plate format. With this screen we propose analyzing diatoms response on multiple levels, including diatom viability, silica content, and silica patterning. We will determine a method of consistent measurement of cell viability using cell count or chlorophyll content. We test both colorimetric and fluorescent methods of silica quantification. We test a variety of plate processing methods, focusing on removal of background signal from the cells. Much of the focus of this work looks at the first two parts of the workflow

represented in Figure 1: studying the biology of *T. pseudonana* and silica biomineralization, and optimizing the assay conditions in an HT format.

Experimental Methods

Materials

Thalassiosira pseudonana (CCMP1335) was obtained from Bigelow National Center for Marine Algae and Microbiota. LysoSensor Yellow/Blue DND-160 (L7545), CountBright counting beads (C36950), and size calibration beads (F13838) were purchased from Life Technologies. Chitin Magnetic Beads (E8036S) were purchased from New England BioLABs, Inc. Poly(ethyleneimine)-coated Magnetic Beads, 1 μm (MHE-1000-50) and 50 nm (MHE-50-25) were purchased from Ocean NanoTech LLC. Chlorophyll Reference Standard beads (898) and DAPI Reference Standard beads (906) for flow cytometry were obtained from Bangs Laboratories, Inc. A variety of 96-well and 384-well filtration plates were purchased from Millipore. 96-well v-shaped plates (3897 and 3357) were obtained from Costar. 96-deep well, large volume plates from Biotix were used. Costar flat bottom plates (3631) were used. An Aurum Vacuum Manifold (732-6470) was purchased from Bio-Rad. A 96-well plate magnet rack from EdgeBio was used. All other reagents were supplied by Sigma-Aldrich or Fisher Scientific.

Culture Conditions

Stock cultures were maintained in modified Artificial Seawater Medium recipe^{9, 30, 117} under 100 to 150 PAR in a 14:10 light:dark cycle at 18-20°C; these are typical growth conditions for *T. pseudonana*, and they grew well and didn't need further condition changes.^{118, 119} Stock solutions were maintained in autoclave sterilized 125 mL Erlenmeyer flasks, with 51 mL of culture. Approximately every 4 days, 1 mL of old cell culture was inoculated into 50 mL of fresh media.

Silica Quantification

In order to quantitate the silica of the diatom frustules, the more sensitive colorimetric assay, the reduced beta-silicomolybdate blue assay is used. Using NaOH to dissolve the frustule into silicic acid prevents formation of colorimetric complex. Thus, the assay needs to be modified to allow for dissolution by ammonium fluoride. However, NH₄F also prevents the development of the colorimetric complex (Figure 33). Using results by Proost et al, boric acid can be incorporated into the assay to reduce fluoride interference. Optimization of this was performed by a titration of ammonium

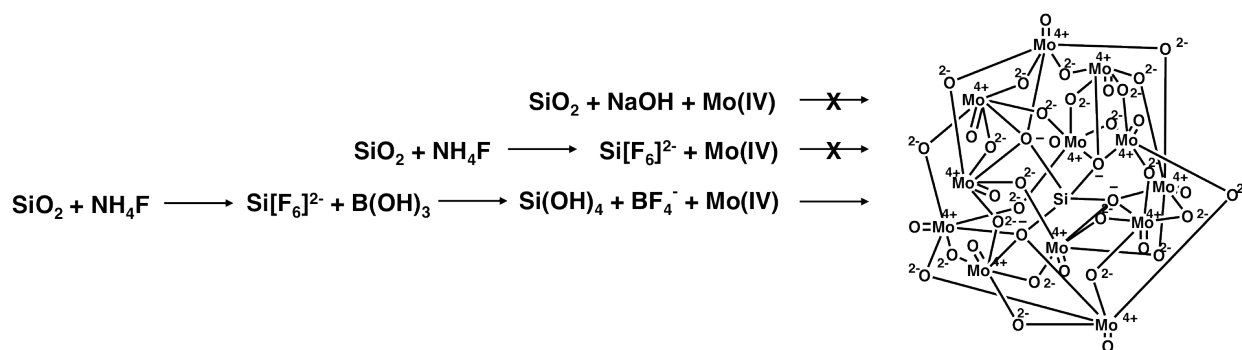


Figure 33. Schematic of the process of optimizing the Molybdenum Blue colorimetric reaction for the quantification of silicon

fluoride content with boric acid. A concentration of 400 mM ammonium fluoride for the sample was chosen, and the colorimetric assay was determined to be consistent and reliable (Figure 34). Thus, in order to quantitate silica of frustules, cell samples were

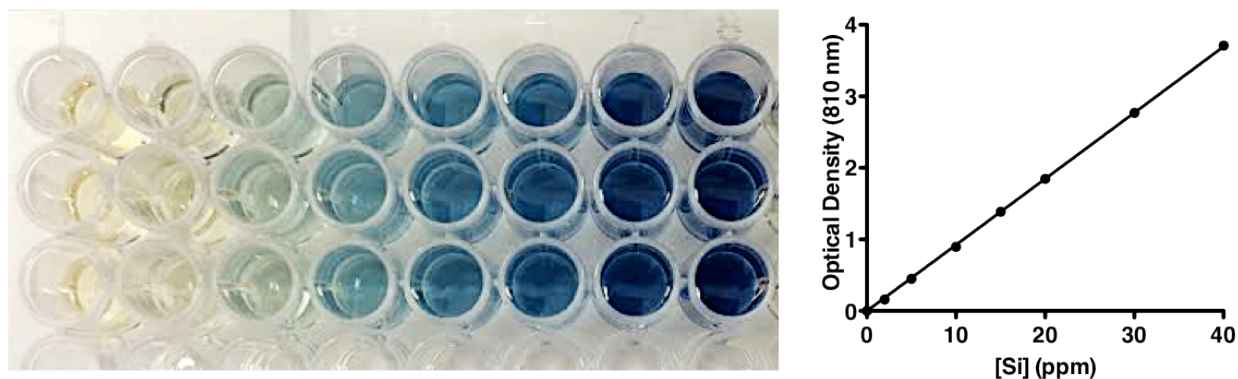


Figure 34. Optimized Mo Blue assay calibration curve, points represent mean of n=3 and error bars represent S.D.

dissolved in 400 mM ammonium fluoride at a pH of 5, 40 μ L aliquots were used in the colorimetric assay, and absorbance at 810 nm was measured using a BioTek Synergy H4 Hybrid Reader. Si content was determined by comparison with a standard curve ranging from 0.5 to 40 ppm run at each sample time.

In order to show that the colorimetric assay is accurate with respect to our conditions (*Thalassiosira pseudonana* cells), the silica content of cultures ranging in cell density from 10^5 to $4 \cdot 10^6$ was determined. A study by Hildebrand et al⁹ found that cells of *T. pseudonana* have Si contents of about 50 fmol/cell, with 20 fmol in each valve, and 4 fmol in a girdle band; the average cell has 2 girdle bands. Because these cells do not grow smaller through cell division, the cell size and silica content remains consistent over generations, a unique advantage to these cells.⁹ Using 50 fmol Si/cell as the theoretical value in Figure 35, we see that the experimental and expected results line up well across a range of cell densities. With this proof of the validity of the assay,

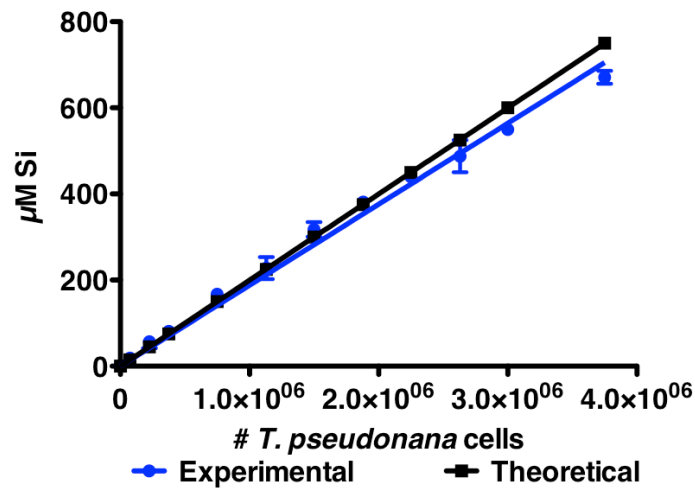


Figure 35. Experimental vs theoretical amount of Si in *T. pseudonana* using optimized Mo Blue colorimetric assay

we can use this method to quantify between 712 nM and 1.42 mM Si, which translates to ~1425 cells up to ~2.85 million cells in a 40µL sample.

Flow Cytometry

Flow cytometry analysis was performed on a BD Fortessa or Accuri C6. When samples were prepared in a 96 or 384 well plate, the HyperCyt adapter and software were used. Natural chlorophyll a fluorescence of cells was used to count and monitor cells; addition of a dye was not required. Silica content of the cells was measured with the fluorescent probe PDMPO (LysoSensor Yellow/Blue DND-160). To samples prepared in Falcon tubes, counting beads were added to get a cell count and cell density of the solution. Samples in a plate format were counted during flow cytometry analysis.

Imaging

Cells were imaged using scanning electron microscopy on a Hitachi 4600 or Zeiss MERLIN. Atomic force microscopy on cells was done on a. Transmission electron microscopy of cells was done on a CM20 Phillips. A PerkinElmer Opera Microscope was used to image samples in a plate format.

Plate Analysis and Processing

When cells were translated to the microtiter plate format, cell growth was monitored using a BioTek H4 Synergy Hybrid Reader. Chlorophyll A, present in the photosynthetic algae, was excited at approximately 380 nm and emission was monitored at 685 nm. This led to growth curves of the cells. Well-to-well variability of the chlorophyll *in vivo* fluorescence (IVF) was determined across 96-well and 384-well plates. To maintain consistency and reliability, a BioTek MultiFlo liquid handler was used to dispense reagents when possible.

In order to separate excess Si or PDMPO in the media from the cells, a number of different methods were tested. Different plate types were centrifuged to pellet the cells at the bottom of the plate, and the supernatant was removed. Supernatant cell content was measured by IVF, as described above. Filter plates were also centrifuged into a receiver plate below. Filter plates were also processed using a Bio-Rad Aurum Vacuum Manifold. Another method tested was using magnetic beads to capture the cells and magnetically draw them to the bottom of the plate with a 96-well plate magnet. Plates were washed using Si free artificial seawater medium (ASWm –Si) The number

of plate washes necessary was monitored by the amount of Si or PDMPO left in the cell media.

An alternative to separating Si and PDMPO from the media was attempted, using flow cytometry as described above. Using flow cytometry, only the fluorescence of particles, or solids in solution, like cells, that scatter light is detected. Thus, background PDMPO fluorescence in the cell medium would not be an issue.

Results and Discussion

Culturing and Cell Growth

Once a culture of *T. pseudonana* (CCMP 1335) was obtained, we determined the best inoculation conditions for continuous culturing. At the NCMA at Bigelow Laboratories, CCMP 1335 is maintained at 14°C but is viable between 4°C and 25°C. We established a culturing environment between 18°C to 20°C. In order to provide light for the photosynthetic algae, we used cool fluorescent light bulbs. Previous studies using *T. pseudonana* have light conditions between 100 and 150 PAR (photosynthetically active radiation, $\mu\text{mol photons} \cdot \text{m}^{-2} \cdot \text{s}^{-1}$), and we maintained our cultures under these conditions.^{9, 120} Light output was measured in lux using a VWR International Traceable Dual-range light meter and converted to PAR using the conversion for cool white fluorescent light of $0.013 \cdot \text{lux} = \text{PAR}$.¹¹⁹ We set our light cycle on a 14h:10h light:dark schedule.

Culture growth and cell content was measured by hemocytometer cell counts, chlorophyll a absorbance and chlorophyll a (ChlA) fluorescence in 200 μL samples in a

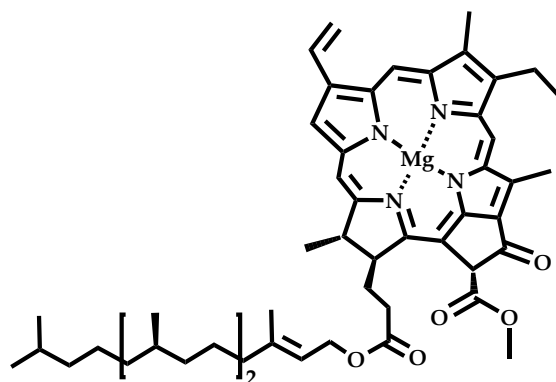


Figure 36. Structure of chlorophyll A

96-well plate. ChlA (Figure 36) absorbs light in the ultraviolet region, as well as partially at 685 nm. If excited in the UV region, at 380 nm, ChlA will emit at 685 nm, even within cells. This process is called *in vivo fluorescence* (IVF) and is commonly used as a proxy for cell content. The more cells there are, the more chlorophyll a there is, and the higher the IVF signal. While chlorophyll a content can vary across diatom species, and even within a species, diatoms maintained under consistent conditions will have stable ChlA content per cell. In fact, across a wide range of cell densities (taken from 6 different cultures over time), from <100,000 cells/mL to over 20 million cells/mL (Figure

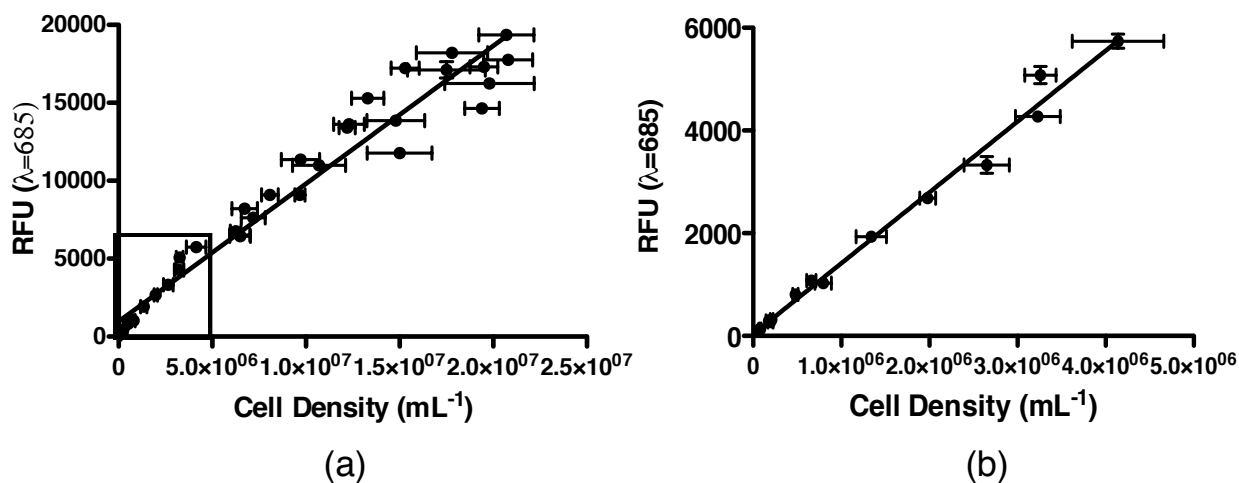


Figure 37. IVF versus cell densities (counted by hemocytometer); (a) samples of 6 different cultures counted by hemocytometer, square box represents zoomed in portion in (b)

37a), there is a linear relationship between the cell count and IVF ($r^2=0.9571$, error in slope 2.49%, $n=37$) of *T. pseudonana* cells cultured under our conditions described above. When looking at cell densities less than 5 million/mL (Figure 37b), which is a conservative limit for our assay, the correlation between IVF and cell count improves ($r^2=0.9892$, error in slope 1.98%, $n=15$).

In order to determine inoculation conditions, we added ratios of stock culture to fresh media of 1:20, 1:25, 1:50, 1:75, and 1:100 with 101 mL in a 250 mL (Figure 38a) and 51 in a 125 mL (Figure 38b) Erlenmeyer flask. Growth was then monitored over 3 weeks, and inoculation conditions of 1:50 in a 125 mL flask were chosen; inoculation was typically done every 4 days, but anywhere between 4 and 10 days would work for basic stock culture maintenance.

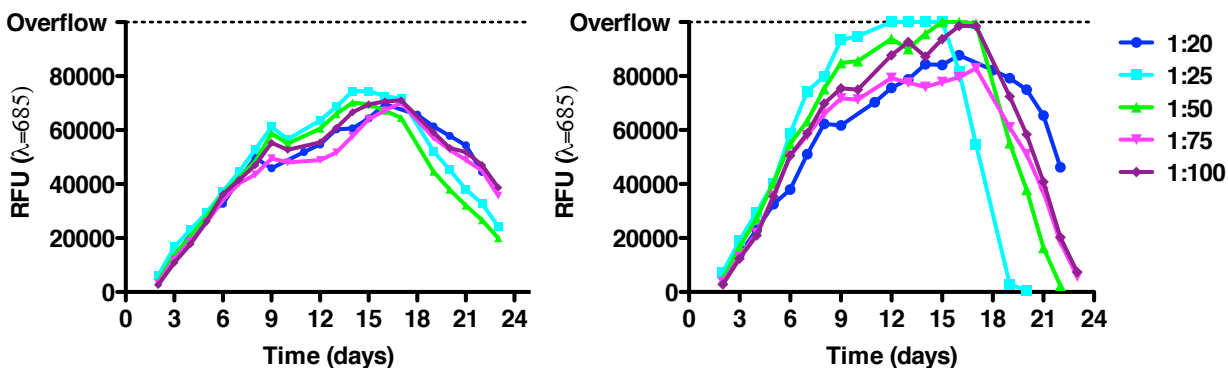


Figure 38. inoculations of stock cultures with fresh media in (a) 250 mL Erlenmeyer flasks and (b) 125 mL Erlenmeyer flasks

Under these conditions, cell growth was consistent. Cell densities of 6 different cultures were measured over the course of 7 to 9 days and found to be reliable (counts in Figure 37).

Translation to Microtiter Plate Format

In order to make the screen high throughput, we needed to translate cell growth to a microtiter plate format. The more wells/plate, the higher throughput the assay. Cells grew successfully in 24-, 96-, and 384-well plates, so we further analyzed 96- and 384-well plates for well-to-well reliability. In both the 96-well (Figure 39) and 384-well plates, the edge wells brought down the overall consistency of the plates. This is not unusual, as plate edges tend to evaporate faster than others, which affects cell

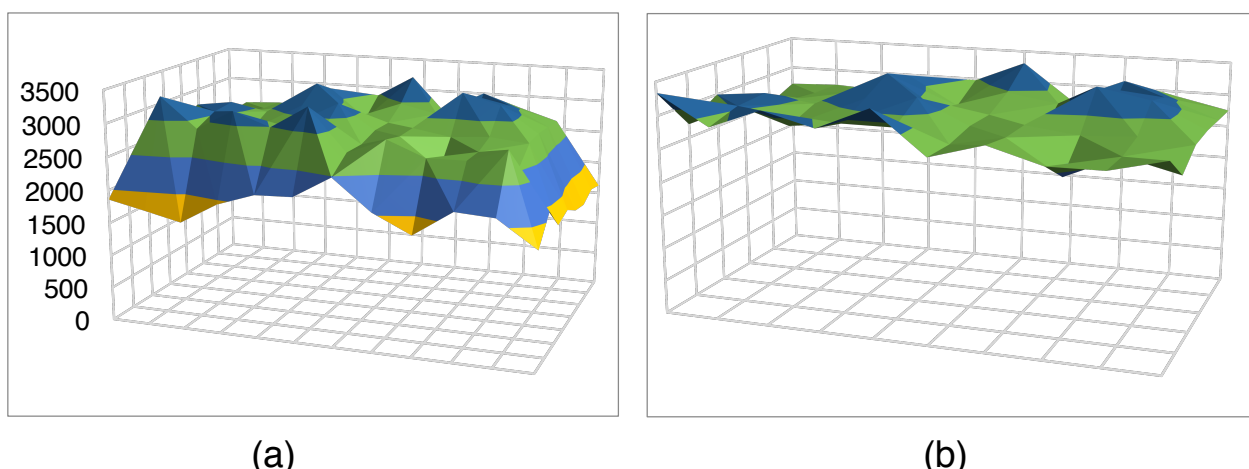


Figure 39. Edge effects of 96-well plate on Day 2 of growth; (a) all wells (b) center wells; z-axis is IVF from 0 to 3500. Blue: 3000-3500, Orange: 2500-3000, Light blue: 2000-2500, Purple: 1500-2000 growth.¹²¹ Additionally, the edge wells are not blocked on all sides by other wells, as center wells are, which may affect the amount of light hitting edge wells when compared to center wells. The edge wells in either format can be reserved for media as a blank and wells for a colorimetric standard curve or PDMPO calibration curve.

DMSO Resistance

High-throughput screening libraries, including the main set at Vanderbilt University, contain millions of stock compounds stored in DMSO. The library

compounds are added directly to the screening assay, meaning the effects of DMSO on cell growth and the cell phenotype that will be monitored must be determined. To do this, DMSO was titrated into cell culture in a 96-well plate and incubated over 4 days. The IVF was measured each day (DMSO causes no interference), and the limit to DMSO concentration that did not diminish cell growth by more than 10% was determined to be 0.1% DMSO (Figure 40). Typically, library compounds are kept in

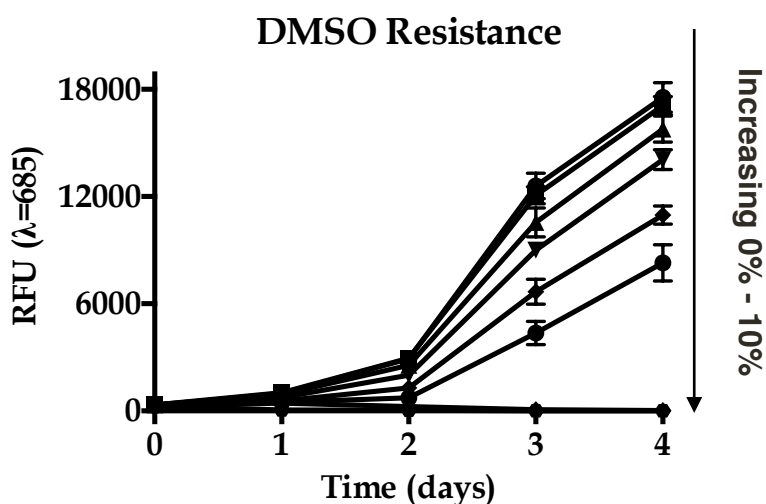


Figure 40. DMSO resistance of *T. pseudonana* culture from 0% to 10% DMSO in a 96-well plate format

stocks of 10 mM, so a 0.1% DMSO concentration limit would correlate to a maximum drug concentration of 10 μ M. While this may seem high compared to other screening assays, it should not pose a problem for this screen. In many cell-based assays, cell death is the desired phenotype since drug-discovery and therapeutics is a common goal. In our assay, however, we want *T. pseudonana* to prosper, and we only want to affect the silicon content and/or placement in their frustule. Therefore, higher

concentrations of drugs are better, so as not to cause cell death. For instance, a dose-response curve of *trans,trans*-2,4-decadienal, which causes cell death in *Thalassiosira weissflogii*¹²² reveals that after two days, the IC50 of IVF (representing cell death) is $1.147 \pm 0.008 \mu\text{M}$ (Figure 41a). Cells with low concentrations of drug, those less than 1

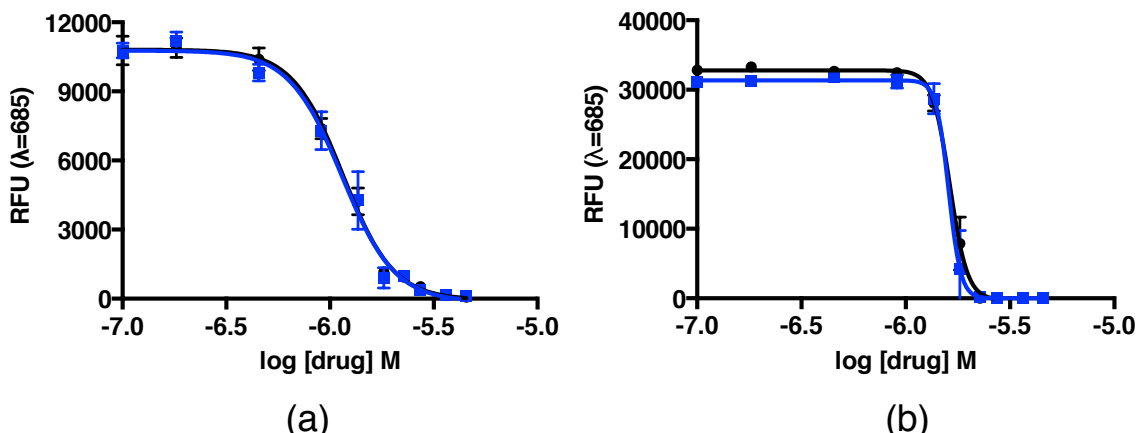


Figure 41. Dose-response curves of *T. pseudonana* after (a) 2 days and (b) 6 days incubated with *trans, trans*-2,4-decadienal in a 96-well plate format. Cell viability is measured by IVF; blue and black lines represent different trials, points represent triplicate means and S.D. error bars μM began to recover their growth slightly, and by day 6, the IC50 is $1.61 \pm 0.02 \mu\text{M}$ (Figure 41b). From this we can see that, at least for this drug, concentrations of $1 \mu\text{M}$ may start to affect cell viability, measured by IVF. Therefore, performing this screening assay at DMSO concentrations less than 0.1% will not be an issue.

PDMPO Fluorescent Probe for Silica Quantification and Imaging

The formation of new silica can be tracked and monitored by using the pH dependent fluorophore, PDMPO (Figure 42). This probe, {2-(4-pyridyl)-5-((4-(2-dimethylaminoethylaminocarbonyl)methoxy)phenyl)oxazole}, is a dual excitation/emission probe that can be taken up by the diatom into acidic environments,

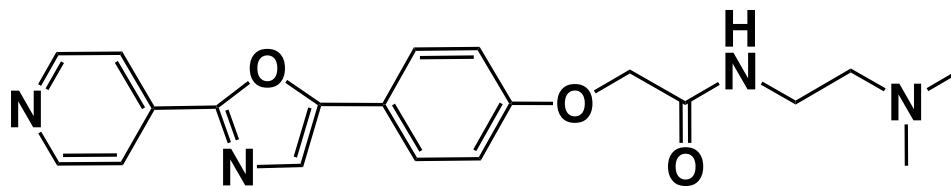


Figure 42. Structure of PDMPO (LysoSensor Yellow/Blue DND-160).

such as the silicon deposition vesicle (SDV). Here, as polymerization occurs, the probe is incorporated into the growing frustule as new silicic acid is polymerized¹²³. This probe can then be used to monitor changes in the amount of silica that has formed in the wells, as well as to image the resulting frustules. Because PDMPO has dual excitation/emission properties that correspond to pH environment, it is typically used as a ratiometric pH monitor. At pH 3 or below, the emission of PDMPO centers around 540 nm. As the pH increases over 3, the emergence of a second peak, or shoulder, at 450 nm occurs (Figure 43a). The differences in these profiles allows a ratio of the two peaks to be taken to determine the pH. Interestingly, this emission change is also

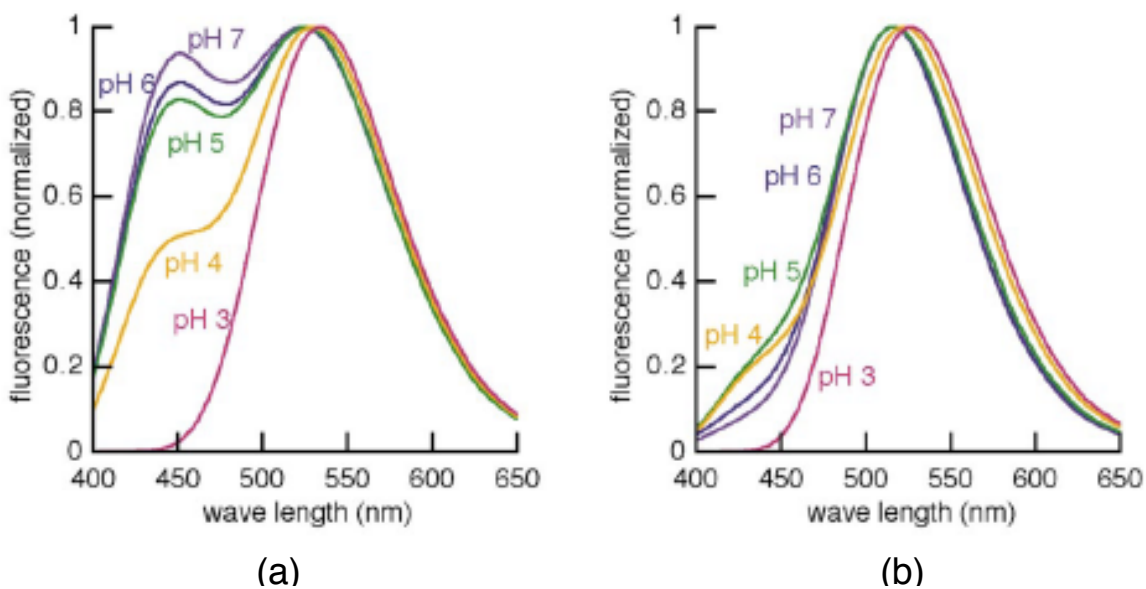


Figure 43. PDMPO fluorescence and emission profiles at varying pH conditions in the (a) absence and (b) presence of polymerized silicic acid (silica) as observed by Shimizu et al⁵; PDMPO is added to buffer

induced by the incorporation of PDMPO into polymerized silica.⁵ When it is incorporated into silicic acid oligomers, the emission profile at any pH will be one peak centered around 510 nm (Figure 43b) rather than two peaks at 450nm and 510nm when pH conditions are above 3. Therefore, in a neutral or basic conditions, like those of ASWm used to culture cells, the PDMPO profile in the background medium is different than the PDMPO profile in silica (Figure 44a).

In order to investigate this property, we wanted to verify the different profiles of PDMPO outside of biological conditions. In ASWm (pH 8), we added 1 μ M PDMPO to all samples. In triplicate, we titrated in silicic acid from 0 to 80 mM.⁵ At concentrations above \sim 2 mM, silicic acid will self-condense into silica oligomers. Therefore, we can see that as the concentration of $\text{Si}(\text{OH})_4$ increases, the ratio of the fluorescence at 510 to 450 increases (Figure 44b), as the emission profile shifts from two peaks at 450 and 550 nm (Figure 44a, blue) to one peak at 510 (Figure 44a, black). While this concentration of silica is much higher than would be found in the frustules of diatoms,

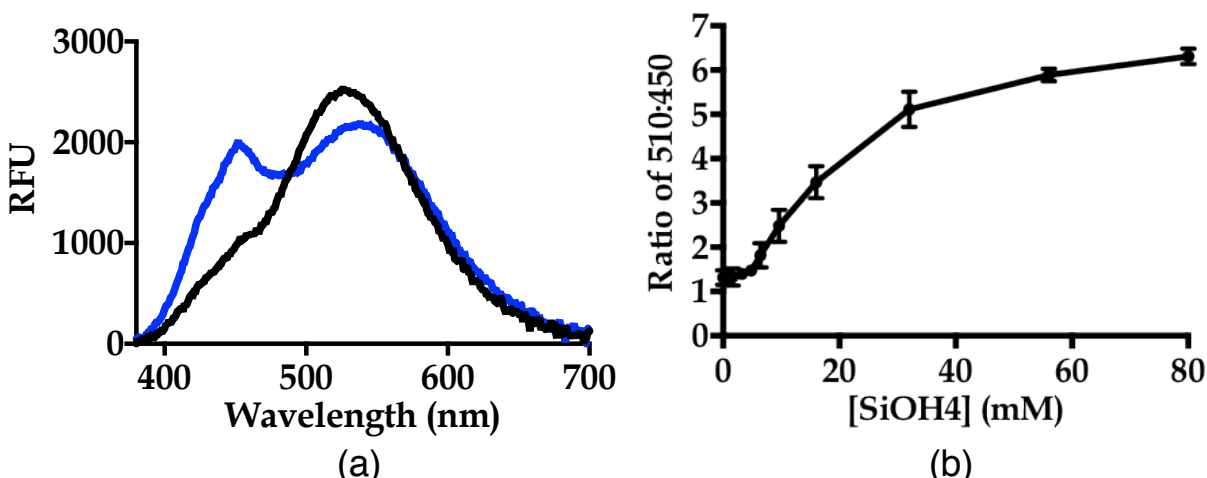


Figure 44. (a) PDMPO emission in the presence (black) and absence (blue) of silicic acid at pH 8 (b) ratio of PDMPO fluorescence at 510 to 450 as a function of silicic acid concentration, collected by Summer Arrowood

we need to use high concentrations to induce condensation of silicic acid to oligomers at pH 8. In the screen, however, *T. pseudonana* will condense the available silicic acid and PDMPO into silica.

In order to test this probe for our assay, we needed to determine how it would interact with *T. pseudonana*. In order to do this, we starved cells of Si, an essential nutrient for their growth, in order to synchronize them according to previously published work.⁹ After 24 hours, cells were plated into a 96-well plate and treated with PDMPO and either Si or media. Cells that had Si added back to them would begin growing, and cells where Si was not added would remain arrested at the same stage in their cell cycle. Therefore, we expected the ratio of fluorescence at 510 to the fluorescence at 450 to be the same for all conditions where Si was solely in the media, and for the ratio to differ only in those wells where cells were actively growing, making new frustules, and had PDMPO in the media. This is exactly what we saw (Figure 45). In two separate trials, we saw consistent values for the ratio of the 510:450 emissions of

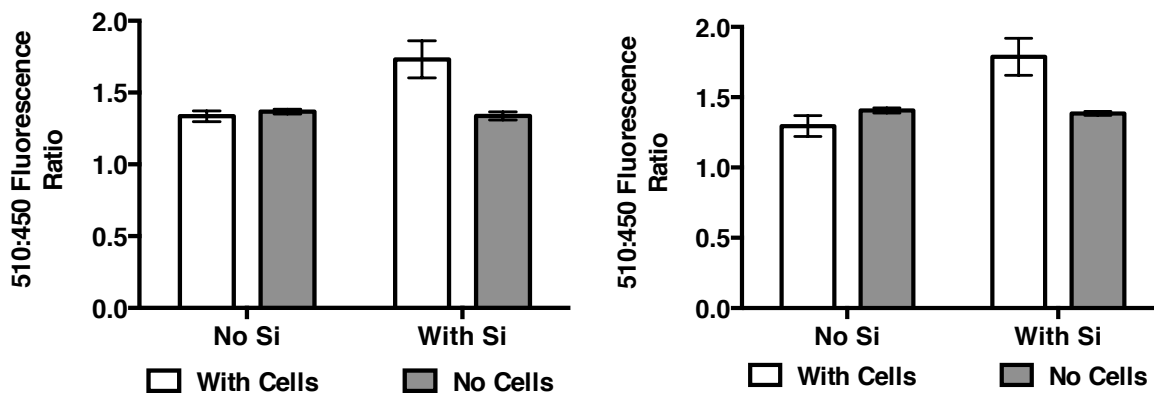


Figure 45. Two different trials of cells or media incubated with PDMPO with or without silica. White bars represent mean of n=15 and grey bars represent mean of n=3; error bars are S.D.

PDMPO, in the presence of cells that were not actively growing and in media where there were no cells, and therefore no polymerized silica.

Due to the low linear range available for PDMPO incorporated into a frustule vs left in the media, we run into a similar issue as with Si colorimetric quantification: there will be excess background signal that will interfere with our ability to detect cell Si and frustule changes. Like with Si, we don't want to limit the PDMPO available to cells, both of these need to be in excess concentrations. Therefore, we need to impose washing steps in order to separate media from the cells.

Plate Processing by Cell Separation

In order to remove excess elements of the media that may interfere with detection (either Si or PDMPO), we attempted a few separation techniques. One typical method for harvesting diatom and other alga cells involves centrifugation at low speeds to pellet the cells. We used centrifugation of plates to pellet cells at the bottom of the

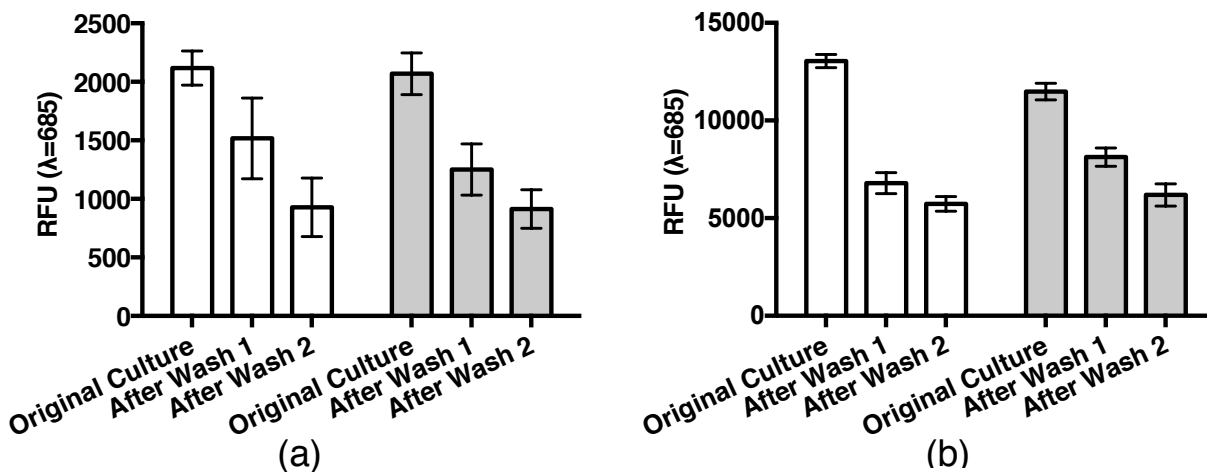


Figure 46. 250 μ L of cell culture in 96-well plates were washed after (a) 1 day and (b) 3 days of growth; white and gray bars represent 2 different trials of n=60

plate; the supernatant was then removed and tested for cell content and Si content. In flat bottom plates, the cells essentially coat the entire bottom, and the loss of cells when removing the supernatant is significant (Figure 46). However, silicon in the media is negligible after two washes. An alternative to this that still retain the high-throughput format are v-well plates, which will allow the cells to pellet specifically into the trough of each well.

In a 96-well v-shaped plate, cells were added to the center 80 wells (columns 2-11) and ASWm was added to the outer 16 wells in columns 1 and 12. The plate was centrifuged at 3000 rpm, and the supernatant was removed and added to a second plate. ASWm was added to the original plate, and the process was repeated twice. Each step was measured for IVF. While most cells were retained and very few were lost, after 2 washes the %CV across the plate was larger than 10% (Figure 47), which is above the threshold for a good high-throughput screening assay. This means that the few that were lost were randomly distributed across the plate, increasing the error across the plate as a whole.

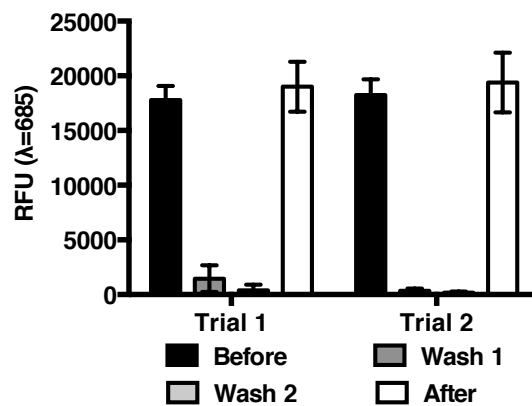


Figure 47. IVF of *T. pseudonana* during series of washing steps in 2 96-well v-bottom plates

To avoid centrifugation to pellet the cells, we studied 96-well and 384-well plates that have a filter bottom to retain material, typically using a molecular weight or size cut-off, in the wells. We used 0.4 μm filter sizes that would let the media and subsequent wash steps flow through and retain the cells ($\sim 2 \times 2 \times 4 \mu\text{m}$). We used two techniques to separate through the filter: centrifugation into a receiver plate or an Aurum Vacuum Manifold.

For an HTS assay, the number of transfer steps should be minimized, and ideally there would be none. We tested how well the filter would stand up to NH_4F to determine if the cells could be digested in the plate. 12 samples of 40 ppm Si in 200 mM NH_4F were added to each of two different plates. 12 samples of 0 ppm Si in 200 mM NH_4F were also added to each plate. Plates were incubated for 1 hour and centrifuged at 1800 rpm, followed by colorimetric determination of the stocks before filtration and the samples after filtration (Figure 48) in a new plate. There was no background signal from 0 ppm Si in 200 mM NH_4F above the limit of detection. We

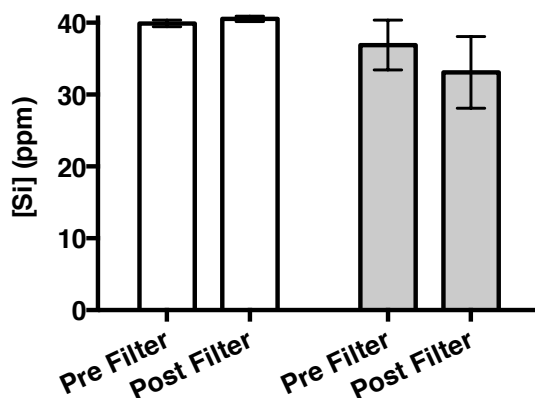
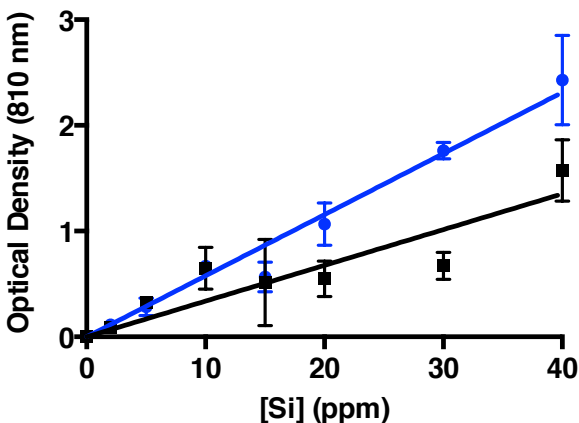


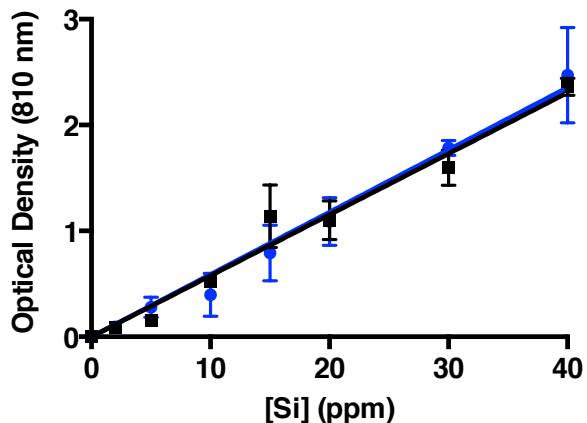
Figure 48. 40 ppm Si samples from pre and post filtration through a 96-well filter plate; grey and white represent different trials

concluded that cell samples could be dissolved using NH_4F without destruction of the filters and without interference in a subsequent colorimetric assay.

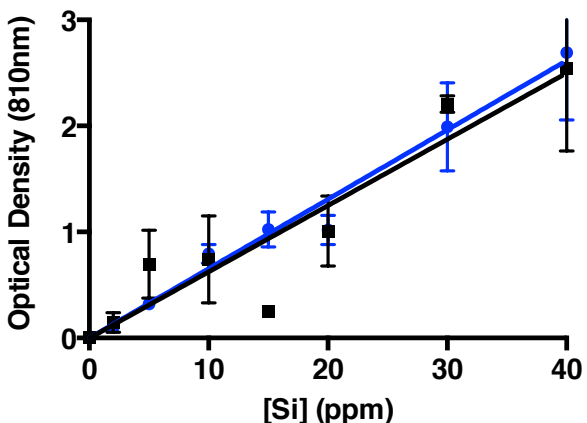
To determine the accuracy of how well samples would flow through the filter, so as to eliminate the need to transfer some of the sample to a new plate using liquid handlers, we added Si standards (Figure 49a-c) and Si samples of 40 ppm (Figure 49e) to 3 96-well plates. In this case, we did not add excess volume; we added 40 μL samples. In this way, the receiver plate could be directly used for colorimetric detection. We used the vacuum manifold to process the plates. We found that while the samples did average an accurate concentration, the variability across the samples was much higher than 10%, even as high as almost 30%. We also found that the standard samples had very high variability, and the sensitivity of the colorimetric assay suffered compared with typical conditions (Figure 49d). Essentially, eliminating the transfer step after filtration is not going to be possible for a robust assay. This also means cells will be dissolved in more than 40 μL of NH_4F , diluting the end signal. Using centrifugation to filter through the plates, rather than the vacuum manifold, saw similar results, with very high error across the samples and a decreased sensitivity of the colorimetric assay.



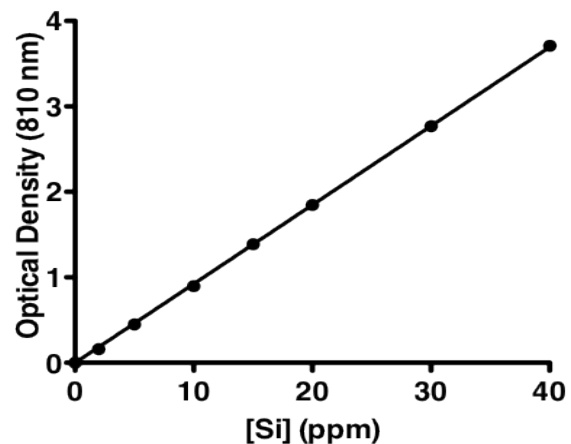
(a)



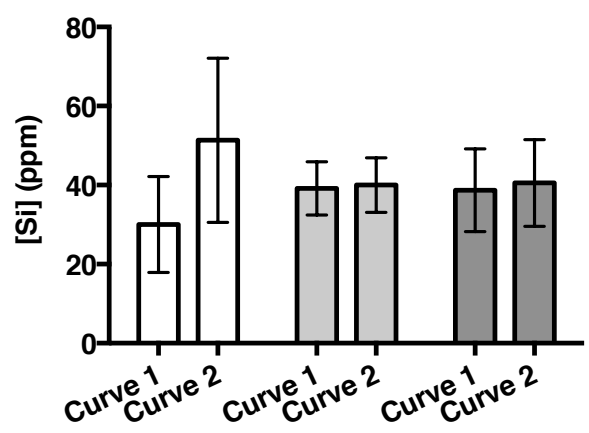
(b)



(c)



(d)



(e)

Figure 49. (a-c) calibration curves from 3 different filter plates after filtration *via* centrifugation, with decreased sensitivity when compared to (d) a calibration curve unfiltered, and (e) Si content of 40 ppm Si samples in 3 different plates (different shades of gray)

Lastly, cells do not grow well in 96-well filter plates (Figure 50a, blue), and they do not prosper at all in 384-well filter plates (Figure 50b, blue). Cells would have to be incubated in a normal plate for the assay and transferred to the filter plate for processing before analysis. Therefore, without a better technique for separating cells from the media, we needed a new way to analyze the cells.

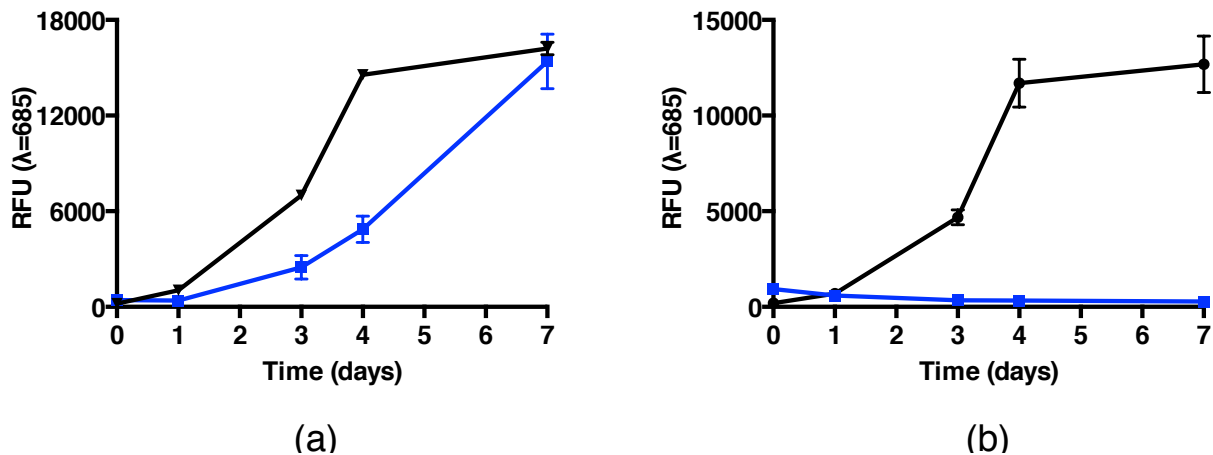


Figure 50. *T. pseudonana* growth measured by IVF in flat bottom (black) or filter (blue) (a) 96-well plates or (b) 384-well plates

Most of the problems discussed so far arise from the fact that these are non-adherent cells, yet they need to be washed for either PDMPO or colorimetric detection. We hypothesized that if we could capture the cells onto magnetic beads during processing, we could make them essentially 'adherent' using a plate magnet. One way of separating recombinant proteins is by expressing them with a chitin binding domain (CBD) and purifying them using chitin magnetic beads. Many cells express proteins with chitin binding domains naturally, and at least one has been identified in the cell wall of *Thalassiosira pseudonana*.¹²⁴ *Thalassiosira pseudonana* cells produce chitin, some of which is associated with the cell wall¹²⁵, and therefore it is likely there are multiple

CBDs associated with their frustules. Using this information, we incubated *T. pseudonana* culture (~2 million cells/mL) with chitin magnetic beads in a 1:1 v/v ratio or with chitin binding buffer and measured the IVF of the supernatant after one hour. Even with the bead stock undiluted, there was no statistical difference between the supernatant of cells incubated with beads and those without (Figure 51).

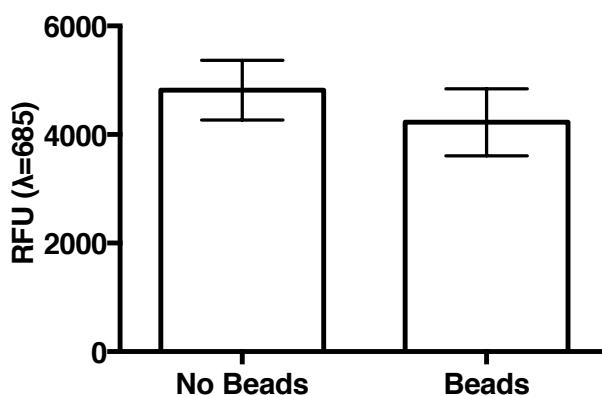


Figure 51. IVF content of supernatant of *T. pseudonana* culture incubated in the presence and absence of chitin magnetic beads

We also investigated electrostatic interactions to separate cells from the surrounding media. Algae have been studied as a source of biofuel¹²⁶⁻¹²⁸, so their harvesting has become an area of interest in recent years.¹²⁹ A newer harvesting method involves the magnetic separation of cells by tagging algal with magnetic particles *via* electrostatic interactions between the negative alga and a positively coated magnetic particle.¹³⁰ Magnetite particles are typically coated with a cationic natural or synthetic polymer, and polymers such as polyethyleneimine (PEI) and chitosan have been studied.¹³¹ We titrated PEI-coated magnetite (Fe₃O₄) particles (50 nm) into cell

culture in microcentrifuge tubes; we measured the supernatant for cell content using IVF (Figure 52). As the number of beads added to the culture increases, the cell content in

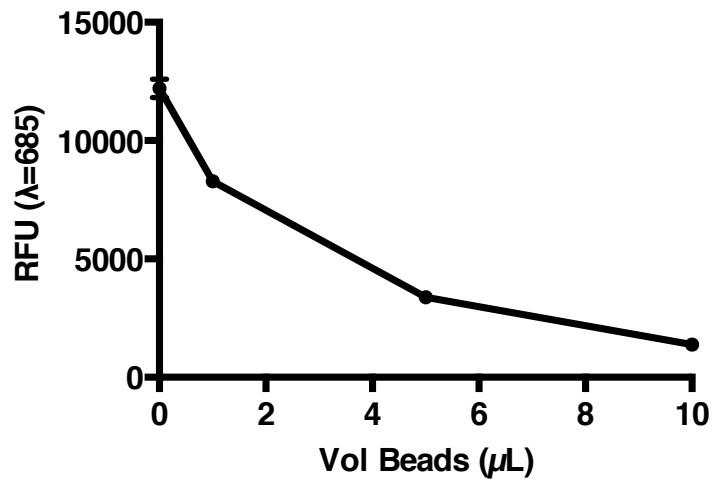


Figure 52. IVF of cell culture supernatant when treated with varying amounts of PEI-coated magnetic particles

the supernatant decreases. When translating this method to a plate format, the beads tended to spread across the bottom and would get caught in the supernatant of washes. While doing this by hand allows the operator to carefully try and avoid the beads, an automatic liquid handler may get the beads. To facilitate the beads grouping at the edge of the wells, the surfactant tween-20 was added to the bead stock. This helps to reduce the interaction of the magnetic particles with the polystyrene plate. Repeating the titration in a plate format (cell density $1 \times 10^6 \text{ mL}^{-1}$), we found that with just 5 μL of beads (50 μg), we could capture 100% of cells from the media. Using 10 μL of beads (100 μg) reduced the amount of cells lost in one wash to less than 10%, according to IVF (Figure 53). Two washes sufficed to remove excess silicon from the media and one wash was enough to remove PDMPO.

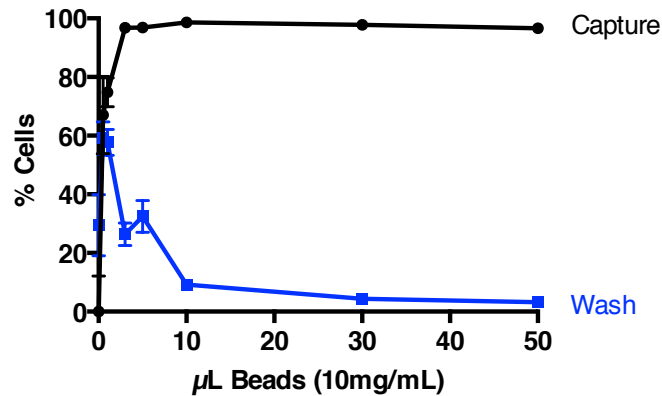


Figure 53. Percentage of cells captured (black) by PEI magnetic particles and washed away in one water wash (blue)

In order to elute the cells off the beads once the capture and washes are complete, we used different methods to disrupt the electrostatics. We used both high and low pH conditions to elute cells from the beads; we incubated cells with beads, washed them twice, and then used NaOH (Figure 54a) and HCl (Figure 54b) to elute off the beads. Subsequent titrations revealed that altering the pH of the solution would not be the

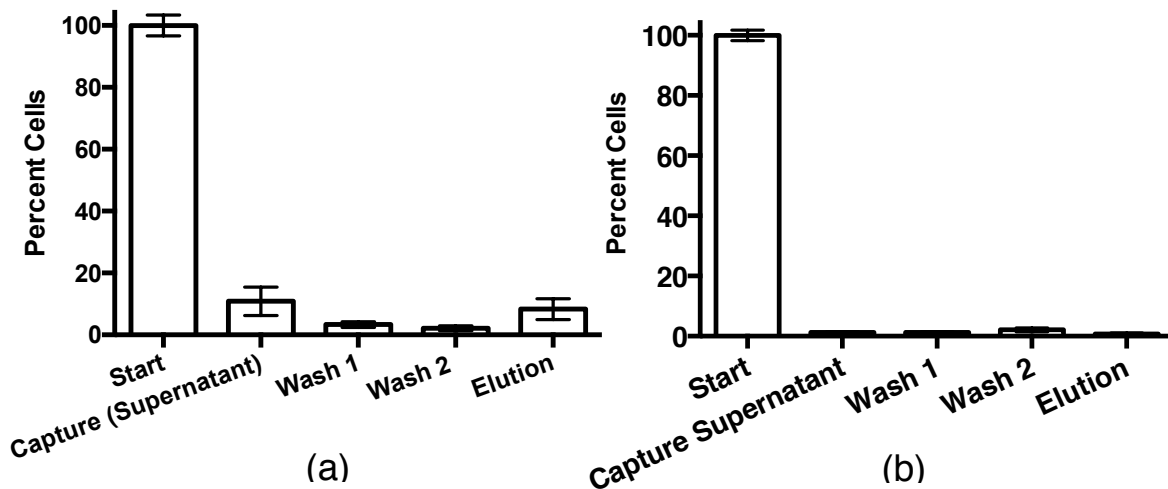


Figure 54. Percentage of cells in the supernatant of various steps in the processing of cells with elution steps by (a) high pH and (b) low pH conditions

strategy for elution in this assay. A titration of salt conditions is the next step for using this avenue for the screening assay. However, as this part of the project progressed, I also investigated developing this project as a flow cytometry screening assay.

Flow Cytometry as an Alternative to Washing

Flow cytometry is a technique that allows for the detection and analysis of cells as they flow one-by-one past a laser. Due to this, signal is only generated when a solid particle (such as a cell) interrupts the laser beam, and small molecules dissolved in solution, like the PDMPO probe, won't be detected.

Using a 384-well plate format, the cell counting using flow cytometry versus a hemocytometer was compared. As seen in Figure 55, these techniques line up well, particularly at concentrations of 6 million cells/mL, which is far more than would be found in our assay.

We needed to verify that the PDMPO probe would be detected by flow cytometry when it was incorporated in the frustule. Cells were incubated overnight in silicon-free

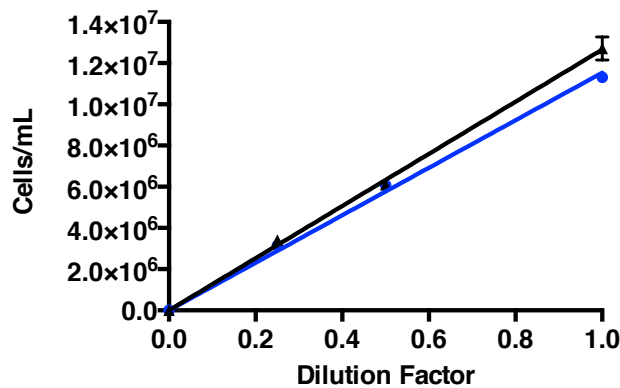


Figure 55. Comparison of cell density calculated by hemocytometer counting (blue) and flow cytometry (black)

media. In triplicate, cells were given a combination of Si or H₂O and PDMPO or DMSO: +Si/+PDMPO, +Si/-PDMPO, -Si/+PDMPO, -Si/-PDMPO. Cells were then allowed to grow overnight and were analyzed by flow cytometry. 20 μ L from each well was sampled. As seen in Figure 56a, cells grew when incubated with Si, and PDMPO (grey) did not affect *T. pseudonana* growth. Event populations were gated as PDMPO positive or PDMPO negative, and cell wells not incubated with PDMPO showed less than 0.1% positive cell events. There was a statistical difference in cells incubated with PDMPO in the presence vs the absence of silicon (Figure 56b). However, this difference was very slight. Over 80% of cells still showed PDMPO incorporation. In order to use this as a

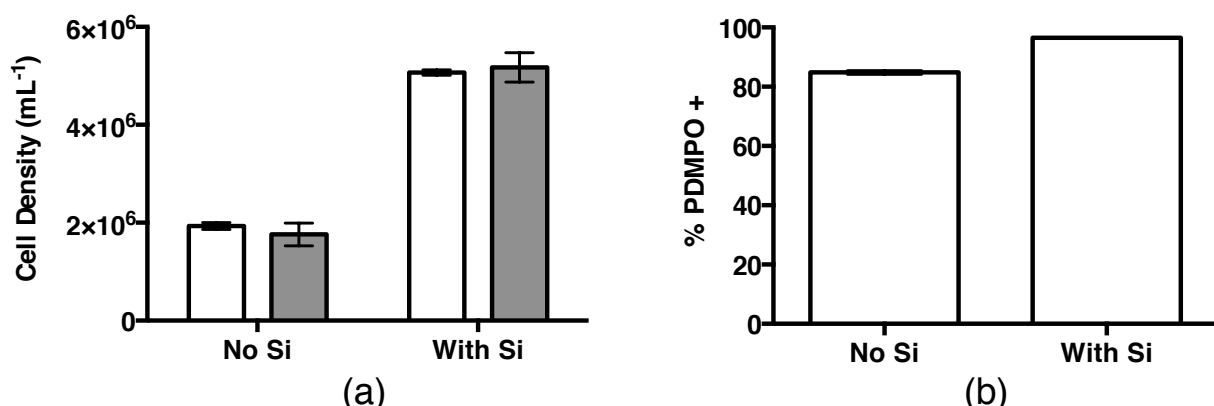


Figure 56. Flow cytometry analysis of cells incubated with or without PDMPO in the presence or absence of Si, (a) cell densities show PDMPO does not affect growth, and Si increases cell density and (b) percentage of PDMPO positive cells increases when actively growing (+Si)

reliable method of detection in the HTS assay, we needed to bring down the background signal of non-actively growing cells incubated with PDMPO. To find a more ideal concentration, cells were incubated in silicon-free media and titrated with PDMPO to determine if the concentration of PDMPO was too in excess. However, analysis by flow shows that even concentrations as low as 50 nm would lead to 80% PDMPO positive cells (Figure 57).

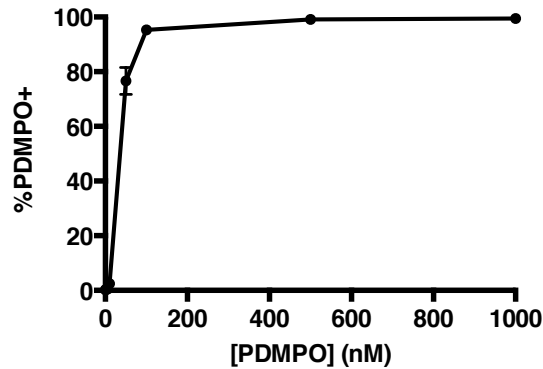


Figure 57. Percentage of PDMPO positive cells as a function of PDMPO concentration

We hypothesized that the signal could be due to PDMPO incorporation by passive uptake as PDMPO diffuses into the cell across the concentration gradient. To investigate this, we proposed lysing the cells so that any internal PDMPO, not incorporated into the frustule, would be part of the background media that is undetectable by flow.

Cell lysis disrupts the PDMPO signal inside the cell, but it also disrupts the chlorophyll a signal. Because this signal was the main method of determining positive cells in flow cytometry, we needed to determine if cells could be positively identified without the ChIA signal. To do this, we compared both unlysed and lysed samples. Interestingly, we found that the Triton X-100 surfactant used to lyse open cells enhanced the chlorophyll a fluorescence; any small bits of chlorophyll a left associated with the cell frustule were picked up on flow easily regardless of the cell's pre-lysed state (actively growing or not). Other features of flow cytometry measurements were altered by lysis as well, including the "forward scatter", which represents the way the laser scatters as the cell passes through. Due to this, we could not confidently gate cells without the IVF signal (Figure 58).

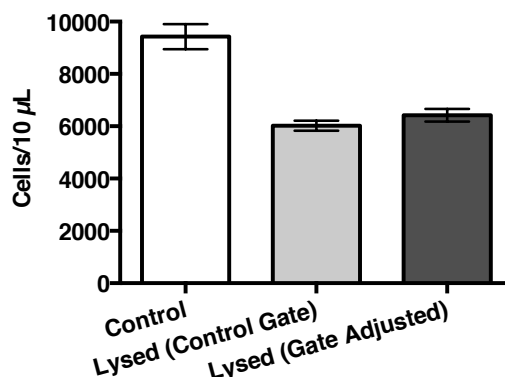


Figure 58. Cell counts in cells unlysed vs lysed, using the same gate (white and light gray), and by gating the lysed population directly (dark gray): lysis affects cell detection by flow cytometry

Limitations and Future Work

During development of this screening assay, a lot of progress was made towards understanding the best growth conditions, and the different types of analysis that could be used to quantitate and image silica in diatom frustules. Unfortunately, there are a number of technological limitations hindering this assay.

One current limitation is in the resolution of confocal, plate imaging. A high content, imaging screen was originally designed to be a secondary screen, to image only the compounds identified as hits during the primary screen. However, it is possible to use an imaging screen as the primary screen. At $\sim 2 \times 2 \mu\text{m}$, these cells are smaller than many cells used in typical assays. In order to investigate the differences between frustules, the resolution of a confocal microscope with a plate adaptor would need to be increased. For instance, using the OPERA confocal microscope on *Navicula radiosa* cells ($\sim 10 \mu\text{m} \times 40 \mu\text{m}$ cells) stained with PDMPO, we still don't see clear patterns in the frustule (Figure 59).

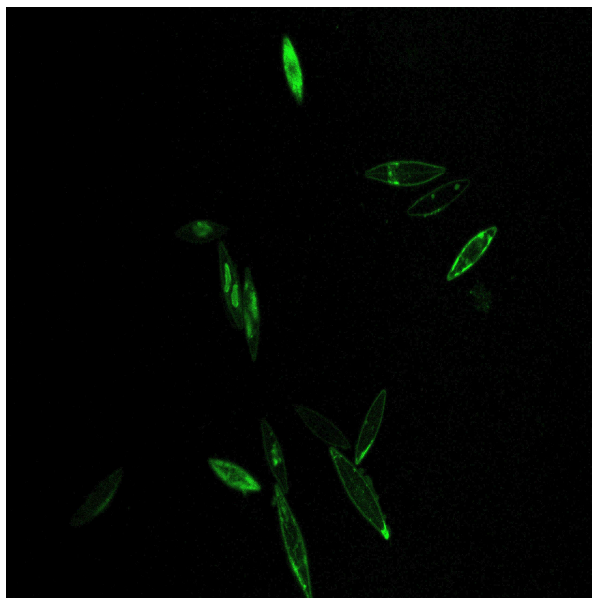


Figure 59. Confocal microscopy image of *Navicula radiosa* diatoms stained with PDMPO

Another limitation that plays into the limitation in imaging is the fluorescent probe PDMPO. This probe has a high background signal, regardless of silica presence or pH, because it fluoresces under all aqueous conditions. This puts a significant limit to the linear range between the negative signal and the positive signal. Additionally, there appears to be serious probe signal in non-growing cells, whether by passive diffusion or simple association with the outside of the cell, that decreases the linear range between negative and positive signal. Various other probes that were expected to give no fluorescence in basic conditions, like those of the background media, did not perform well with *T. pseudonana*. The development of a probe like PDMPO that will fluoresce in the presence of polymerized silica, but not in acidic conditions like the silicon deposition vesicle or basic conditions like the growth media, would significantly increase the linear range and the differentiation between positive and negative signal.

A third limitation is the methods available for separation of non-adherent cells. Essentially, none of the current techniques described above are viable options except for magnetic separation, which has the potential to work. Unfortunately, the scope of this research did not fully uncover the possibilities of this technique. The most important next step in developing this assay without separate technological advancements would be exploring the elution of *T. pseudonana* cells from PEI-magnetic particles or investigating another magnetic tagging method.

CHAPTER VI

RESEARCH SYNOPSIS AND FINAL THOUGHTS

This dissertation focused on the *in vitro* and *in vivo* studies of biosilicification in two different biological systems: diatoms and sea sponges. In Chapter II, we investigated PAMAM dendrimers with varying terminating groups to determine their ability to precipitate silica and titania from their respective precursors. We found that the PAMAM dendrimers reacted with TMOS, TEOS, and TiBALDH to form a range of sizes of silica and titania particles. The size of the resulting particles and the reactivity of the dendrimers was particularly affected by electrostatic interactions between the precursors, the growing metal oxide, and the dendrimers themselves. While we found that we could control the size of metal oxide spheres, we still did not have control over the overall patterning of the material.

In Chapter III, the protease enzymes trypsin and papain were studied as biomimics of the sea sponge enzyme, silicatein. We hoped to discover the role of the hydrolytic active site of the proteases in the formation of the metal oxides silica and titania. We found that, despite being a member of the same family as silicatein, papain was not a direct biomimic of silicatein; the active site of papain was not responsible for hydrolyzing the TMOS substrate. Trypsin, on the other hand, did require the active site to hydrolyze the TMOS substrate. We hypothesize that this difference is due to the decreased positive charge of the trypsin surface compared to the papain surface, which

doesn't allow for as much localization of the relatively negative TMOS, or the hydrolysis by amine groups. Neither enzyme requires the active site to hydrolyze TiBALDH, likely due to the increased susceptibility to nucleophilic attack with respect to TMOS. Like in Chapter II, we found interesting differences in the reactions and morphologies of metal oxides precipitated using these protease enzymes, but we still lacked control over the overall patterning.

Chapter IV focused on increasing our control over metal oxide material patterning using a variation on nanosphere lithography. By combining the results and knowledge gained from Chapter III with a twist on a current bottom-up approach, we were able to precipitate interesting silica 'flowers' into an organized fashion on a substrate. While our control was limited to two-dimensions, I believe that future work developing this technique could begin to see control over the third-dimension. Metal oxide features could be grown up vertically from the pores, and a variety of templates could be created using different masking conditions.

Lastly, Chapter V investigated a new approach to material development. Instead of mimicking biological processes, we aimed to allow these processes to occur in their biological environment, while probing different results using small molecules. We worked towards developing a screening assay of the diatom *T. pseudonana* to probe the silicon metabolic cycle with small molecules in order to affect the frustule formation and patterning. While a lot of interesting information came out of this work, there are still questions to be answered in order to finalize the screen. The most important question to answer to move this project forward without waiting for other technological

or scientific advancements is “can we separate cells from background media in a robust, reproducible fashion?” I believe that with magnetic beads bound to cells, whether through electrostatics or another tagging method, this goal can be achieved.

The work described in this dissertation adds knowledge to biomimetics, enzyme silicification in sea sponges, and nanolithography approaches, and paves the way for increased information about the biosilicification processes in *Thalassiosira pseudonana* and other diatoms as well as the enzymatic control in sea sponges.

REFERENCES

1. Hagino, K.; Bendif, E.; Young, J. R.; Kogame, K.; Probert, I.; Takano, Y.; Horiguchi, T.; de Vargas, C.; Okada, H., NEW EVIDENCE FOR MORPHOLOGICAL AND GENETIC VARIATION IN THE COSMOPOLITAN COCCOLITHOPHORE EMILIANA HUXLEYI (PRYMNESIOPHYCEAE) FROM THE COX1b-ATP4 GENES. *Journal of Phycology* **2011**, *47* (5), 1164-1176.
2. Kroeger, N.; Deutzmann, R.; Sumper, M., Silica-precipitating peptides from diatoms: The chemical structure of silaffin-1A from *Cylindrotheca fusiformis*. *Journal of Biological Chemistry* **2001**, *276* (28), 26066-26070.
3. Foo, C. W. P.; Huang, J.; Kaplan, D. L., Lessons from seashells: silica mineralization via protein templating. *Trends in Biotechnology* **2004**, *22* (11), 577-585.
4. Otzen, D., The Role of Proteins in Biosilicification. *Scientifica* **2012**, *2012*.
5. Shimizu, K.; Del Amo, Y.; Brzezinski, M. A.; Stucky, G. D.; Morse, D. E., A novel fluorescent silica tracer for biological silicification studies. *Chemistry & Biology* **2001**, *8* (11), 1051-1060.
6. Service, N. O. NOAA ocean service education.
7. Colson, P.; Henrist, C.; Cloots, R., Nanosphere Lithography: A Powerful Method for the Controlled Manufacturing of Nanomaterials. *Journal of Nanomaterials* **2013**.
8. Schroeder, H. C.; Krasko, A.; Brandt, D.; Wiens, M.; Tahir, M. N.; Tremel, W.; Mueller, W. E. G., Silicateins, silicase and spicule-associated proteins: synthesis of demosponge silica skeleton and nanobiotechnological applications. *Museu Nacional Serie Livros* **2007**, *28*, 581-592.
9. Hildebrand, M.; Frigeri, L. G.; Davis, A. K., Synchronized growth of *Thalassiosira pseudonana* (Bacillariophyceae) provides novel insights into cell-wall synthesis processes in relation to the cell cycle. *Journal of Phycology* **2007**, *43* (4), 730-740.
10. Cha, J. N.; Shimizu, K.; Zhou, Y.; Christiansen, S. C.; Chmelka, B. F.; Stucky, G. D.; Morse, D. E., Silicatein filaments and subunits from a marine sponge direct the polymerization of silica and silicones in vitro. *Proceedings of the National Academy of Sciences of the United States of America* **1999**, *96* (2).
11. Wang, X. H.; Wiens, M.; Schroder, H. C.; Hu, S. X.; Mugnaioli, E.; Kolb, U.; Tremel, W.; Pisignano, D.; Muller, W. E. G., Morphology of Sponge Spicules: Silicatein a Structural Protein for Bio-Silica Formation. *Advanced Engineering Materials* **2010**, *12* (9), B422-B437.

12. Addadi, L.; Gal, A.; Faivre, D.; Scheffel, A.; Weiner, S., Control of Biogenic Nanocrystal Formation in Biomineralization. *Israel Journal of Chemistry* **2016**, *56* (4), 227-241.
13. Mann, S., *Biomineralization: Principles and Concepts in Bioinorganic Materials Chemistry*. Oxford University Press Inc.: New York, 2001; Vol. 5.
14. Mann, S., *Biomineralization Principles and Concepts in Bioinorganic Materials Chemistry*. Oxford University Press Inc., New York: United States, 2001; p 191.
15. Prozorov, T., Magnetic microbes: Bacterial magnetite biomineralization. *Seminars in Cell & Developmental Biology* **2015**, *46*, 36-43.
16. Stolz, J. F.; Chang, S. B. R.; Kirschvink, J. L., MAGNETOTACTIC BACTERIA AND SINGLE-DOMAIN MAGNETITE IN HEMIPELAGIC SEDIMENTS. *Nature* **1986**, *321* (6073), 849-851.
17. Nudelman, F., Nacre biomineralisation: A review on the mechanisms of crystal nucleation. *Seminars in Cell & Developmental Biology* **2015**, *46*, 2-10.
18. Brownlee, C.; Wheeler, G. L.; Taylor, A. R., Coccolithophore biomineralization: New questions, new answers. *Seminars in Cell & Developmental Biology* **2015**, *46*, 11-16.
19. Falini, G.; Fermani, S.; Goffredo, S., Coral biomineralization: A focus on intra-skeletal organic matrix and calcification. *Seminars in Cell & Developmental Biology* **2015**, *46*, 17-26.
20. Berendsen, A. D.; Olsen, B. R., Bone development. *Bone* **2015**, *80*, 14-18.
21. Habraken, W.; Habibovic, P.; Epple, M.; Böhner, M., Calcium phosphates in biomedical applications: materials for the future? *Materials Today* **2016**, *19* (2), 69-87.
22. Wang, X.; Schroeder, H. C.; Brandt, D.; Wiens, M.; Lieberwirth, I.; Glasser, G.; Schlossmacher, U.; Wang, S.; Mueller, W. E. G., Sponge Biosilica Formation Involves Syneresis Following Polycondensation in vivo. *ChemBiochem* **2011**, *12* (15), 2316-2324.
23. Muller, W. E. G.; Krasko, A.; Le Pennec, G.; Schroder, H. C., Biochemistry and cell biology of silica formation in sponges. *Microscopy Research and Technique* **2003**, *62* (4), 368-377.
24. Fairhead, M.; Johnson, K. A.; Kowatz, T.; McMahon, S. A.; Carter, L. G.; Oke, M.; Liu, H.; Naismith, J. H.; van der Walle, C. F., Crystal structure and silica condensing activities of silicatein alpha-cathepsin L chimeras. *Chemical Communications* **2008**, (15), 1765-1767.

25. Schroder, H. C.; Brandt, D.; Schlossmacher, U.; Wang, X. H.; Tahir, M. N.; Tremel, W.; Belikov, S. I.; Muller, W. E. G., Enzymatic production of biosilica glass using enzymes from sponges: basic aspects and application in nanobiotechnology (material sciences and medicine). *Naturwissenschaften* **2007**, *94* (5), 339-359.
26. Murr, M. M.; Morse, D. E., Fractal intermediates in the self-assembly of silicatein filaments. *Proceedings of the National Academy of Sciences of the United States of America* **2005**, *102* (33), 11657-11662.
27. Muller, W. E. G. W., DE); Schroder, H. W., DE); Krasko, A. M., DE) Decomposition and modification of silicate and silicone by silicase and use of the reversible enzyme 2007.
28. Schröder, H. C.; Krasko, A.; Le Pennec, G.; Adell, T.; Wiens, M.; Hassanein, H.; Müller, I. M.; Müller, W. E., Silicase, an enzyme which degrades biogenous amorphous silica: contribution to the metabolism of silica deposition in the demosponge *Suberites domuncula*. *Prog Mol Subcell Biol* **2003**, *33*, 249-68.
29. Sumper, M.; Brunner, E., Silica biomineralisation in diatoms: The model organism *Thalassiosira pseudonana*. *Chembiochem* **2008**, *9* (8).
30. Thamatrakoln, K.; Hildebrand, M., Analysis of *Thalassiosira pseudonana* silicon transporters indicates distinct regulatory levels and transport activity through the cell cycle. *Eukaryotic Cell* **2007**, *6* (2), 271-279.
31. Curnow, P.; Senior, L.; Knight, M. J.; Thamatrakoln, K.; Hildebrand, M.; Booth, P. J., Expression, Purification, and Reconstitution of a Diatom Silicon Transporter. *Biochemistry* **2012**, *51* (18).
32. Martin-Jezequel, V.; Hildebrand, M.; Brzezinski, M. A., Silicon metabolism in diatoms: Implications for growth. *Journal of Phycology* **2000**, *36* (5).
33. Iler, R., *The Chemistry of Silica: Solubility, Polymerization, Colloid and Surface Properties, and Biochemistry*. John Wiley & Sons, Inc.: New York, 1979.
34. Groeger, C.; Sumper, M.; Brunner, E., Silicon uptake and metabolism of the marine diatom *Thalassiosira pseudonana*: Solid-state Si-29 NMR and fluorescence microscopic studies. *Journal of Structural Biology* **2008**, *161* (1), 55-63.
35. Tesson, B.; Hildebrand, M., Extensive and Intimate Association of the Cytoskeleton with Forming Silica in Diatoms: Control over Patterning on the Meso- and Micro-Scale. *Plos One* **2010**, *5* (12).
36. Hildebrand, M., Biological processing of nanostructured silica in diatoms. *Progress in Organic Coatings* **2003**, *47* (3-4), 256-266.

37. Armbrust, E. V.; Berges, J. A.; Bowler, C.; Green, B. R.; Martinez, D.; Putnam, N. H.; Zhou, S. G.; Allen, A. E.; Apt, K. E.; Bechner, M.; Brzezinski, M. A.; Chaal, B. K.; Chiovitti, A.; Davis, A. K.; Demarest, M. S.; Detter, J. C.; Glavina, T.; Goodstein, D.; Hadi, M. Z.; Hellsten, U.; Hildebrand, M.; Jenkins, B. D.; Jurka, J.; Kapitonov, V. V.; Kroger, N.; Lau, W. W. Y.; Lane, T. W.; Larimer, F. W.; Lippmeier, J. C.; Lucas, S.; Medina, M.; Montsant, A.; Obornik, M.; Parker, M. S.; Palenik, B.; Pazour, G. J.; Richardson, P. M.; Rynearson, T. A.; Saito, M. A.; Schwartz, D. C.; Thamatrakoln, K.; Valentin, K.; Vardi, A.; Wilkerson, F. P.; Rokhsar, D. S., The genome of the diatom *Thalassiosira pseudonana*: Ecology, evolution, and metabolism. *Science* **2004**, *306* (5693), 79-86.
38. Hildebrand, M.; Wetherbee, R., Components and control of silicification in diatoms. *Silicon biomineralization: Biology, biochemistry, molecular biology, biotechnology* **2003**, *Volume 33*.
39. Gordon, R.; Losic, D.; Tiffany, M. A.; Nagy, S. S.; Sterrenburg, F. A. S., The Glass Menagerie: diatoms for novel applications in nanotechnology. *Trends in Biotechnology* **2009**, *27* (2), 116-127.
40. Kröger, N.; Lorenz, S.; Brunner, E.; Sumper, M., Self-assembly of highly phosphorylated silaffins and their function in biosilica morphogenesis. *Science* **2002**, *298* (5593), 584-6.
41. Gröger, C.; Lutz, K.; Brunner, E., Biomolecular self-assembly and its relevance in silica biomineralization. *Cell Biochem Biophys* **2008**, *50* (1), 23-39.
42. Lechner, C. C.; Becker, C. F. W., Modified silaffin R5 peptides enable encapsulation and release of cargo molecules from biomimetic silica particles. *Bioorganic & Medicinal Chemistry* **2013**, *21* (12), 3533-3541.
43. Stote, R. E.; Filocamo, S. F.; Lum, J. S., Silaffin primary structure and its effects on the precipitation morphology of titanium dioxide. *Journal of Materials Research* **2016**, *31* (10), 1373-1382.
44. Miller, S. A.; Hong, E. D.; Wright, D., Rapid and efficient enzyme encapsulation in a dendrimer silica nanocomposite. *Macromolecular Bioscience* **2006**, *6* (10), 839-845.
45. Knecht, M. R.; Sewell, S. L.; Wright, D. W., Size control of dendrimer-templated silica. *Langmuir* **2005**, *21* (5), 2058-2061.
46. Sewell, S. L.; Rutledge, R. D.; Wright, D. W., Versatile biomimetic dendrimer templates used in the formation of TiO₂ and GeO₂. *Dalton Transactions* **2008**, (29), 3857-3865.
47. Deravi, L. F.; Sumerel, J. L.; Sewell, S. L.; Wright, D. W., Piezoelectric Inkjet Printing of Biomimetic Inks for Reactive Surfaces. *Small* **2008**, *4* (12), 2127-2130.

48. Fabijanic, K. I.; Perez-Castillejos, R.; Matsui, H., Direct enzyme patterning with microcontact printing and the growth of ZnO nanoparticles on the catalytic templates at room temperature. *Journal of Materials Chemistry* **2011**, *21* (42), 16877-16879.
49. de la Rica, R.; Matsui, H., Urease as a nanoreactor for growing crystalline ZnO nanoshells at room temperature. *Angewandte Chemie-International Edition* **2008**, *47* (29), 5415-5417.
50. Daiko, Y., Proton conduction in glasses prepared via sol-gel and melting techniques. *Journal of the Ceramic Society of Japan* **2013**, *121* (1415), 539-543.
51. Vaidhyathan, B.; Ganguli, M.; Rao, K. J., A NOVEL METHOD OF PREPARATION OF INORGANIC GLASSES BY MICROWAVE IRRADIATION. *Journal of Solid State Chemistry* **1994**, *113* (2), 448-450.
52. Allcock, H., *Introduction to Materials Chemistry*. John Wiley & Sons, Inc.: Hoboken, New Jersey, 2008; p 432.
53. Ciriminna, R.; Fidalgo, A.; Pandarus, V.; Beland, F.; Ilharco, L. M.; Pagliaro, M., The Sol-Gel Route to Advanced Silica-Based Materials and Recent Applications. *Chemical Reviews* **2013**, *113* (8), 6592-6620.
54. Danks, A. E.; Hall, S. R.; Schnepf, Z., The evolution of 'sol-gel' chemistry as a technique for materials synthesis. *Materials Horizons* **2016**, *3* (2), 91-112.
55. Livage, J.; Henry, M.; Sanchez, C., SOL-GEL CHEMISTRY OF TRANSITION-METAL OXIDES. *Progress in Solid State Chemistry* **1988**, *18* (4), 259-341.
56. Kumari, A.; Singla, R.; Guliani, A.; Yadav, S. K., NANOENCAPSULATION FOR DRUG DELIVERY. *Excli Journal* **2014**, *13*, 265-286.
57. Abbasi, E.; Aval, S. F.; Akbarzadeh, A.; Milani, M.; Nasrabadi, H. T.; Joo, S. W.; Hanifehpour, Y.; Nejati-Koshki, K.; Pashaei-Asl, R., Dendrimers: synthesis, applications, and properties. *Nanoscale Research Letters* **2014**, *9*.
58. Fan, X. H.; Zhao, Y. L.; Xu, W.; Li, L. B., Linear-dendritic block copolymer for drug and gene delivery. *Materials Science & Engineering C-Materials for Biological Applications* **2016**, *62*, 943-959.
59. Ghobril, C.; Rodriguez, E. K.; Nazarian, A.; Grinstaff, M. W., Recent Advances in Dendritic Macromonomers for Hydrogel Formation and Their Medical Applications. *Biomacromolecules* **2016**, *17* (4), 1235-1252.
60. Yellepeddi, V. K.; Ghandehari, H., Poly(amido amine) dendrimers in oral delivery. *Tissue Barriers* **2016**, *4* (2).

61. Parisi, O. I.; Scrivano, L.; Sinicropi, M. S.; Picci, N.; Puoci, F., Engineered Polymer-Based Nanomaterials for Diagnostic, Therapeutic and Theranostic Applications. *Mini-Reviews in Medicinal Chemistry* **2016**, *16* (9), 754-761.
62. Evtyugin, G. A.; Stoikova, E. E., Electrochemical biosensors based on dendrimers. *Journal of Analytical Chemistry* **2015**, *70* (5), 517-534.
63. Tsiourvas, D.; Tsetsekou, A.; Papavasiliou, A.; Arkas, M.; Boukos, N., A novel hybrid sol-gel method for the synthesis of highly porous silica employing hyperbranched poly(ethyleneimine) as a reactive template. *Microporous and Mesoporous Materials* **2013**, *175*, 59-66.
64. Ivanov, A. A.; Botvin, V. V.; Filimoshkin, A. G., Dendrimer polyaluminosilicates as a matrix for filled coatings. *Russian Journal of Applied Chemistry* **2014**, *87* (2), 135-140.
65. Lai, Y. C.; Lai, C. S.; Tai, J. T.; Nguyen, T. P.; Wang, H. L.; Lin, C. Y.; Tsai, T. Y.; Ho, H. C.; Wang, P. H.; Liao, Y. C.; Tsai, D. H., Understanding ligand-nanoparticle interactions for silica, ceria, and titania nanopowders. *Advanced Powder Technology* **2015**, *26* (6), 1676-1686.
66. Jones, S. M., Amine catalyzed condensation of tetraethylorthosilicate. *Journal of Non-Crystalline Solids* **2001**, *291* (3), 206-210.
67. Delak, K. M.; Sahai, N., Amine-catalyzed biomimetic hydrolysis and condensation of organosilicate (vol 17, pg 3221, 2005). *Chemistry of Materials* **2005**, *17* (16).
68. Coradin, T.; Eglin, D.; Livage, J., The silicomolybdic acid spectrophotometric method and its application to silicate/biopolymer interaction studies. *Spectroscopy-an International Journal* **2004**, *18* (4), 567-576.
69. Delak, K. M.; Sahai, N., Mechanisms of amine-catalyzed organosilicate hydrolysis at circum-neutral pH. *Journal of Physical Chemistry B* **2006**, *110* (36).
70. Knecht, M. R.; Wright, D. W., Dendrimer-mediated formation of multicomponent nanospheres. *Chemistry of Materials* **2004**, *16* (24), 4890-4895.
71. Frigeri, L. G.; Radabaugh, T. R.; Haynes, P. A.; Hildebrand, M., Identification of proteins from a cell wall fraction of the diatom *Thalassiosira pseudonana* - Insights into silica structure formation. *Molecular & Cellular Proteomics* **2006**, *5* (1), 182-193.
72. Kisailus, D.; Truong, Q.; Amemiya, Y.; Weaver, J. C.; Morse, D. E., Self-assembled bifunctional surface mimics an enzymatic and templating protein for the synthesis of a metal oxide semiconductor. *Proceedings of the National Academy of Sciences of the United States of America* **2006**, *103* (15).

73. de La Rica, R.; Fabijanic, K. I.; Baldi, A.; Matsui, H., Biomimetic Crystallization Nanolithography: Simultaneous Nanopatterning and Crystallization. *Angewandte Chemie-International Edition* **2010**, *49* (8), 1447-1450.
74. Truffi, M.; Fiandra, L.; Sorrentino, L.; Monieri, M.; Corsi, F.; Mazzucchelli, S., Ferritin nanocages: A biological platform for drug delivery, imaging and theranostics in cancer. *Pharmacological Research* **2016**, *107*, 57-65.
75. da Costa, F.; Souza, P. C. T.; Klein, D. E.; Bove, C. P., Application of acetolysis in phytoliths extraction. *Review of Palaeobotany and Palynology* **2016**, *228*, 93-97.
76. Haynes, R. J., A contemporary overview of silicon availability in agricultural soils. *Journal of Plant Nutrition and Soil Science* **2014**, *177* (6), 831-844.
77. Neethirajan, S.; Gordon, R.; Wang, L. J., Potential of silica bodies (phytoliths) for nanotechnology. *Trends in Biotechnology* **2009**, *27* (8), 461-467.
78. Uriz, M. J.; Turon, X.; Becerro, M. A., Silica deposition in demosponges. *Silicon biomineralization: Biology, biochemistry, molecular biology, biotechnology* **2003**, *Volume 33*, 163-193.
79. Wang, X.; Schlossmacher, U.; Wiens, M.; Batel, R.; Schroeder, H. C.; Mueller, W. E. G., Silicateins, silicatein interactors and cellular interplay in sponge skeletogenesis: formation of glass fiber-like spicules. *Febs Journal* **2012**, *279* (10).
80. Mueller, W. E. G.; Schlossacher, U.; Wang, X.; Boreiko, A.; Brandt, D.; Wolf, S. E.; Tremel, W.; Schroeder, H. C., Poly(silicate)-metabolizing silicatein in siliceous spicules and silicasomes of demosponges comprises dual enzymatic activities (silica polymerase and silica esterase). *Febs Journal* **2008**, *275* (2), 362-370.
81. Apweiler, R.; Bairoch, A.; Wu, C. H., Protein sequence databases. *Current Opinion in Chemical Biology* **2004**, *8* (1), 76-80.
82. Rai, A.; Perry, C. C., Facile Fabrication of Uniform Silica Films with Tunable Physical Properties Using Silicatein Protein from Sponges. *Langmuir* **2010**, *26* (6), 4152-4159.
83. Shimizu, K.; Cha, J.; Stucky, G. D.; Morse, D. E., Silicatein alpha: Cathepsin L-like protein in sponge biosilica. *Proceedings of the National Academy of Sciences of the United States of America* **1998**, *95* (11).
84. Tahir, M. N.; Theato, P.; Muller, W. E. G.; Schroder, H. C.; Borejko, A.; Faiss, S.; Janshoff, A.; Huth, J.; Tremel, W., Formation of layered titania and zirconia catalysed by surface-bound silicatein. *Chemical Communications* **2005**, (44), 5533-5535.

85. Sumerel, J. L.; Yang, W. J.; Kisailus, D.; Weaver, J. C.; Choi, J. H.; Morse, D. E., Biocatalytically templated synthesis of titanium dioxide. *Chemistry of Materials* **2003**, *15* (25), 4804-4809.
86. Kisailus, D.; Choi, J. H.; Weaver, J. C.; Yang, W. J.; Morse, D. E., Enzymatic synthesis and nanostructural control of gallium oxide at low temperature. *Advanced Materials* **2005**, *17* (3), 314-+.
87. Schechte.I; Berger, A., ON SIZE OF ACTIVE SITE IN PROTEASES .I. PAPAINE. *Biochemical and Biophysical Research Communications* **1967**, *27* (2), 157-&.
88. Guex, N.; Peitsch, M. C., SWISS-MODEL and the Swiss-PdbViewer: An environment for comparative protein modeling. *Electrophoresis* **1997**, *18* (15), 2714-2723.
89. Li, L.; Li, C.; Zhang, Z.; Alexov, E., On the 'Dielectric "Constant" of Proteins: Smooth Dielectric Function for Macromolecular Modeling and Its Implementation in DelPhi. *Journal of Chemical Theory and Computation* **2013**, *9* (4), 2126-2136.
90. Smith, G. P.; Baustian, K. J.; Ackerson, C. J.; Feldheim, D. L., Metal oxide formation by serine and cysteine proteases. *Journal of Materials Chemistry* **2009**, *19* (44), 8299-8306.
91. Knecht, M. R.; Wright, D. W., Amine-terminated dendrimers as biomimetic templates for silica nanosphere formation. *Langmuir* **2004**, *20* (11), 4728-4732.
92. Kroger, N.; Deutzmann, R.; Sumper, M., Polycationic peptides from diatom biosilica that direct silica nanosphere formation. *Science* **1999**, *286* (5442), 1129-1132.
93. Knecht, M. R.; Wright, D. W., Functional analysis of the biomimetic silica precipitating activity of the R5 peptide from *Cylindrotheca fusiformis*. *Chemical Communications* **2003**, (24), 3038-3039.
94. Naik, R. R.; Whitlock, P. W.; Rodriguez, F.; Brott, L. L.; Glawe, D. D.; Clarson, S. J.; Stone, M. O., Controlled formation of biosilica structures in vitro. *Chemical Communications* **2003**, (2), 238-239.
95. Pearson, R. G., HARD AND SOFT ACIDS AND BASES HSAB .2. UNDERLYING THEORIES. *Journal of Chemical Education* **1968**, *45* (10), 643-&.
96. Darwent, B., Bond Dissociation Energies in Simple Molecules. Commerce, D. o., Ed. 1970; p 52.
97. Allison, D. P.; Dufrene, Y. F.; Doktycz, M. J.; Hildebrand, M., Biomineralization at the Nanoscale: Learning from Diatoms. *Methods in Nano Cell Biology* **2008**, *90*.

98. Picas, L.; Milhiet, P. E.; Hernandez-Borrell, J., Atomic force microscopy: A versatile tool to probe the physical and chemical properties of supported membranes at the nanoscale. *Chemistry and Physics of Lipids* **2012**, *165* (8), 845-860.
99. Albisetti, E.; Carroll, K. M.; Lu, X.; Curtis, J. E.; Petti, D.; Bertacco, R.; Riedo, E., Thermochemical scanning probe lithography of protein gradients at the nanoscale. *Nanotechnology* **2016**, *27* (31).
100. Li, M.; Liu, L. Q.; Xi, N.; Wang, Y. C., Applications of Atomic Force Microscopy in Exploring Drug Actions in Lymphoma-Targeted Therapy at the Nanoscale. *Bionanoscience* **2016**, *6* (1), 22-32.
101. Xia, Y. N.; Whitesides, G. M., Soft lithography. *Angewandte Chemie-International Edition* **1998**, *37* (5), 551-575.
102. Merghni, A.; Kammoun, D.; Hentati, H.; Janel, S.; Popoff, M.; Lafont, F.; Aouni, M.; Mastouri, M., Quantification of Staphylococcus aureus adhesion forces on various dental restorative materials using atomic force microscopy. *Applied Surface Science* **2016**, *379*, 323-330.
103. Li, Q.; Zhang, T.; Pan, Y. G.; Ciacchi, L. C.; Xu, B. Q.; Wei, G., AFM-based force spectroscopy for bioimaging and biosensing. *Rsc Advances* **2016**, *6* (16), 12893-12912.
104. Koseki, S.; Inoue, K.; Morito, S.; Ohba, T.; Usuki, H., Comparison of TiN-coated tools using CVD and PVD processes during continuous cutting of Ni-based superalloys. *Surface & Coatings Technology* **2015**, *283*, 353-363.
105. Englade-Franklin, L. E.; Morrison, G.; Verberne-Sutton, S. D.; Francis, A. L.; Chan, J. Y.; Garno, J. C., Surface-Directed Synthesis of Erbium-Doped Yttrium Oxide Nanoparticles within Organosilane Zeptoliter Containers. *Acs Applied Materials & Interfaces* **2014**, *6* (18), 15942-15949.
106. An, W. F.; Tolliday, N., Cell-Based Assays for High-Throughput Screening. *Molecular Biotechnology* **2010**, *45* (2), 180-186.
107. Ilouga, P. E.; Hesterkamp, T., On the Prediction of Statistical Parameters in High-Throughput Screening Using Resampling Techniques (vol 17, pg 705, 2012). *Journal of Biomolecular Screening* **2012**, *17* (8), 1113-1113.
108. Macarron, R.; Hertzberg, R. P., Design and Implementation of High Throughput Screening Assays. *Molecular Biotechnology* **2011**, *47* (3), 270-285.
109. Saboski, E. M., EFFECTS OF MERCURY AND TIN ON FRUSTULAR ULTRASTRUCTURE OF THE MARINE DIATOM, NITZSCHIA LIEBETHRUTTI. *Water, Air, and Soil Pollution*, 1977; Vol. 8, pp 461-466.

110. Townley, H. E.; Woon, K. L.; Payne, F. P.; White-Cooper, H.; Parker, A. R., Modification of the physical and optical properties of the frustule of the diatom *Coscinodiscus wailesii* by nickel sulfate. *Nanotechnology* **2007**, *18* (29).
111. Cohn, S. A.; Nash, J.; Pickettheaps, J. D., THE EFFECT OF DRUGS ON DIATOM VALVE MORPHOGENESIS. *Protoplasma* **1989**, *149* (2-3), 130-143.
112. Parkinson, J.; Gordon, R., Beyond micromachining: the potential of diatoms. *Trends in Biotechnology* **1999**, *17* (5), 190-196.
113. Bismuto, A.; Setaro, A.; Maddalena, P.; De Stefano, L.; De Stefano, M., Marine diatoms as optical chemical sensors: A time-resolved study. *Sensors and Actuators B-Chemical* **2008**, *130* (1), 396-399.
114. Losic, D.; Mitchell, J. G.; Voelcker, N. H., Diatomaceous Lessons in Nanotechnology and Advanced Materials. *Advanced Materials* **2009**, *21* (29), 2947-2958.
115. Jeffryes, C.; Campbell, J.; Li, H.; Jiao, J.; Rorrer, G., The potential of diatom nanobiotechnology for applications in solar cells, batteries, and electroluminescent devices. *Energy & Environmental Science* **2011**, *4* (10), 3930-3941.
116. Butcher, K. S. A.; Ferris, J. M.; Phillips, M. R.; Wintrebert-Fouquet, M.; Wah, J. W. J.; Jovanovic, N.; Vyverman, W.; Chepurinov, V., A luminescence study of porous diatoms. *Materials Science & Engineering C-Biomimetic and Supramolecular Systems* **2005**, *25* (5-8), 658-663.
117. Darley, W. M.; Volcani, B. E., ROLE OF SILICON IN DIATOM METABOLISM . A SILICON REQUIREMENT FOR DEOXYRIBONUCLEIC ACID SYNTHESIS IN DIATOM CYLINDROTHECA-FUSIFORMIS REIMANN AND LEWIN. *Experimental Cell Research* **1969**, *58* (2-3), 334-&.
118. Bigelow National Center for Marine Algae and Microbiota. <https://ncma.bigelow.org/>.
119. Creswell, L., Phytoplankton Culture for Aquaculture Feed. Agriculture, U. D. o., Ed. Southern Regional Aquaculture Center: 2010.
120. Franklin, D. J.; Airs, R. L.; Fernandes, M.; Bell, T. G.; Bongaerts, R. J.; Berges, J. A.; Malin, G., Identification of senescence and death in *Emiliana huxleyi* and *Thalassiosira pseudonana*: Cell staining, chlorophyll alterations, and dimethylsulfoniopropionate (DMSP) metabolism. *Limnology and Oceanography* **2012**, *57* (1), 305-317.
121. Iversen, P. W.; Beck, B.; Chen, Y.-F.; Dere, W.; Devanarayan, V.; Eastwood, B. J.; Farnen, M. W.; Iturria, S. J.; Montrose, C.; Moore, R. A.; Weidner, J. R.;

Sittampalam, G. S., *HTS Assay Validation*. Eli Lilly & Company and the National Center for Advancing Translational Sciences: Bethesda, MD, 2012.

122. Casotti, R.; Mazza, S.; Brunet, C.; Vantrepotte, V.; Ianora, A.; Miralto, A., Growth inhibition and toxicity of the diatom aldehyde 2-trans, 4-trans-decadienal on *Thalassiosira weissflogii* (Bacillariophyceae). *Journal of Phycology* **2005**, *41* (1), 7-20.

123. Shimizu, K.; Del Amo, Y.; Brzezinski, M. A.; Stucky, G. D.; Morse, D. E., A novel fluorescent silica tracer for biological silicification studies. *Chemistry & Biology* **2001**, *8* (11), 1051-1060.

124. Davis, A. K.; Hildebrand, M.; Palenik, B., A stress-induced protein associated with the girdle band region of the diatom *Thalassiosira pseudonana* (Bacillariophyta). *Journal of Phycology* **2005**, *41* (3), 577-589.

125. Durkin, C. A.; Mock, T.; Armbrust, E. V., Chitin in Diatoms and Its Association with the Cell Wall. *Eukaryotic Cell* **2009**, *8* (7), 1038-1050.

126. Lehahn, Y.; Ingle, K. N.; Golberg, A., Global potential of offshore and shallow waters macroalgal biorefineries to provide for food, chemicals and energy: feasibility and sustainability. *Algal Research-Biomass Biofuels and Bioproducts* **2016**, *17*, 150-160.

127. Chaffin, J. D.; Mishra, S.; Kuhaneck, R. M.; Heckathorn, S. A.; Bridgeman, T. B., Environmental controls on growth and lipid content for the freshwater diatom, *Fragilaria capucina*: A candidate for biofuel production. *Journal of Applied Phycology* **2012**, *24* (5), 1045-1051.

128. Liu, J.; Mao, X. M.; Zhou, W. G.; Guarnieri, M. T., Simultaneous production of triacylglycerol and high-value carotenoids by the astaxanthin-producing oleaginous green microalga *Chlorella zofingiensis*. *Bioresource Technology* **2016**, *214*, 319-327.

129. Ummalyma, S. B.; Mathew, A. K.; Pandey, A.; Sukumaran, R. K., Harvesting of microalgal biomass: Efficient method for flocculation through pH modulation. *Bioresource Technology* **2016**, *213*, 216-221.

130. Wang, S. K.; Stiles, A. R.; Guo, C.; Liu, C. Z., Harvesting microalgae by magnetic separation: A review. *Algal Research-Biomass Biofuels and Bioproducts* **2015**, *9*, 178-185.

131. Ge, S.; Agbakpe, M.; Zhang, W.; Kuang, L., Heteroaggregation between PEI-coated magnetic nanoparticles and algae: effect of particle size on algal harvesting efficiency. *ACS Appl Mater Interfaces* **2015**, *7* (11), 6102-8.

Jenny E. Nesbitt

jenny.e.nesbitt@vanderbilt.edu

Work Address:

1234 Stevenson Center Lane
Vanderbilt University
Nashville, TN 37235
(615) 322-5516

Home Address:

189 Wallace Road
Apt D-104
Nashville, TN 37211
(513) 256-3072

EDUCATION

Vanderbilt University, Nashville, TN

2010-2016

Ph.D. in Chemistry, focus: bioanalytical & bioinorganic materials

Wake Forest University, Winston-Salem, NC

2006-2010

B.S. in Chemistry with honors, concentration in materials

Minor in French

GPA: 3.5/4

Université de Bourgogne, Dijon, France

2008

Study Abroad Program

RESEARCH EXPERIENCE

Vanderbilt University, Department of Chemistry, Nashville, TN

2010-2016

Graduate Research Assistant

Advisor: Dr. David Wright

Thesis: "Oceanic inspiration for biomaterial formation – investigations into biomimetic synthesis and characterization of inorganic oxide materials inspired by sea sponges and diatoms"

High Throughput Assay Development for Material Fabrication

- A novel approach to material development by utilizing biological methods *in vivo*. Diatoms, a subset of algae, are photosynthetic single-cell eukaryotes that biomineralize a silica cell wall, or frustule, that is both species-specific and nano-patterned.
- This screening assay will probe the silicon metabolic cycle of diatoms, searching for compounds that may interact with the biomineralization process. By identifying these compounds, we hope to fabricate, with a high degree of reproducibility, a large amount of non-orthogonal three-dimensional structures with nanoscale patterning. We also hope to gather more insight into the mechanism by which these cells control the biomineralization of their frustules.
- We used *Thalassiosira pseudonana*, a strain of diatoms that has had the genome sequenced, to allow future chemical biology studies with the hit compounds.
- Cells were cultured using sterile technique, and plates are handled using automation and liquid handling instrumentation.
- A fluorescent probe, LysosensorTM Yellow/Blue DND-160, was investigated as a method of tracking and measuring silica formation.

- Cell processing using flow cytometry, a colorimetric silicon quantitation assay, fluorescence measurements, centrifugation, or magnetic beads was explored

***In Vitro* Biom mineralization of Inorganic Oxides**

- Papain and trypsin were studied as mimics for the silica-precipitating enzyme, silicatein, found in sea sponges.
- The properties of silica and titania precipitation by these enzymes were explored, including kinetics, yield, composition, and size.
- Enzyme reactions were further investigated by inhibition and denaturation studies.

Variation on Nanosphere Lithography

- Zeptoliter sized reaction pores were templated using nanosphere lithography
- Papain and TMOS were reacted in these reaction pores to form templated silica ‘flowers’
- Substrates were imaged using SEM and AFM

Wake Forest University, Department of Chemistry, Winston-Salem, NC

2009-2010

Honors Thesis Researcher

Advisor: Dr. Abdessadek Lachgar

Thesis: “Synthesis, Structure, and Characterization of Novel Hybrid Inorganic-Organic Materials and their Ion Exchange Properties”

- Gallium phosphonate oxalate metal-organophosphates (MOPs) were synthesized using a mild solvothermal synthesis (autoclave).
- Characterization of these materials was performed using single crystal and powder X-ray diffraction, IR spectroscopy, thermogravimetric analysis, and inductively coupled plasma atomic emission spectroscopy.
- Ion exchange was performed using LiCl to replace the materials’ amine groups with smaller Li⁺ ions and was characterized using powder XRD.

TEACHING EXPERIENCE

Vanderbilt University

Teaching Fellow

Senior Capstone Class, Fall 2014-Spring 2015

- Senior undergraduate researchers are led through 6-week modules and individual research projects to develop independence and creative thinking in the laboratory.
- Two units introduce students to a wide variety of instrumentation, and the teaching fellows assist student training. The chromatography unit explores proteins and pigments using ion-exchange chromatography, size-exclusion chromatography, HILIC, 2D-PAGE, LC-MS, and ESI-MS. The inorganic synthesis model explores CdSe quantum dots and ruthenium coordination complexes using TEM, cyclic voltammetry, fluorescence quantum yield, SEM, and ICP-OES.
- After students complete these modules, teaching fellows assist them in developing their own independent research project. These projects range from organic synthesis to diagnostics to nanoparticle-based assays.
- Teaching fellows assist students in putting together a poster to represent their research. This is often their first experience with poster development and presentation.
- Due to the infancy of this course, I also help modify and further develop the modules.

Teaching Assistant

Senior Capstone Class, Fall 2013-Fall 2015 (see above)

General Chemistry II, Spring 2012, Spring 2016
Analytical Chemistry, Spring 2011
General Chemistry I, Fall 2010, Fall 2011

Wake Forest University

Undergraduate Teaching Assistant

Physical Chemistry I (Thermodynamics & Kinetics), Spring 2010

- Held weekly help sessions & graded weekly problem sets

Tutor

Chemistry (General and Organic), Fall 2009 – Spring 2010

Physics, Fall 2009 – Spring 2010

HONORS/AWARDS

Vanderbilt University

D. Stanley and Ann T. Tarbell Graduate Research Fellowship, 2015

Teaching Fellowship, 2014-2015

Hercules Fellowship, 2010-2012

Wake Forest University

American Chemical Society Undergraduate Award in Analytical Chemistry, 2009

PUBLICATIONS

Nesbitt, J.E.; Wright, D.W.; Investigations of enzyme biomimics for *in vitro* inorganic oxide material formation. *Bioinspiration & Biomimetics* **2016**; *Submitted*

Sandlin, R. D.; Fong, K. Y.; Stiebler, R.; Gulka, C. P.; **Nesbitt, J. E.**; Oliveira, M. P.; Oliveira, M. F.; Wright, D. W., Detergent-Mediated Formation of beta-Hematin: Heme Crystallization Promoted by Detergents Implicates Nanostructure Formation for Use as a Biological Mimic. *Crystal Growth & Design* **2016**, *16* (5), 2542-2551.

OUTREACH/SERVICE

Vanderbilt University

Vanderbilt Students Volunteering in Science (VSVS)

Weekly outreach at local urban middle schools

- Provides hands-on laboratory experiences for students with little access.
- Robotics unit teaches kids programming using Lego® Mindstorms®.
- Chemistry unit explores physical properties vs chemical properties, magnetism, pH, elements, compounds, and mixtures, diffusion, and UV radiation.

Tennessee State Collaborative on Reforming Education (TN-SCORE)

High school field trips hosted at Vanderbilt University

- Introduces solar energy as a renewable energy source in a hands-on manner.
- Students extract blackberry juice and soak it with TiO₂ coated glass, coat conductive glass with graphite, and build a solar cell.
- Students learn about scanning electron microscopy (SEM) and are able to image TiO₂ substrates.

Materials Outreach in Rural Education (MORE)

Outreach at rural middle and high schools in Tennessee

- Kits were provided for rural schools that often lack funds to support laboratory experiments.
- Teachers were trained on activities to continue hands-on experiences afterwards
- Kit activities introduce phenotypes vs genotypes, electrical circuits, and chemical vs physical changes.

SELECTED CONFERENCES/COURSES ATTENDED

Nesbitt, J.E.; Wright, D.W. “Development of a screening assay platform as a novel approach to material fabrication and design”, poster presented at the High Throughput Chemistry & Chemical Biology Gordon Conference, New London, NH, **June 2015**

Nesbitt, J.E.; Wright, D.W. “Development of a screening assay platform as a novel approach to material fabrication and design”, poster presented at Southeastern regional meeting of the American chemical society (SERMACS), Nashville, TN, **October 2014**

Nesbitt, J.E.; Travis, A.R.; Wright, D.W. “Biologically Inspired Control of Silicon Dioxide Formation”, poster presented at Vanderbilt Institute of Chemical Biology (VICB) symposium, Nashville, TN, **August 2012**

Attended an *Algal Culturing Techniques Course* at the National Center for Marine Algae and Microbiota, East Boothbay, ME, **June 2012**

Attended a *Managing Algal Cultures Workshop* at the Algae Collection at the University of Texas, Austin, TX, **April 2012**

OTHER SKILLS

Language: French (proficient, 12 years)

Programs/Technical:

Familiar:

- Gas chromatography
- High performance liquid chromatography
- Electrochemistry
- High throughput and automation techniques and instrumentation

Proficient:

- Cell culture
- Mass spectrometry/analysis: ESI, MALDI, LC-MS
- ICP-OES
- NMR and analysis
- Microscopy
- Flow cytometry
- Atomic force microscopy
- Transmission electron microscopy

Expert:

- UV/Vis Spectrophotometry including Synergy Biotek Plate Reader
- Algal culture
- Sterile technique
- Microsoft Office, FlowJo, ChemDraw
- Scanning electron microscopy